2000

Design and implementation of haptic interactions

Naci Zafer
Iowa State University

INFORMATION TO USERS

This manuscript has been reproduced from the microfilm master. UMI films the text directly from the original or copy submitted. Thus, some thesis and dissertation copies are in typewriter face, while others may be from any type of computer printer.

The quality of this reproduction is dependent upon the quality of the copy submitted. Broken or indistinct print, colored or poor quality illustrations and photographs, print bleedthrough, substandard margins, and improper alignment can adversely affect reproduction.

In the unlikely event that the author did not send UMI a complete manuscript and there are missing pages, these will be noted. Also, if unauthorized copyright material had to be removed, a note will indicate the deletion.

Oversize materials (e.g., maps, drawings, charts) are reproduced by sectioning the original, beginning at the upper left-hand corner and continuing from left to right in equal sections with small overlaps.

Photographs included in the original manuscript have been reproduced xerographically in this copy. Higher quality 6" x 9" black and white photographic prints are available for any photographs or illustrations appearing in this copy for an additional charge. Contact UMI directly to order.

Bell & Howell Information and Learning
300 North Zeeb Road, Ann Arbor, MI 48106-1346 USA
800-521-0600

UMI®

Design and implementation of haptic interactions

by

Naci Zafer

A dissertation submitted to the graduate faculty

in partial fulfillment of the requirements for the degree of

DOCTOR OF PHILOSOPHY

Major: Mechanical Engineering

Major Professor: Greg R. Luecke

Iowa State University

Ames, Iowa

2000

Graduate College
Iowa State University

This is to certify that the Doctoral dissertation of

Naci Zafer

has met the dissertation requirements of Iowa State University

Signature was redacted for privacy.

Major Professor

Signature was redacted for privacy.

For the Major Program

Signature was redacted for privacy.

For the Graduate College

To my loving wife, Ozdem

TABLE OF CONTENTS

ABSTRACT

This thesis addresses current haptic display technology where the user interacts with a virtual environment by means of specialized interface devices. The user manipulates computer generated virtual objects and is able to feel the sense of touch through haptic feedback. The objective of this work is to design high performance haptic interactions by developing multi-purpose virtual tools and new control schemes to implement a PUMA 560 robotic manipulator as the haptic interface device. This study focuses on engineering applications where the interaction is with computer generated physical models of dynamic systems and mechanisms. Thus, the research presented in this dissertation focuses on introducing and using new modeling techniques in designing haptic interactions. The interactions are modeled by coupling the motions of the virtual tool with those of the PUMA 560 robotic manipulator.

Kane's method is introduced to model dynamics of virtual tools. The resulting model is used to develop an approach to dynamic simulation for use in interacting haptic display, which includes multibody systems switching constraints. Multibody dynamics of a virtual simulator, a dumbbell, is developed and the advantages of the Kane's method in handling the non-holonomic constraints are presented. Experimental data is also collected to show various contact configurations.

A two-degree of freedom virtual manipulator is modeled to feel the surface of a taurus shape. An optimal position controller is designed to achieve stable interactions. The controller is designed to achieve kinematic coupling between the virtual manipulator and the haptic display device to impose motion constraints and the virtual interactions.

Stability of the haptic interface is also studied and proved using Lyapunov's direct method. Experimental data in various positions of the robotic manipulator is obtained to justify theoretical results. A shift mechanism is then implemented on the taurus shape, thus the motions of the robotic manipulator is further constrained. The difficulties in handling the motion constraints are discussed and an alternative approach is presented.

The work presented in this dissertation uses both kinematic and dynamic based virtual manipulators as virtual simulators to address problems associated in both free and constrained motions. Implementation of both haptic display simulations in an experimental interaction system allows for the evaluation of the performance of the haptic interaction. Both implementations are general enough to allow researchers with any six degree-of-freedom robot to apply the approaches and continue in this area of research. The results are expected to improve on the current haptic display technology by a new type of optimal position controller and better algorithms to handle both holonomic and nonholonomic constraints.

1. INTRODUCTION

1.1 Background

With the amazing advancements in computer technology, researchers are trying to imitate the world artificially. The ultimate goal is to create a realistic virtual environment using new interfaces that convince the human that the dream world looks and feels real. Conventional interfaces such as the keyboard, monitor and the mouse are widely used as interfaces to current computer generated applications. However, with these devices, the user can only see and manipulate the graphical environment with limited realism. More complex tools such as six degree-of-freedom input-output (6D I/O) devices (trackballs), head-mounted displays (HMDs), and datagloves have also been designed and implemented. These tools allow the user to move in the virtual environment and manipulate computer-generated objects. The HMD is equipped with an optical position sensor to track the head position and the dataglove enables the user to point and move in a certain direction.

Interface devices such as joysticks, hand masters, grip handles and exoskeletons have also been designed and implemented to feel the physical characteristics of the virtual environment. These devices are usually called haptic devices because they are provide tactile and force feedback. They allow the user to feel inertia, friction, and full dynamics of virtual objects in the virtual environment. These interface devices have the ability to exert forces on the human arm, hand, fingers, etc. to exploit human sensory perceptions in the virtual

environment. The haptic device, also called a haptic display, can be designed and manufactured to serve a unique purpose. It can be a robotic manipulator or an exoskeleton. These haptic devices enable the user to kinesthetically interact with virtual or real dynamic systems through the human hand contact forces. These devices usually emulate a handle through which the user interacts with virtual objects. Because the quality of the interaction is dependent on the dynamics of the haptic device, the need for dynamic compensation is obvious. The majority of these haptic interface devices currently are of high cost, custom built and therefore unique. Design and manufacture of multi purpose haptic devices that will satisfy the need in both industry and research are needed, and is a goal of this work. Since robotic manipulators are quite common in industry and have been available to researchers for several decades now, many researchers have started using existing robotic manipulators as haptic interface devices. The coupling of the user with these devices also has the additional advantage of limiting the user reachable space. They guarantee a safe working space for the user so the virtual reality participant does not collide with real world objects. The robotic manipulator much like many other custom built haptic devices, can be equipped with a force transducer to measure the user's hand or finger movements or the forces exerted. These forces are then used to create the desired change in the virtual environment. The resultant forces are exerted on the user's hand or fingers by the robot manipulator.

The virtual haptic feedback is hard to generate artificially. The user must first be convinced by the realistic images of the virtual environment. Whenever the virtual environment is manipulated or deformed, it must feel as real as possible. The changes in the virtual environment must reflect the motion and force inputs from the user.

Haptic interaction deals with the force information between the user and the environment. The user applies the forces to create effects in the virtual environment and feels the change in the virtual environment with a force generated by computer simulations. The development of better force display technology has therefore been a vast research area, which accelerated in the late 1990s. One main problem is that measuring or generating force information accurately is very difficult. Although force transducers have been employed to measure forces, this approach has not proven to be a very effective way. The force measuring devices have to sense and record forces generated by the user hand movements, however small they are. This is not a task easily accomplished. Since these devices carry noise with the force information they supply, filters must be implemented to remove the noise. However, filters create further problems. They result in time delays that may distort the virtual environment or even cause instability. The forces fed back to the user, on the other hand, are created by motors in the joints of the haptic interface device or the robotic manipulator. Thus, transparent haptic interface devices are needed to inrease haptic display performance.

1.2 Motivation

The haptic device used in this work is an industrial six-degree of freedom robotic manipulator equipped with a handle at the end effector. The robotic manipulator is used to develop force interactions and kinematic constraints. Unlike custom built haptic devices, the device used in this work is a common manipulator in the research community, and the results

obtained here are easy to verify and follow to other research areas. In addition, the interface hardware and software for joint level control are commonly available to researchers everywhere. The robot is equipped with position sensors at each joint, so the encoder readings are used to compute and track the position of the user hand movements. Although force measurement is not used in some of the applications, a force transducer is also attached to the handle and used in dynamic simulations of virtual objects.

The dynamic model of a multibody system is derived using Kane's method. The introduction of Kane's method to derive the dynamics of the multibody system leads to generalized coordinates, which are able to handle non-holonomic and changing constraints. Kane's method produces models in independent coordinates and therefore presents efficiency of formulation. Dependent coordinates can be found by solving the position problem or integrating the constraint equations along with the rest of the system equations. The resulting model is also computationally efficient.

A dumbbell is chosen as the multibody system to show how the haptic display can be designed to replace application-oriented expensive interfaces. Although the user always feels six degree-of-freedom, the dumbbell has eight degree-of-freedom, which is due to the fact that its wheels rotate. Thus, the dumbbell may allow the user to feel the dynamics exerted by the additional degrees of freedom. Because it is a six degree-of-freedom model, torque feedback in addition to force feedback is also felt by the user. Depending on the motion constraints, the system may have degrees-of-freedom between two and eight.

An approach to providing force and motion constraints is developed using the idea of coupling the actual robot with a virtual robot. The virtual robot kinematics constrain the

actual robot motion, allowing motion to simulate specific virtual mechanisms. A two-degree of freedom virtual manipulator is implemented to study system redundancies in this application. Because a major concern in kinematically redundant systems is stability of the kinematically constrained systems, the search for a stable controller is the objective of this application. The designed controller must filter out the forces and torques resulting in motions away from the desired direction of motion.

The two-degree of freedom virtual manipulator is further constrained to implement a shift mechanism. The motion of the virtual manipulator end effector is designed to act like a stick shift, and the controller implementation constrains the haptic interface to move in this manner. The stability problems associated with changing unilateral constraints are also addressed. Although this application does not require force measurements, the forces applied by the user are measured to compensate for friction. The user-applied forces are measured to predict the desired direction of motion, and the motion is then accelerated in that direction by applying a slight torque at the joints of the manipulator. To further imitate the behavior of a real stick shift mechanism, a detent is also created as the user pushes the shift in. As the user pushes in and out, the motion is first resisted and then released. Thus, the push feels like a click action.

Although it is not implemented, inertial effects of the stick shift might be added to this model. This can be done by assigning dynamic characteristics to the virtual manipulator and using the measured forces to design interactions.

1.3 Contributions

This thesis contributes to the current haptic display technology in various ways. Kane's method is introduced to model multibody dynamic systems for the purpose of trajectory following in haptic force feedback control. The representation of the system using generalized velocities provides advantages in designing and handling both holonomic and non-holonomic constraints as well as switching constraints.

A virtual manipulator concept is developed that couples the actual robot kinematics with the constraints of a simulated manipulator. An impedance based optimal controller is presented in this approach to handle system redundancies. The controller does not require force sensor measurements and offers a stable haptic force control framework. Finally, the stability problems encountered in motion constraints are analyzed and a possible solution is presented.

1.4 Preview of dissertation

In Chapter 2, a brief historical development of haptic display technology is presented. The need for developing high degree-of-freedom virtual systems for interaction is emphasized and the literature in developing dynamic models for simulation of these high degree-of-freedom systems is reviewed. Finally, kinamatically redundant systems are described and an overview of methods to handling redundancies mentioned.

In chapter 3, kinematics and dynamics of both the robotic manipulator and the virtual manipulators to be used are analyzed. A brief summary of dynamics of the robot manipulator is first given. Next, Kane's method is used to derive the dynamics of a virtual dumbbell system. The kinematics of a two degree-of-freedom virtual mechanism is derived. Finally, for use as a virtual shift mechanism, the method of implementing the virtual system using an industrial six degree-of-freedom robot is presented.

Chapter 4 comprises a description of haptic interactions in the virtual environment. The interaction with a high degree-of-freedom tool, a dumbbell, is described and the controller is designed for stable interactions. An optimal impedance type position controller is also described to make the robot mimic the motions of a two degree-of-freedom virtual manipulator. The methods of handling switching constraints are presented.

In chapter 5, stability proof of the virtual manipulator optimal position controller is given. The position of the robot is used to describe the closest achievable position by the virtual manipulator. An impedance controller is then employed to move the robot to that location. The forces and torques applied by the user at the end effector of the robot are filtered to resist the motions not achievable by the virtual manipulator. The Lyapunov stability theory is finally used to prove the stability of the haptic display.

In chapter 6, experimental results from both virtual systems are presented and discussed. The dumbbell motions in free space are shown to illustrate the success of force and torque feedback to the user. Then, contact motions as the dumbbell contacts a surface and rolls on it are studied. The optimal position controller is then employed to make the robot act like the two degree-of-freedom virtual manipulator. The performance of the controller is discussed.

Finally, the two degree-of-freedom manipulator is forced to move in a shift pattern. The switching unilateral constraints are studied.

A summary of results and a brief discussion about the direction of future research conclude the dissertation in Chapter 8.

2. LITERATURE REVIEW

2.1 Introduction

The study presented in this research addresses haptic display and simulation technology. The term haptic display is used to name a mechanical device with which a human can kinesthetically interact with virtual objects in a virtual environment (VE). The haptic system includes the human user, the haptic display device and the computer simulation of the virtual world or the environment. While interacting with the VE by means of the haptic display device, the user is able to view it using specially designed visual aid instruments. Although the main focus area of this thesis is the design and implementation of the haptic display technology, the historical development of the stereoscopic vision technology will also be briefly mentioned to show an overall perspective.

Because the computer graphics technology has drastically matured since the introduction in the1970s, the graphical representation of complex virtual environments is commonly achieved even for real time interactions. With recent advancements in graphics technology, the potential is enormous. The user can now exploit his physical and perceptual senses and gain experience in training and analysis that is directly applicable to real world. Moreover, the cost of implementing the virtual experience is decreasing as the capabilities increase. Examples of the use of this technology include educational [10] [25] and medical [37] purposes.

The user is immersed in the VE through a graphic display, which may be as simple as a monitor, and interacts with it using specific interface devices like a keyboard, mouse or a trackball. Recently, other display and interface devices have come into use which are designed and implemented to improve the sense of immersion in user interactions in the VE. Most of these devices, especially the proprioceptive user interfaces, are still very primitive and face problems with both hardware and software implementation. Thus, the focus of most VR research is in the area of the user interaction and experience with the computer created environment.

In addition to a conventional monitor display, devices have been designed and implemented to achieve stereoscopic vision. The liquid crystal shutter glasses provide 3-D depth perception. This is achieved by occluding the right eye image from the left eye and vice versa. Another display device is a head mounted display, HMD, which may be equipped with an optical position tracker and a headphone. These devices use a separate display monitor for each eye, thus the surroundings are occluded and therefore it is a more immersive technique. The disadvantage in such technique is that the user cannot see his or her surroundings, field of view, latency, so the safety becomes a big concern. Because the user cannot also see his hands, graphical representations of hands may be required. A problem then arises with the registration of the real objects with alignment of the virtual display. In another stereoscopic vision technique, the user is placed inside a room in which the stereoscopic images are projected on to the walls and the floor. The user wears shutter glasses. This method eliminates the need for modeling and display of virtual hands, but any real object or another person in the same room will occlude the user vision. The user may not be able to see all that is projected on to the walls and the floor.

With the graphical representation of the VE commonly presented to the user, the next step is to address the interface devices that allow the user to interact with the virtual objects. This objective is achieved traditionally by using a mouse and a keyboard. Because these devices can not handle 3-D interactions effectively, devices like a wand and a glove have been designed and implemented.

A wand is a hand-held interface that is equipped with a sensor at its tip and a six-degree-of-freedom sensor at its base that give position and the orientation information. Some wands have push buttons and switches, which are used to carry digital input commands to the computers controlling the VE. The data is used to make changes to the VE in real time. Some types emit a laser beam, which may be used to select an object in the VE. A glove worn by the user is equipped with position sensors and it provides the information needed to locate the position and orientation of the user's hands and fingers. The computer simulations are programmed so the graphical world responds to data that these devices provide. The flow of data that creates effects or changes is usually in the direction towards the VE, and not vice versa. Therefore, these interfaces are passive devices. However, some gloves can even reflect signals back to the user. These sensations can be heat, pressure or tactile sensing. These types of gloves can make the dexterous manipulation of the VE possible.

Recent research had led to development of haptic devices to augment and improve the capabilities provided by the more commonly used interface devices. Using haptic interface devices, the user can exert forces in the VE and provide the user with a reaction force from the virtual environment [53]. In many cases, haptic interaction is achieved by the use of specially designed devices capable of specific sensory feedback. The haptic interaction

makes it possible to grasp and manipulate the virtual objects. Thus, virtual force [15] and tactile feedback [50] are possible.

The haptic interface technology is closely related to teleoperation [8] [11] [58] and telerobotics field of research [35] [41]. In these applications, the master provides force and motion feedback to the operator from the motion and force experienced by the slave. This research field has also come to include the remote control of a variety of virtual systems which include simulated robots, prototype vehicles and virtual manufacturing applications.

Kazerooni [41] gives description of a framework for designing a telerobotic system controller. Dynamics of the master and slave robots are coupled. Only the forces are transferred between master and slave. The human pushes against the master arm while the slave pushes against environment. The human senses scaled down forces using this device from the slave. A two-degree of freedom XY table is the master, while a three degree of freedom composite robot with high structural stiffness and low mass of links (allowing wide bandwidth) is the slave. A computed torque method and a PD controller were used for the slave. The computed torque cancels the robot nonlinear terms while the PD controller reduces error and develop robustness in modeling errors. In the research presented in this dissertation to model admittance type haptic interactions, the same computed torque controller and a PD controller is used to compensate for the PUMA 560 robot dynamics and to minimize the position error. This is because the haptic display performance requires transparent haptic interface devices to provide a low inertia display. The dynamic compensation of the PUMA 560 manipulator is therefore essential to model dynamic interactions.

In the case of virtual systems, the slave is a simulated system, and the forces and motion reflected to the operator are computer generated rather than measured. The approach used in this work uses a virtual tool as the slave. The operator manipulates the master to control the virtual slave. This is achieved by direct attachment of the master and the slave using a virtual tool between the two mechanisms. The quality of the haptic interaction with the virtual system therefore depends on not only the mechanical interface but also the virtual tool dynamics used to generate force [28] or motion feedback to the user.

The realism of the haptic display is maximized by the design of more transparent haptic interface devices [12] [43] [35]. Transparent interface devices are usually defined as a low inertia, low friction and back driveable manipulators. The dynamics of the interface device must also be compensated to achieve transparency. For this reason, researchers [3] [4] have been mainly concerned with the stability and performance of haptic interactions, namely the instabilities due to sampling the data (or the limit cycle) and the dynamic range of impedance (or the Z-width [18]).

Although the interaction with the virtual world occurs through a mechanical interface, the virtual simulation must reflect forces and motion consistent with the user input. Because a good haptic display is usually described as a low inertia, low friction and back driveable manipulator, this definition rules out most industrial manipulators. However, work in this research is to develop control interaction strategies that allow the use of the common mechanical devices for use in haptic display.

Many types of haptic interface devices have been developed, some are unique for research purposes and others serve commercial needs. These devices categorize into three groups.

The first category includes grip interaction devices. Force joysticks are the cheapest available grip interaction devices. A two-degree of freedom force joystick can be used to simulate the feel of springs, yo-yos [55], dampers and walls [5]. The PUMA 560 manipulator used in this research belong also in this category. A handle is attached at the end effector of the manipulator through which the user interacts with the virtual environment. The device, PHANToM [49], is desk based and provides force feedback to a thimble worn by the user's finger. The device is able to measure the user finger tip position. Thus, The user can interact with virtual objects to feel and manipulate them. Bejczy [8] uses the PHANToM to perform tasks remotely. The motion of the PHANToM robot image on the computer monitor predicts the motion of the real robot. In comparison with applications performed without force feedback, force feedback to the user is shown to increase performance. Kazerooni and Her [40] have designed a two-degree of freedom haptic device to generate a broader range of impedances. The force imposed on the user by the device was an arbitrary function of the force exerted on the device by the environment. Milman et. al. [54] present a more complex, four-degree of freedom, haptic device. The device emulates a handle through which the user interacts with virtual objects. Adachi [1] used a SPace Interface deviCE (SPICE) manipulator, a 6 degree of freedom robot with joints controlled by direct drive motors, to interact with computer generated virtual objects. The grip of the manipulator held by the user traces virtual object surfaces with different hardness.

The second group devices are intended to use finger(s) where forces are generated by and applied to the finger(s). CyberGlove by [Virtual Technologies Inc.] is a commercially available hand master with force feedback. The device uses six electromechanical actuators connected to each finger and the palm. Luecke [47] uses a force reflecting exoskeleton to

interact with simulated environments by providing contact forces using an electro-magnetic interface between the digits of the human finger and the virtual environment.

Shimoga [64] uses multi-fingered robotic hands in applications of teleoperation. The hands are usually three or four fingered and actuated by electric, hydraulic or pneumatic means. They are equipped with force feedback to fingers and the wrist of the human operator. The design aims to providing the user with the sensation of grasping forces exerted by the slave robot fingers. It is also pointed out in this work that the operator can transmit motion commands to the hand master at 5-10 Hz, and demands the position and force feedback signals at no less than 20-30 Hz. The human hand is reportedly not able to discriminate between two forces at frequencies above 320 Hz. A survey of existing touch display technologies, visual, pneumatic, vibro-tactile, electro-tactile, and neuromuscular stimulation is also presented. An evaluation of the existing master gloves capable of providing touch feedback, and their drawbacks and method of improvements are given.

The third category contains highly specialized devices. A-four-degree-of-freedom surgical simulator by [EXOS Inc.] provides force feedback to user's hand and arm. The surgeons use this technology to train and practice on a virtual patient without any risk to real people. The surgeons provided with surgical instruments designed for haptic interactions perform and practice techniques on the graphically represented body tissues [37]. Forces are generated by touching virtual organ tissues. Another haptic interface device designed by Shuichi provides force feedback to user's elbow joint. The exoskeletons [16] [48] shows the complexity and cost of higher degree of freedom haptic devices.

Although they don't qualify as good haptic devices, many researchers [17] [47] [46] [68] have started using in hand robotic manipulators as haptic interface devices for obvious

reasons. Because higher degree of freedom haptic devices are required for generalized haptic simulations, robotic manipulators can provide that. Another reason is that research developed using robotic manipulators can be easily applied to an ideal or a generalized haptic interface device [54] [29] whenever it becomes available. It is in general true that the more the degrees of freedom, the lower the performance of the haptic interface. This is because these devices imply more complex control algorithms and hard to achieve dynamic compensations. However, position and force controllers [30] [38] [66] [24] [28] and the full dynamics [6] [23] [44] [22] [42] for many robot manipulators have been studied for decades, and are well-understood. Therefore, robotic manipulators have some advantages for use as haptic displays. Industrial robots allow researchers to avoid the time, expense, and effort of designing custom haptic displays. One drawback in use of industrial manipulators is that new control algorithms are needed to model haptic interactions in order to assure stability and to increase performance.

There are two types of controllers used to mimic the dynamic behavior of a virtual object. In the first approach, the motion is sensed and forces are reflected to the user. This is called an impedance type controller [36] [49] [52]. In the second approach, the applied forces are measured and the motion is produced. This is an admittance type controller [1] [2] [51]. The use of impedance control has been more common in the area of haptic feedback design. One reason that these methods have been so successful is that most virtual simulations are limited to simple motions that are restricted to a plane where motions are modeled by spring –damper connections. These applications include virtual walls [1] [20] and push-buttons [2].

Haptic interface research so far has been a search for a flexible hardware interface device and the development of robust control algorithms to achieve high fidelity interactions in the VE. In this work, the robotic manipulator generates force feedback to the user to feel and manipulate virtual objects using either admittance or impedance control. The force generation [59] [55] describes the force and motion relation between the user and the virtual object.

2.2 Multibody dynamics

As the haptic display technology advances, algorithms need to be developed to address complex virtual environment simulations [13] and contact configurations. In most existing research, the study of stable virtual interaction in the VE has usually used primitive virtual objects which are static or modeled by spring-damper mechanisms. These systems usually deal with unilateral constraints [20] [62]. Recently, research effort has been made to develop high degree-of-freedom systems that use more complex constraint conditions. There have been studies on the stability and implementations of nonholonomic and changing constraints [19] [21] [69] [34]. Formulation of rolling constraints is given in [63] [69]. Colgate [21] has designed a one-degree of freedom bicycle like robotic device "cobot" to handle non-holonomic constraints. This device can steer in any direction while providing constraints at the edge of the workspace.

Gillespie presents a study of dynamic interactions in a virtual environment [32] and gives a survey of multibody dynamics for virtual simulations [33]. A comparison of

Newton-Euler, Lagrange and Kane formalisms is given [32] to evaluate which formalism handles changing constraints more effectively. Although the Newton-Euler equations have been traditionally used to model the system dynamics, Lagrange multipliers need to be employed in these models to handle constraints [57]. On the other hand, Kane's method [39] handles nonholonomic and changing constraints better because the equations of motion are expressed in terms of independent coordinates. Dependent coordinates can be obtained by integrating the constraint equations or solving the position problem. The advantage in using the Kane's method over using Lagrange multipliers is probably best stated by Thomas R. Kane [39] as "It enables one to deal directly with nonholonomic systems without having to introduce and subsequently eliminate Lagrange multipliers".

2.3 Kinematically redundant systems

In part of the research presented in this dissertation, a PUMA 560 robotic manipulator is used as the haptic interface device and forced to behave like a virtual manipulator or a mechanism. Because the robot always has more degrees of freedom than the virtual manipulator, the controller is designed to handle system redundancies [56] [60]. The system redundancies or kinematic constraints [14] enforced on the robot servos are created by the virtual manipulator motions and they are the same as the constraints generated by a hybrid position/force controller [31] [61] [65] [67]. The hybrid controller enforces the desired directions of motion imposed by a position and force controller. The controller requires the inverse of the jacobian of the kinematically redundant manipulator. The calculation of the

inverse of the jacobian does not present a unique solution and it may lead to dimensionally inconsistent products. The solution to the inverse problem has been shown to yield infinite number of robot manipulator configurations [45]. The research has led to the development of generalized inverses which use the Moore-Penrose theory of generalized inverses [26]. The stability of hybrid control is studied and tested using a PUMA 560 industrial manipulator in [27].

3. ANALYTICAL DEVELOPMENT

This chapter presents analytical development required in the design and the implementation of the haptic interactions. First, a brief summary on the kinematics and the dynamics of the robot manipulator is given. Then, dynamics of a multibody system, a dumbbell, is developed. The analysis is performed so the implementation of haptic interactions between the user and this virtual dynamic system will use an admittance controller. Finally, a virtual manipulator kinematics is derived to be implemented with an impedance controller to design haptic interactions.

3.1 Robotic manipulator

Most haptic devices used in designing haptic interactions are custom built and unique. Industrial manipulators have therefore been an attractive and an inexpensive tool to help design and implement haptic displays. Advances in computer control have also allowed for accurate compensation of robot dynamics. One disadvantage in using the robot manipulators as haptic interface devices is that their links are heavy and compensation for friction and backlash is difficult.

Since PUMA 560 manipulator is a very commonly used robotic device, its kinematics and dynamics have been studied and reported by many researchers. For this reason, only a brief background information will be given. A schematic of the robot is shown in Figure 3.1.

The PUMA 560 manipulator is a positioning device, with six revolute joints, seven links. Each joint is controlled via a DC servomotor. Each motor shaft incorporates an optical

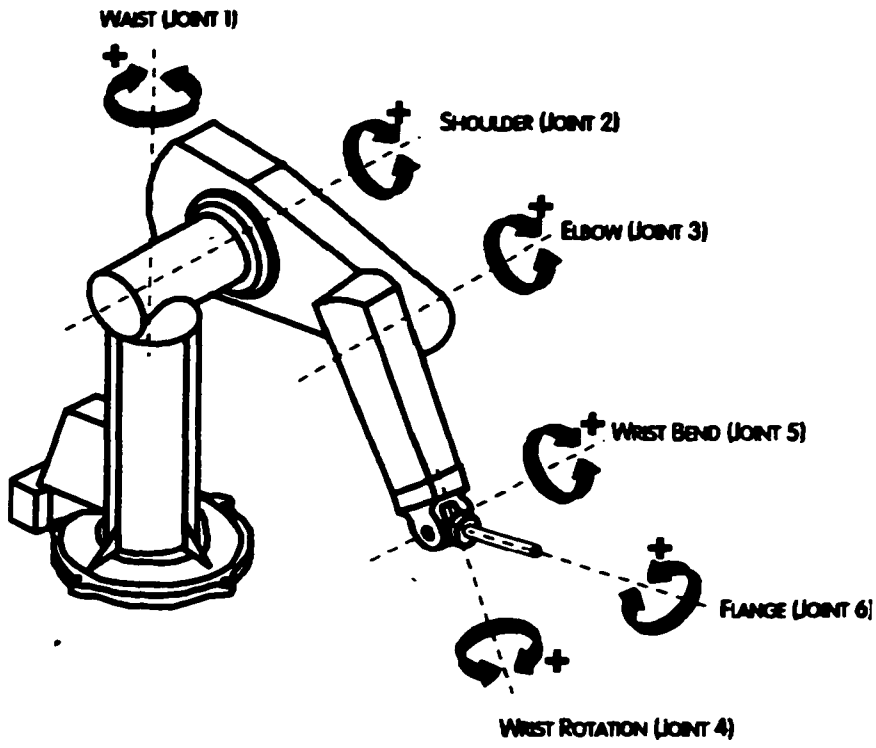

Figure 3.1 Puma 560 Schematic

encoder for position sensing purpose. The overall problem in control is to compute the joint torques required to achieve predefined positions, velocities and accelerations.

The end effector frame relative to the base frame is described by the following homogenous transformation (See Appendix A)

$$ {}^{0}_{6}T = \begin{bmatrix} r_{11} & r_{12} & r_{13} & x_1 \\ r_{21} & r_{22} & r_{23} & x_2 \\ r_{31} & r_{32} & r_{33} & x_3 \\ 0 & 0 & 0 & 1 \end{bmatrix} \tag{3.1} $$

where subscript 6 represents the sixth joint or the end effector and 0 is the stationary base of the robot. This transformation defines the end effector position

$$ {}^{F}x_r = \begin{bmatrix} x_1 \\ x_2 \\ x_3 \end{bmatrix} \tag{3.2} $$

and the orientation

$$ R_r = \begin{bmatrix} r_{11} & r_{12} & r_{13} \\ r_{21} & r_{22} & r_{23} \\ r_{31} & r_{32} & r_{33} \end{bmatrix} \tag{3.3} $$

with respect to the base frame F.

The velocity of the end effector is generally expressed in terms of joint velocities and angular positions by

$$ \dot{x}_r = J_r \dot{q} \tag{3.4} $$

where J_r (see Appendix A) is the Jacobian matrix and it provides a linear relationship between the end effector speed and the joint velocities.

The dynamics of a general six-degree of freedom robotic manipulator in the joint space is expressed by

$$ H(q)\ddot{q} + C(q,\dot{q})\dot{q} + f_r\dot{q} + g(q) = \tau - J_r^T \cdot {}^{R}F_r \tag{3.5} $$

where $H(q)$ is a 6×6 symmetric inertia matrix, $C(q,\dot{q})\dot{q}$ is a 6×1 vector of coriolis and centrifugal terms, f_r is a 6×1 vector of frictional terms, $g(q)$ is a 6×1 vector of gravitational terms, ${}^{R}F_r$ is a 6×1 external Cartesian force and torque vector in the end effector coordinates (R), τ is the 6×1 joint actuator torque vector.

Since this thesis is the study and the design of virtual interactions in a VE by the use of a PUMA 560 industrial manipulator, developing the equations of motion for the robot is an essential first step. There are two ways to determine the robot dynamics, either

analytically or by direct measurement. The analytical methods employed derive the dynamics of the system by employing Newton-Euler or Lagrange equations. The process usually includes the use of symbolic approaches, due to complexity of calculations. A symbolic processing software such as Maple can derive and optimize these equations. The first study in literature to experimentally identify the system parameters of a PUMA 560 was reported by Armstrong et al. [7]. This approach required disassembling the robot to measure inertial parameters. Because all Puma 560 robot mechanical compenents are essentially the same, this set of parameter values is used to describe the Puma 560 used in this work. The Maple software was employed to arrive at the final equations given in Appendix A.

3.2 Dumbbell

This study presents the full dynamics of a dumbbell modeled with two steerable sharp-edged drive wheels mounted at the extremities of a rigid cylindrical axle (as shown in Figure 3.2). The axis of the axle coincides with those of the wheels. The motion of each wheel can be constrained to roll when in contact with a flat surface, which results in both holonomic and non-holonomic motions. Kane's Method is used to derive the unconstrained and constrained dynamic equations of motion for the hardware. The objective is to couple the robotic arm with the multibody simulation dynamics to provide the user with dynamically consistent virtual motion sensations.

The process in determining the multibody dynamics starts by assigning a coordinate frame to the dumbbell (shown in Figure 3.2), and then deriving the kinematics and dynamics of the system.

Let us first consider a simple case where the wheels rotate together with the shaft. In other words, the wheels are rigidly mounted to the axle. The orientation of the dumbbell can then be easily related to the orientation of a fixed reference coordinate frame F. This can be done by a transformation described by the ZYX Euler angles defined by three successive rotations. First, a rotation of a about the Z-axis in F, then a rotation of β about the Y-axis of the current frame, and finally a rotation of γ about the X-axis of the current frame. The resulting coordinate frame is D, which is attached to the rigid cylindrical axle as shown in Figure 3.2. This transformation is given by

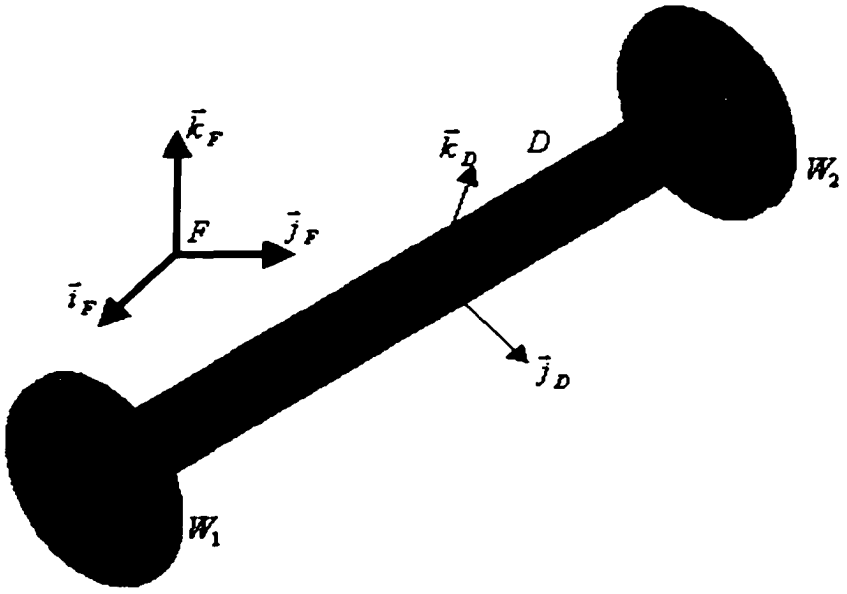

Figure 3.2 Dumbbell Coordinate Axis in Free SpaceMotion

$$\begin{bmatrix} \vec{i}_D \\ \vec{j}_D \\ \vec{k}_D \end{bmatrix} = \begin{bmatrix} 1 & 0 & 0 \\ 0 & c\gamma & s\gamma \\ 0 & -s\gamma & c\gamma \end{bmatrix} \begin{bmatrix} c\beta & 0 & -s\beta \\ 0 & 1 & 0 \\ s\beta & 0 & c\beta \end{bmatrix} \begin{bmatrix} ca & sa & 0 \\ -sa & ca & 0 \\ 0 & 0 & 1 \end{bmatrix} \begin{bmatrix} \vec{i}_F \\ \vec{j}_F \\ \vec{k}_F \end{bmatrix} \tag{3.6}$$

which implies

$$\begin{bmatrix} \vec{i}_F \\ \vec{j}_F \\ \vec{k}_F \end{bmatrix} = {}^F R^D \begin{bmatrix} \vec{i}_D \\ \vec{j}_D \\ \vec{k}_D \end{bmatrix} \tag{3.7}$$

where

$${}^F R^D = \begin{bmatrix} cac\beta & cas\beta s\gamma - sac\gamma & cas\beta c\gamma + sas\gamma \\ sac\beta & sas\beta s\gamma + cac\gamma & sas\beta c\gamma - cas\gamma \\ -s\beta & c\beta s\gamma & c\beta c\gamma \end{bmatrix} \tag{3.8}$$

where (i_F, j_F, k_F) are the unit vectors in $F(X,Y,Z)$, and (i_D, j_D, k_D) are the unit vectors in $D(X,Y,Z)$. $(ca\ ,\ c\beta\ ,\ c\gamma)$ are the cosine, and $(sa\ ,\ s\beta\ ,\ s\gamma)$ the sine of angles a, β and γ, respectively.

If the orientation is already known and given by

$$\begin{bmatrix} \vec{i}_F \\ \vec{j}_F \\ \vec{k}_F \end{bmatrix} = \begin{bmatrix} r_{11} & r_{12} & r_{13} \\ r_{21} & r_{22} & r_{23} \\ r_{31} & r_{32} & r_{33} \end{bmatrix} \begin{bmatrix} \vec{i}_D \\ \vec{j}_D \\ \vec{k}_D \end{bmatrix} \tag{3.9}$$

then the three successive rotations can be found by solving the inverse problem which results in

$$\begin{aligned} \beta &= \text{atan2}(-r_{31}, \sqrt{r_{11}^2 + r_{21}^2}) \\ a &= \text{atan2}(r_{21}/c\beta, r_{11}/c\beta) \\ \gamma &= \text{atan2}(r_{32}/c\beta, r_{33}/c\beta) \end{aligned} \tag{3.10}$$

where atan2 (Y, X) is the four quadrant arctangent of the real parts of the elements of X and Y. Note that this solution is not valid if $c\beta = 0$. In designing the haptic interactions, the

dumbbell will be oriented in such a way that the motion singularity at $c\beta = 0$ will coincide with the Puma 560 singularity, which happens when the fourth and the sixth joint angles are both zero.

The angular velocity of frame D is defined by these rotations as

$$^F\vec{w}^D = \dot{a}\vec{k}_F + \dot{\beta}(ca\vec{j}_F - sa\vec{i}_F) + \dot{\gamma}\vec{i}_D \tag{3.11}$$

$$^F\vec{w}^D = (-\dot{a}s\beta + \dot{\gamma})\vec{i}_D + (\dot{a}c\beta s\gamma + \dot{\beta}c\gamma)\vec{j}_D + (\dot{a}c\beta c\gamma - \dot{\beta}s\gamma)\vec{k}_D \tag{3.12}$$

$$^F\vec{w}^D = u_1\vec{i}_D + u_2\vec{j}_D + u_3\vec{k}_D \tag{3.13}$$

where the generalized velocity terms are defined by

$$u_1 = -\dot{a}s\beta + \dot{\gamma},\ u_2 = \dot{a}c\beta s\gamma + \dot{\beta}c\gamma,\ u_3 = \dot{a}c\beta c\gamma - \dot{\beta}s\gamma \tag{3.14}$$

By differentiating the angular velocity, the angular acceleration is obtained

$$^F\vec{a}^D = \dot{u}_1\vec{i}_D + \dot{u}_2\vec{j}_D + \dot{u}_3\vec{k}_D \tag{3.15}$$

If dumbbell center of gravity position vector is given by

$$\overrightarrow{FD^*} = p_x\vec{i}_F + p_F\vec{j}_A + p_z\vec{k}_F \tag{3.16}$$

Then, the velocity of the center of gravity of the system becomes

$$^F\vec{V}^{D^*} = \dot{p}_x\vec{i}_F + \dot{p}_y\vec{j}_F + \dot{p}_z\vec{k}_F = u_4\vec{i}_F + u_5\vec{j}_F + u_6\vec{k}_F \tag{3.17}$$

where three more generalized velocity terms are defined by

$$u_4 = \dot{p}_x,\ u_5 = \dot{p}_y,\ u_6 = \dot{p}_z \tag{3.18}$$

The six generalized velocities suffice to characterize the motion of the dumbbell. Thus, the system has six degree-of-freedom. The total velocity of D in Cartesian frame D can now be written in matrix form as

$$\dot{x} = J_v u \tag{3.19}$$

where

$$u = [u_1 \quad u_2 \quad u_3 \quad u_4 \quad u_5 \quad u_6]^T \tag{3.20}$$

$$J_v = \begin{bmatrix} 0 & 0 & 0 & cac\beta & sac\beta & -s\beta \\ 0 & 0 & 0 & cas\beta s\gamma - sac\gamma & sas\beta s\gamma + cac\gamma & c\beta s\gamma \\ 0 & 0 & 0 & cas\beta c\gamma + sas\gamma & sas\beta c\gamma - cas\gamma & c\beta c\gamma \\ 1 & 0 & 0 & 0 & 0 & 0 \\ 0 & 1 & 0 & 0 & 0 & 0 \\ 0 & 0 & 1 & 0 & 0 & 0 \end{bmatrix} \tag{3.21}$$

Time differential of ${}^F\vec{V}^{D^*}$ is the acceleration

$${}^F\vec{a}^{D^*} = \dot{u}_4\vec{i}_F + \dot{u}_5\vec{j}_F + \dot{u}_6\vec{k}_F \tag{3.22}$$

Now, let us derive the equations that define torques and forces in the system. The inertia torque is given by

$$\vec{T}^D = -{}^F\vec{a}^D \cdot \underline{\underline{I}}^D - {}^F\vec{w}^D \times \underline{\underline{I}}^D \cdot {}^F\vec{w}^D \tag{3.23}$$

where the central inertia dyadic in the principle axis is

$$\underline{\underline{I}}^D = I_1\vec{i}_D\vec{i}_D + I_2(\vec{j}_D\vec{j}_D + \vec{k}_D\vec{k}_D) \tag{3.24}$$

Then,

$$\vec{T}^D = -I_1\dot{u}_1\vec{i}_D - (I_2\dot{u}_2 - Iu_1u_3)\vec{j}_D - (I_2\dot{u}_3 + Iu_1u_2)\vec{k}_D \tag{3.25}$$

where

$$I = I_2 - I_1 \tag{3.26}$$

If the shaft has a mass m_D, radius r, and length L, and the wheels have masses m_{W_1} and m_{W_2} with the same radius R, and neglectable thickness h, then

$$I_1 = \frac{1}{2}m_D r^2 + \frac{1}{2}(m_{W_1} + m_{W_2})R^2 \tag{3.27}$$

$$I_2 = \frac{1}{4}m_D r^2 + \frac{1}{4}(m_{W_1} + m_{W_2})R^2 + \frac{1}{12}m_D L^2 + (m_{W_1} + m_{W_2})\frac{L^2}{4} \tag{3.28}$$

The inertia force is

$$\vec{R}^{D^*} = -m \cdot {}^F\vec{a}^{D^*} \tag{3.29}$$

where m is the total mass of the system,

$$m = m_D + m_{W_1} + m_{W_2} \tag{3.30}$$

The non-holonomic generalized inertia forces are then given by

$$F_{gi}^* = {}^F\vec{w}_{u_i}^D \cdot \vec{T}^D + {}^F\vec{V}_{u_i}^{D^*} \cdot \vec{R}^{D^*}, \text{ for } i = 1,2,...,6, \tag{3.31}$$

and the non-holonomic generalized active forces by

$$F_{gi} = \vec{F}^{D^*} \cdot {}^F\vec{V}_{u_i}^{D^*} + \vec{M}^{D^*} \cdot {}^F\vec{w}_{u_i}^D, \text{ for } i = 1,2,...,6, \tag{3.32}$$

where the non-zero partial velocity terms are

$${}^A\vec{w}_{u_1}^D = \vec{i}_D, \; {}^A\vec{w}_{u_2}^D = \vec{j}_D, \; {}^A\vec{w}_{u_3}^D = \vec{k}_D \tag{3.33}$$

$${}^F\vec{V}_{u_4}^{D^*} = \vec{i}_F, \; {}^F\vec{V}_{u_5}^{D^*} = \vec{j}_F, \; {}^F\vec{V}_{u_6}^{D^*} = \vec{k}_F \tag{3.34}$$

The forces and torques applied at D^* are

$$\begin{aligned} \vec{F}^{D^*} &= F_1\vec{i}_D + F_2\vec{j}_D + F_3\vec{k}_D - mg\vec{k}_F \\ \vec{M}^{D^*} &= M_1\vec{i}_D + M_2\vec{j}_D + M_3\vec{k}_D \end{aligned} \tag{3.35}$$

Then, Kane's dynamical equations are then given by

$$F_{gi}^* + F_{gi} = 0 \tag{3.36}$$

which results in the following equations

$$I_1\dot{u}_1 - M_1 = 0 \tag{3.37}$$

$$I_2\dot{u}_2 - Iu_1u_3 - M_2 = 0 \tag{3.38}$$

$$I_2\dot{u}_3 + Iu_1u_2 - M_3 = 0 \tag{3.39}$$

$$m\dot{u}_4 - F_1 = 0 \tag{3.40}$$

$$m\dot{u}_5 - F_2 = 0 \tag{3.41}$$

$$m\dot{u}_6 - F_3 + mg = 0 \tag{3.42}$$

These equations when integrated give the generalized velocities in (3.20).

Equations in (3.14) can be rewritten as

$$\begin{bmatrix} -s\beta & 0 & 1 \\ c\beta s\gamma & c\gamma & 0 \\ c\beta c\gamma & -s\gamma & 0 \end{bmatrix} \begin{bmatrix} \dot{a} \\ \dot{\beta} \\ \dot{\gamma} \end{bmatrix} = \begin{bmatrix} u_1 \\ u_2 \\ u_3 \end{bmatrix} \tag{3.43}$$

which implies

$$\begin{aligned} \dot{a} &= (s\gamma u_2 + c\gamma u_3)/c\beta \\ \dot{\beta} &= c\gamma u_2 - s\gamma u_3 \\ \dot{\gamma} &= u_1 + (s\gamma u_2 + c\gamma u_3)s\beta/c\beta \end{aligned} \tag{3.44}$$

As long as $c\beta \neq 0$, integration of these equations will give the angles a, β and γ. Then, these equations can be used to determine the orientation of the dumbbell. Finally, integration of equation (3.18) gives the dumbbell position described by equation (3.16).

A more complex case is when the wheels are free to rotate about the axis $\vec{i}_D$, independently from the rotation of the rigid cylindrical axle. Assume that the angular positions of the wheels W_1 and W_2 are given by angles γ_1 and γ_2, respectively. The angular velocities of the wheels about the axis $\vec{i}_D$ are then $\dot{\gamma}_1$ and $\dot{\gamma}_2$. These angular velocity assignments will also be defined as additional generalized velocities,

$$u_7 = \dot{\gamma}_1, \; u_8 = \dot{\gamma}_2 \tag{3.45}$$

Note that the system has eight degrees-of-freedom in this case.

The angular velocities of the wheels can now be expressed by

$$^F\vec{w}^{W_1} = u_7\vec{i}_D + u_2\vec{j}_D + u_3\vec{k}_D \tag{3.46}$$

$$^F\vec{w}^{W_2} = u_8\vec{i}_D + u_2\vec{j}_D + u_3\vec{k}_D \tag{3.47}$$

The time differential of these equations give the angular accelerations

$$^F\vec{a}^{W_1} = \dot{u}_7\vec{i}_D + \dot{u}_2\vec{j}_D + \dot{u}_3\vec{k}_D \tag{3.48}$$

$$^F\vec{a}^{W_2} = \dot{u}_8\vec{i}_D + \dot{u}_2\vec{j}_D + \dot{u}_3\vec{k}_D \tag{3.49}$$

The velocity of center of gravity of the wheel W_1^* is

$$\begin{aligned} ^F\vec{V}^{W_1^*} &= {}^F\vec{V}^{D^*} + 0.5L\dot{\vec{i}}_D = {}^F\vec{V}^{D^*} + 0.5L\,{}^F\vec{w}^D \times \vec{i}_D \\ &= {}^F\vec{V}^{D^*} + 0.5L(u_1\vec{i}_D + u_2\vec{j}_D + u_3\vec{k}_D)\times\vec{i}_D \\ &= u_4\vec{i}_F + u_5\vec{j}_F + u_6\vec{k}_F + 0.5L(u_3\vec{j}_D - u_2\vec{k}_D) \end{aligned} \tag{3.50}$$

$$\begin{aligned} ^F\vec{V}^{W_1^*} &= (u_4 ca c\beta + u_5 sac\beta - u_6 s\beta)\vec{i}_D \\ &+ \left(u_4(cas\beta s\gamma - sac\gamma) + u_5(sas\beta s\gamma + cac\gamma) + u_6 c\beta s\gamma + 0.5Lu_3\right)\vec{j}_D \\ &+ \left(u_4(cas\beta c\gamma + sas\gamma) + u_5(sas\beta c\gamma - cas\gamma) + u_6 c\beta c\gamma - 0.5Lu_2\right)\vec{k}_D \end{aligned} \tag{3.51}$$

Similarly, the velocity of center of gravity of the wheel W_2^* is found to be

$$\begin{aligned} ^F\vec{V}^{W_2^*} &= (u_4 ca c\beta + u_5 sac\beta - u_6 s\beta)\vec{i}_D \\ &+ \left(u_4(cas\beta s\gamma - sac\gamma) + u_5(sas\beta s\gamma + cac\gamma) + u_6 c\beta s\gamma - 0.5Lu_3\right)\vec{j}_D \\ &+ \left(u_4(cas\beta c\gamma + sas\gamma) + u_5(sas\beta c\gamma - cas\gamma) + u_6 c\beta c\gamma + 0.5Lu_2\right)\vec{k}_D \end{aligned} \tag{3.52}$$

Then, the accelerations are obtained by differentiating these equations with respect to time.

$$\begin{aligned} ^F\vec{a}^{W_1^*} &= \frac{\partial\,{}^F\vec{V}^{W_1^*}}{\partial t} = \frac{\partial}{\partial t}\left(u_4\vec{i}_F + u_5\vec{j}_F + u_6\vec{k}_F + 0.5L(u_3\vec{j}_D - u_2\vec{k}_D\right) \\ &= \dot{u}_4\vec{i}_F + \dot{u}_5\vec{j}_F + \dot{u}_6\vec{k}_F + 0.5L(\dot{u}_3\vec{j}_D - \dot{u}_2\vec{k}_D + u_3\,{}^F\vec{w}^D \times \vec{j}_D - u_2\,{}^F\vec{w}^D \times \vec{k}_D) \\ &= \left(\dot{u}_4 ca c\beta + \dot{u}_5 sac\beta - \dot{u}_6 s\beta - 0.5L(u_2^2 + u_3^2)\right)\vec{i}_D \\ &+ \left(\dot{u}_4(cas\beta s\gamma - sac\gamma) + \dot{u}_5(sas\beta s\gamma + cac\gamma) + \dot{u}_6 c\beta s\gamma + 0.5L(\dot{u}_3 + u_1u_2)\right)\vec{j}_D \\ &+ \left(\dot{u}_4(cas\beta c\gamma + sas\gamma) + \dot{u}_5(sas\beta c\gamma - cas\gamma) + \dot{u}_6 c\beta c\gamma - 0.5L(\dot{u}_2 - u_1u_3)\right)\vec{k}_D \end{aligned} \tag{3.53}$$

$$
\begin{aligned}
{}^F\vec{a}^{W_2^*} &= \left(\dot{u}_4 ca c\beta + \dot{u}_5 sac\beta - \dot{u}_6 s\beta + 0.5L(u_2^2 + u_3^2)\right)\vec{i}_D \\
&+ \left(\dot{u}_4(cas\beta s\gamma - sac\gamma) + \dot{u}_5(sas\beta s\gamma + cac\gamma) + \dot{u}_6 c\beta s\gamma - 0.5L(\dot{u}_3 + u_1u_2)\right)\vec{j}_D \\
&+ \left(\dot{u}_4(cas\beta c\gamma + sas\gamma) + \dot{u}_5(sas\beta c\gamma - cas\gamma) + \dot{u}_6 c\beta c\gamma + 0.5L(\dot{u}_2 - u_1u_3)\right)\vec{k}_D
\end{aligned} \tag{3.54}
$$

In order to obtain a dynamic model, let us first find out the non-zero partial velocity terms.

$$
\begin{aligned}
&{}^A\vec{w}_{u_1}^D = \vec{i}_D \\
&{}^A\vec{w}_{u_2}^D = {}^A\vec{w}_{u_2}^{W_1} = {}^A\vec{w}_{u_2}^{W_2} = \vec{j}_D \\
&{}^A\vec{w}_{u_3}^D = {}^A\vec{w}_{u_3}^{W_1} = {}^A\vec{w}_{u_3}^{W_2} = \vec{k}_D \\
&{}^A\vec{w}_{u_7}^{W_1} = {}^A\vec{w}_{u_8}^{W_2} = \vec{i}_D
\end{aligned} \tag{3.55}
$$

$$
\begin{aligned}
&{}^F\vec{V}_{u_2}^{W_1^*} = -{}^F\vec{V}_{u_2}^{W_2^*} = -0.5L\left((cas\beta c\gamma + sas\gamma)\vec{i}_F + (sas\beta c\gamma - cas\gamma)\vec{j}_F + c\beta c\gamma\vec{k}_F\right) = -0.5L\vec{k}_D \\
&{}^F\vec{V}_{u_3}^{W_1^*} = -{}^F\vec{V}_{u_3}^{W_2^*} = 0.5L\left((cas\beta s\gamma - sac\gamma)\vec{i}_F + (sas\beta s\gamma + cac\gamma)\vec{j}_F + c\beta s\gamma\vec{k}_F\right) = 0.5L\vec{j}_D \\
&{}^F\vec{V}_{u_4}^{D^*} = {}^F\vec{V}_{u_4}^{W_1^*} = {}^F\vec{V}_{u_4}^{W_2^*} = \vec{i}_F = cac\beta\vec{i}_D + (cas\beta s\gamma - sac\gamma)\vec{j}_D + (cas\beta c\gamma + sas\gamma)\vec{k}_D \\
&{}^F\vec{V}_{u_5}^{D^*} = {}^F\vec{V}_{u_5}^{W_1^*} = {}^F\vec{V}_{u_5}^{W_2^*} = \vec{j}_F = sac\beta\vec{i}_D + (sas\beta s\gamma + cac\gamma)\vec{j}_D + (sas\beta c\gamma - cas\gamma)\vec{k}_D \\
&{}^F\vec{V}_{u_6}^{D^*} = {}^F\vec{V}_{u_6}^{W_1^*} = {}^F\vec{V}_{u_6}^{W_2^*} = \vec{k}_F = -s\beta\vec{i}_D + c\beta s\gamma\vec{j}_D + c\beta c\gamma\vec{k}_D
\end{aligned} \tag{3.56}
$$

The inertia torque is

$$
\vec{T} = -{}^F\vec{a}\cdot\underline{\underline{I}} - {}^F\vec{w}\times\underline{\underline{I}}\cdot{}^F\vec{w} \tag{3.57}
$$

which yields

$$
\vec{T}^D = -I_1^D\dot{u}_1\vec{i}_D - (I_2^D\dot{u}_2 - I^Du_1u_3)\vec{j}_D - (I_2^D\dot{u}_3 + I^Du_1u_2)\vec{k}_D \tag{3.58}
$$

where

$$
I_1^D = \frac{1}{2}m_Dr^2,\ I_2^D = \frac{1}{4}m_Dr^2 + \frac{1}{12}m_DL^2,\ I^D = I_2^D - I_1^D \tag{3.59}
$$

and

$$
\vec{T}^{W_1} = -I_1^{W_1}\dot{u}_7\vec{i}_D - (I_2^{W_1}\dot{u}_2 - I^{W_1}u_7u_3)\vec{j}_D - (I_2^{W_1}\dot{u}_3 + I^{W_1}u_7u_2)\vec{k}_D \tag{3.60}
$$

$$\vec{T}^{W_2} = -I_1^{W_2}\dot{u}_8\vec{i}_D - (I_2^{W_2}\dot{u}_2 - I^{W_2}u_8u_3)\vec{j}_D - (I_2^{W_2}\dot{u}_3 + I^{W_2}u_8u_2)\vec{k}_D \tag{3.61}$$

where

$$I_1^{W_1} = \frac{1}{2}m_{W_1}R^2,\ I_2^{W_1} = \frac{1}{4}m_{W_1}R^2,\ I^{W_1} = I_2^{W_1} - I_1^{W_1} \tag{3.62}$$

$$I_1^{W_2} = \frac{1}{2}m_{W_2}R^2,\ I_2^{W_2} = \frac{1}{4}m_{W_2}R^2,\ I^{W_2} = I_2^{W_2} - I_1^{W_2} \tag{3.63}$$

Forces and torques applied at D^* are given in (3.35). Forces and torques applied at W_1^* and W_2^* are assumed all zero.

The forces resultant of all contact and distance forces are

$$\vec{R}^{D^*} = -m_D \cdot {}^F\vec{a}^{D^*},\ \vec{R}^{W_1^*} = -m_{W_1} \cdot {}^F\vec{a}^{W_1^*},\ \vec{R}^{W_2^*} = -m_{W_2} \cdot {}^F\vec{a}^{W_2^*} \tag{3.64}$$

The generalized inertia and active forces are

$$F_{gi}^* = {}^F\vec{w}_{u_i}^{D} \cdot \vec{T}^{D} + {}^F\vec{V}_{u_i}^{D^*} \cdot \vec{R}^{D^*} + {}^F\vec{w}_{u_i}^{W_1} \cdot \vec{T}^{W_1} + {}^F\vec{V}_{u_i}^{W_1^*} \cdot \vec{R}^{W_1^*} + {}^F\vec{w}_{u_i}^{W_2} \cdot \vec{T}^{W_2} + {}^F\vec{V}_{u_i}^{W_2^*} \cdot \vec{R}^{W_2^*} \tag{3.65}$$

$$F_{gi} = \vec{F}^{D^*} \cdot {}^F\vec{V}_{u_i}^{D^*} + \vec{M}^{D^*} \cdot {}^F\vec{w}_{u_i}^{D} + \vec{F}^{W_1^*} \cdot {}^F\vec{V}_{u_i}^{W_1^*} + \vec{M}^{W_1^*} \cdot {}^F\vec{w}_{u_i}^{W_1} + \vec{F}^{W_2^*} \cdot {}^F\vec{V}_{u_i}^{W_2^*} + \vec{M}^{W_2^*} \cdot {}^F\vec{w}_{u_i}^{W_2} \tag{3.66}$$

Then, Kane's dynamical equations are again given by (3.36) which results in the following system dynamic equations.

$$I_1^D\dot{u}_1 - M_1 = 0 \tag{3.67}$$

$$I_2\dot{u}_2 - \left(I^D + (m_{W_1} + m_{W_2})\frac{L^2}{4}\right)u_1u_3 - I^{W_1}u_7u_3 - I^{W_2}u_8u_3 - M_2 = 0 \tag{3.68}$$

$$I_2\dot{u}_3 + \left(I^D + (m_{W_1} + m_{W_2})\frac{L^2}{4}\right)u_1u_2 + I^{W_1}u_7u_2 + I^{W_2}u_8u_2 - M_3 = 0 \tag{3.69}$$

$$m\dot{u}_4 - F_1 = 0 \tag{3.70}$$

$$m\dot{u}_5 - F_2 = 0 \tag{3.71}$$

$$m\dot{u}_6 - F_3 + mg = 0 \tag{3.72}$$

$$I_1^{W_1}\dot{u}_7 = 0 \tag{3.73}$$

$$I_1^{W_2}\dot{u}_8 = 0 \tag{3.74}$$

In the case where the wheels are rigidly attached to the axle, $u_7 = u_8 = u_1$ and the last two equations drop out. If the wheels don't rotate, then $u_7 = u_8 = 0$.

Let us now analyze the contact motions where the dumbbell comes in contact with a surface z_F = constant. The case where just one of the wheels contacts the surface is shown in Figure 3.3. The wheel W_1 touches the surface S at point $\hat{W}_1$.

The unit vector tangent to the surface S is $\vec{j}_{W_1}$ and given by

$$\vec{j}_{W_1} = -sa\vec{i}_F + ca\vec{j}_F \tag{3.75}$$

Note also that the unit vector $\vec{i}_{W_1}$ is equal to $\vec{i}_D$. Then, $\vec{k}_{W_1}$ is expressed by

$$\vec{k}_{W_1} = \vec{i}_{W_1} \times \vec{j}_{W_1} = cas\beta\vec{i}_F + sas\beta\vec{j}_F + c\beta\vec{k}_F \tag{3.76}$$

So,

$$\begin{bmatrix} \vec{i}_{W_1} \\ \vec{j}_{W_1} \\ \vec{k}_{W_1} \end{bmatrix} = \begin{bmatrix} cac\beta & sac\beta & -s\beta \\ -sa & ca & 0 \\ cas\beta & sas\beta & c\beta \end{bmatrix} \begin{bmatrix} \vec{i}_F \\ \vec{j}_F \\ \vec{k}_F \end{bmatrix} \tag{3.77}$$

This also implies

$$\begin{bmatrix} \vec{i}_{W_1} \\ \vec{j}_{W_1} \\ \vec{k}_{W_1} \end{bmatrix} = \begin{bmatrix} 1 & 0 & 0 \\ 0 & c\gamma & -s\gamma \\ 0 & s\gamma & c\gamma \end{bmatrix} \begin{bmatrix} \vec{i}_D \\ \vec{j}_D \\ \vec{k}_D \end{bmatrix} \tag{3.78}$$

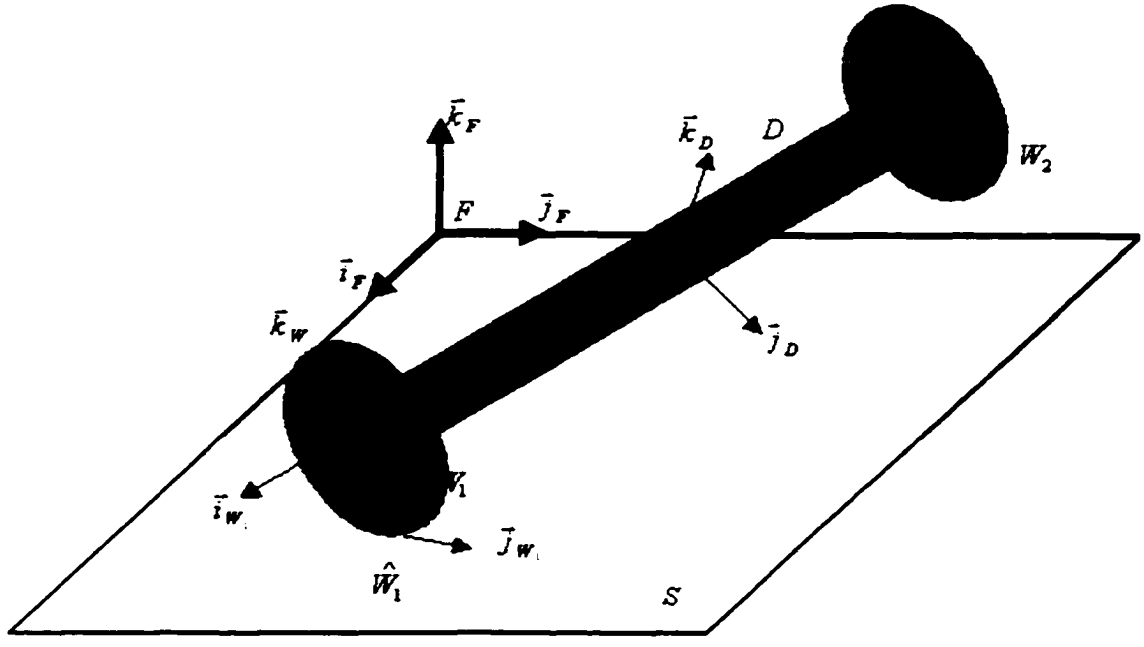

Figure 3.3 Dumbbell Coordinate Axis in Contact Motion

The angular velocity of W_1 is

$$^F\vec{w}^{W_1} = u_7\vec{i}_D + u_2\vec{j}_D + u_3\vec{k}_D \tag{3.79}$$

Let A be a reference frame in which $\vec{i}_{W_1}, \vec{j}_{W_1}, \vec{k}_{W_1}$ are fixed, then the angular velocity of A in F is

$$^F\vec{w}^A = u_2\vec{j}_D + u_3\vec{k}_D \tag{3.80}$$

The angular acceleration of W_1 is

$$\begin{aligned} ^F\vec{a}^{W_1} &= \dot{u}_7\vec{i}_D + \dot{u}_2\vec{j}_D + \dot{u}_3\vec{k}_D + {}^F\vec{w}^A \times {}^A\vec{w}^{W_1} \\ &= \dot{u}_7\vec{i}_D + \dot{u}_2\vec{j}_D + \dot{u}_3\vec{k}_D + (u_2\vec{j}_D + u_3\vec{k}_D)\times(u_7\vec{i}_D) \\ &= \dot{u}_7\vec{i}_D + (\dot{u}_2 + u_3u_7)\vec{j}_D + (\dot{u}_3 - u_2u_7)\vec{k}_D \end{aligned} \tag{3.81}$$

The contact point velocity is then

$$
\begin{aligned}
{}^F\vec{V}^{\hat{W}_1} &= {}^F\vec{V}^{W_1^*} + {}^F\vec{w}^{W_1} \times (-R\vec{k}_{W_1}) = {}^F\vec{V}^{W_1^*} + {}^F\vec{w}^{W_1} \times (-R\vec{k}_{W_1}) \\
&= {}^F\vec{V}^{W_1^*} - R\left(u_7\vec{i}_D + u_2\vec{j}_D + u_3\vec{k}_D\right) \times (s\gamma\vec{j}_D + c\gamma\vec{k}_D) \\
&= {}^F\vec{V}^{W_1^*} - R\left((c\gamma u_2 - s\gamma u_3)\vec{i}_D - u_7 c\gamma\vec{j}_D + u_7 s\gamma\vec{k}_D\right)
\end{aligned}
\tag{3.82}
$$

If the wheel W_2 comes in contact with the surface S at any point $\hat{W}_2$, similar equations given below are obtained.

$$
{}^F\vec{w}^{W_2} = u_8\vec{i}_D + u_2\vec{j}_D + u_3\vec{k}_D \tag{3.83}
$$

$$
{}^F\vec{a}^{W_2} = \dot{u}_8\vec{i}_D + (\dot{u}_2 + u_3u_8)\vec{j}_D + (\dot{u}_3 - u_2u_8)\vec{k}_D \tag{3.84}
$$

$$
{}^F\vec{V}^{\hat{W}_2} = {}^F\vec{V}^{W_2^*} - R\left((c\gamma u_2 - s\gamma u_3)\vec{i}_D - u_8 c\gamma\vec{j}_D + u_8 s\gamma\vec{k}_D\right) \tag{3.85}
$$

Equation (3.57) is employed to find inertia torque terms. Thus,

$$
\vec{T}^{W_1} = -I_1^{W_1}\dot{u}_7\vec{i}_D - (I_2^{W_1}\dot{u}_2 + I_1^{W_1}u_3u_7)\vec{j}_D - (I_2^{W_1}\dot{u}_3 - I_1^{W_1}u_2u_7)\vec{k}_D \tag{3.86}
$$

$$
\vec{T}^{W_2} = -I_1^{W_2}\dot{u}_8\vec{i}_D - (I_2^{W_2}\dot{u}_2 + I_1^{W_2}u_3u_8)\vec{j}_D - (I_2^{W_2}\dot{u}_3 - I_1^{W_2}u_2u_8)\vec{k}_D \tag{3.87}
$$

Forces and torques applied at D^* are

$$
\begin{aligned}
\vec{F}^{D^*} &= F_1\vec{i}_D + F_2\vec{j}_D + F_3\vec{k}_D - m_D g\vec{k}_F \\
\vec{M}^{D^*} &= M_1\vec{i}_D + M_2\vec{j}_D + M_3\vec{k}_D
\end{aligned}
\tag{3.88}
$$

The effect of the reaction forces from the surface can be reflected to the gravitational centers of the wheels to give

$$
\begin{aligned}
\vec{F}^{W_1^*} &= F_{r1}\vec{i}_{W_1} + F_{r2}\vec{j}_{W_1} + F_{r3}\vec{k}_{W_1} - m_{W_1} g k_F \\
&= (F_{r1} + m_{W_1} g s\beta)\vec{i}_D + (F_{r2}c\gamma + F_{r3}s\gamma - m_{W_1} g c\beta s\gamma)\vec{j}_D \\
&\quad + (-F_{r2}s\gamma + F_{r3}c\gamma - m_{W_1} g c\beta c\gamma)\vec{k}_D
\end{aligned}
\tag{3.89}
$$

$$
\vec{M}^{W_1^*} = R(F_{r2}\vec{i}_{W_1} - F_{r1}\vec{j}_{W_1}) = R(F_{r2}\vec{i}_D - F_{r1}c\gamma\vec{j}_D + F_{r1}s\gamma\vec{k}_D) \tag{3.90}
$$

$$\begin{aligned}\vec{F}^{W_2^*} &= F_{r4}\vec{i}_{W_1} + F_{r5}\vec{j}_{W_1} + F_{r6}\vec{k}_{W_1} - m_{W_2}gk_F \\ &= (F_{r4} + m_{W_2}gs\beta)\vec{i}_D + (F_{r5}c\gamma + F_{r6}s\gamma - m_{W_2}gc\beta s\gamma)\vec{j}_D \\ &\quad + (-F_{r5}s\gamma + F_{r6}c\gamma - m_{W_2}gc\beta c\gamma)\vec{k}_D\end{aligned} \tag{3.91}$$

$$\vec{M}^{W_2^*} = R(F_{r4}\vec{i}_{W_1} - F_{r5}\vec{j}_{W_1}) = R(F_{r5}\vec{i}_D - F_{r4}c\gamma\vec{j}_D + F_{r4}s\gamma\vec{k}_D) \tag{3.92}$$

The generalized inertia and active forces are then

$$F_{gi}^* = {}^F\vec{w}_{u_i}^D \cdot \vec{T}^{D^*} + {}^F\vec{V}_{u_i}^{D^*} \cdot \vec{R}^{D^*} + {}^F\vec{w}_{u_i}^{W_1} \cdot \vec{T}^{W_1^*} + {}^F\vec{V}_{u_i}^{W_1^*} \cdot \vec{R}^{W_1^*} + {}^F\vec{w}_{u_i}^{W_2} \cdot \vec{T}^{W_2^*} + {}^F\vec{V}_{u_i}^{W_2^*} \cdot \vec{R}^{W_2^*} \tag{3.93}$$

$$F_{gi} = \vec{F}^{D^*} \cdot {}^F\vec{V}_{u_i}^{D^*} + \vec{M}^{D^*} \cdot {}^F\vec{w}_{u_i}^{D} + \vec{F}^{W_1^*} \cdot {}^F\vec{V}_{u_i}^{W_1^*} + \vec{M}^{W_1^*} \cdot {}^F\vec{w}_{u_i}^{W_1} + \vec{F}^{W_2^*} \cdot {}^F\vec{V}_{u_i}^{W_2^*} + \vec{M}^{W_2^*} \cdot {}^F\vec{w}_{u_i}^{W_2} \tag{3.94}$$

Kane's equations of motion are given by equation (3.36), and they are

$$I_1^D\dot{u}_1 - M_1 = 0 \tag{3.95}$$

$$\begin{aligned}&I_2\dot{u}_2 - \left(I^D + (m_{W_1} + m_{W_2})\frac{L^2}{4}\right)u_1u_3 + I_1^{W_1}u_7u_3 + I_1^{W_2}u_8u_3 - M_2 \\ &\quad + \frac{L}{2}\left((-F_{r2} + F_{r5})s\gamma + (F_{r3} - F_{r6})c\gamma - (m_{W_1} + m_{W_2})gc\beta c\gamma\right) + (F_{r1} + F_{r4})Rc\gamma = 0\end{aligned} \tag{3.96}$$

$$\begin{aligned}&I_2\dot{u}_3 + \left(I^D + (m_{W_1} + m_{W_2})\frac{L^2}{4}\right)u_1u_2 - I_1^{W_1}u_7u_2 - I_1^{W_2}u_8u_2 - M_3 \\ &\quad - \frac{L}{2}\left((F_{r2} - F_{r5})c\gamma + (F_{r3} - F_{r6})s\gamma - (m_{W_1} + m_{W_2})gc\beta s\gamma\right) - (F_{r1} + F_{r4})Rs\gamma = 0\end{aligned} \tag{3.97}$$

$$m\dot{u}_4 - F_1 - (F_{r1} + F_{r4})cac\beta + (F_{r2} + F_{r5})sa - (F_{r3} + F_{r6})cas\beta = 0 \tag{3.98}$$

$$m\dot{u}_5 - F_2 - (F_{r1} + F_{r4})sac\beta - (F_{r2} + F_{r5})ca - (F_{r3} + F_{r6})sas\beta = 0 \tag{3.99}$$

$$m\dot{u}_6 - F_3 + (F_{r1} + F_{r4})s\beta - (F_{r3} + F_{r6})c\beta + mg = 0 \tag{3.100}$$

$$I_1^{W_1}\dot{u}_7 - F_{r2}R = 0 \tag{3.101}$$

$$I_1^{W_2}\dot{u}_8 - F_{r5}R = 0 \tag{3.102}$$

where

$$I_2 = \frac{1}{4}m_D r^2 + \frac{1}{4}(m_{W_1} + m_{W_2})R^2 + \frac{1}{12}m_D L^2 + (m_{W_1} + m_{W_2})\frac{L^2}{4} \tag{3.103}$$

When the wheels W_1 and W_2 roll on the surface S without slipping,

$${}^F\vec{V}^{\hat{W}_1} = {}^F\vec{V}^{W_1^*} - R\left((c\gamma u_2 - s\gamma u_3)\vec{i}_D - u_7 c\gamma \vec{j}_D + u_7 s\gamma \vec{k}_D\right) = 0 \tag{3.104}$$

$$\left({}^F R^D\right)^T \begin{bmatrix} u_4 \\ u_5 \\ u_6 \end{bmatrix} - \begin{bmatrix} R(c\gamma u_2 - s\gamma u_3) \\ -Ru_7 c\gamma + \frac{L}{2}u_3 \\ Ru_7 s\gamma - \frac{L}{2}u_2 \end{bmatrix} = 0 \tag{3.105}$$

$${}^F\vec{V}^{\hat{W}_2} = {}^F\vec{V}^{W_2^*} - R\left((c\gamma u_2 - s\gamma u_3)\vec{i}_D - u_8 c\gamma \vec{j}_D + u_8 s\gamma \vec{k}_D\right) = 0 \tag{3.106}$$

which can also be written in the same form

$$\left({}^F R^D\right)^T \begin{bmatrix} u_4 \\ u_5 \\ u_6 \end{bmatrix} - \begin{bmatrix} R(c\gamma u_2 - s\gamma u_3) \\ -Ru_8 c\gamma - \frac{L}{2}u_3 \\ Ru_8 s\gamma + \frac{L}{2}u_2 \end{bmatrix} = 0 \tag{3.107}$$

where $\left({}^F R^D\right)^T$ is the transpose of the rotation matrix ${}^F R^D$.

Although equation (3.104) is used for simulation of the system dynamics in the case of rolling without slip, this approach is not physically correct. The correct formulation must ensure conservation of total energy of the system.

Equations (3.105) and (3.107) together imply the following non-holonomic constraints

$$\begin{aligned} u_2 &= \frac{R}{L}(u_7 - u_8)s\gamma \\ u_3 &= \frac{R}{L}(u_7 - u_8)c\gamma \end{aligned} \tag{3.108}$$

The time derivative of these equations give

$$\begin{aligned} \dot{u}_2 &= \frac{R}{L}\left((\dot{u}_7 - \dot{u}_8)s\gamma + (u_7 - u_8)u_1 c\gamma + (u_7 - u_8)^2 \frac{Rs\beta c\gamma}{Lc\beta} \right) \\ \dot{u}_3 &= \frac{R}{L}\left((\dot{u}_7 - \dot{u}_8)c\gamma - (u_7 - u_8)u_1 s\gamma - (u_7 - u_8)^2 \frac{Rs\beta s\gamma}{Lc\beta} \right) \end{aligned} \tag{3.109}$$

where equation (3.44) was used to replace $\dot{\gamma}$.

Then,

$${}^F R^D \begin{bmatrix} u_4 \\ u_5 \\ u_6 \end{bmatrix} = \begin{bmatrix} R(c\gamma u_2 - s\gamma u_3) \\ -Ru_7 c\gamma + \frac{L}{2}u_3 \\ Ru_7 s\gamma - \frac{L}{2}u_2 \end{bmatrix} = \begin{bmatrix} 0 \\ -\frac{R}{2}(u_7 + u_8)c\gamma \\ \frac{R}{2}(u_7 + u_8)s\gamma \end{bmatrix} \tag{3.110}$$

which implies the non-holonomic constraints

$$\begin{aligned} u_4 &= \frac{R}{2}(u_7 + u_8)sa \\ u_5 &= -\frac{R}{2}(u_7 + u_8)ca \\ u_6 &= 0 \end{aligned} \tag{3.111}$$

By differentiating these equations,

$$\begin{aligned} \dot{u}_4 &= \frac{R}{2}\left((\dot{u}_7 + \dot{u}_8)sa + (u_7^2 - u_8^2)\frac{Rca}{Lc\beta} \right) \\ \dot{u}_5 &= -\frac{R}{2}\left((\dot{u}_7 + \dot{u}_8)ca - (u_7^2 - u_8^2)\frac{Rsa}{Lc\beta} \right) \\ \dot{u}_6 &= 0 \end{aligned} \tag{3.112}$$

where equation (3.44) was used again to replace $\dot{a}$.

Note that the generalized velocities $u_2, u_3, u_4, u_5,$ and u_6 can all be expressed in terms of u_7 and u_8. This means the system has three degree-of-freedom when the wheels W_1 and W_2 roll on the surface S without slipping. Thus, the velocity of every point of the dumbbell can be expressed in terms of the generalized velocities $u_1, u_7,$ and u_8. Therefore, system dynamics can be expressed by equations (3.95), (3.101), and (3.102). The system dynamics are determined if the reaction forces F_{r2} and F_{r5} are identified. These forces are solved from the remaining equations, equations (3.96) through (3.100). Next, the non-holonomic constraints are employed in these equations. This is done by replacing $\dot{u}_2, \dot{u}_3, \dot{u}_4, \dot{u}_5,$ and $\dot{u}_6$ with the constraint equations (3.109) and (3.112). The calculations involved in process will not be shown here. The resulting equations are

$$
\begin{aligned}
&I_1^D \dot{u}_1 = M_1 \\
&c_6 \dot{u}_7 = (c_1 s\gamma + c_2 c\gamma)(I_1^{W_1} + 2c_5) + (I_1^{W_1} + 2c_4)c_3 \\
&c_6 \dot{u}_8 = -(c_1 s\gamma + c_2 c\gamma)(I_1^{W_2} + 2c_5) + (I_1^{W_2} + 2c_4)c_3
\end{aligned}
\tag{3.113}
$$

where

$$
\begin{aligned}
c_1 &= -\left(I^D + (m_{W_1} + m_{W_2})\frac{L^2}{4} \right) u_1 u_3 + I_1^{W_1} u_7 u_3 + I_1^{W_2} u_8 u_3 - M_2 \\
c_2 &= \left(I^D + (m_{W_1} + m_{W_2})\frac{L^2}{4} \right) u_1 u_2 - I_1^{W_1} u_7 u_2 - I_1^{W_2} u_8 u_2 - M_3 \\
c_3 &= \frac{(-F_2 ca + F_1 sa)R}{2} \\
c_4 &= -\frac{I_2 R^2}{L^2} \\
c_5 &= \frac{mR^2}{4} \\
c_6 &= I_1^{W_1} I_1^{W_2} + (I_1^{W_1} + I_1^{W_2})(c_4 + c_5) + 2c_4 c_5
\end{aligned}
$$

Once these equations are integrated, the generalized velocities $u_1, u_7,$ and u_8 will be obtained. Since, the generalized velocities $u_2, u_3, u_4, u_5,$ and u_6 are all functions of u_7 and u_8, they are easy to calculate using equations (3.108) and (3.111).

Integration of equation (3.16) and (3.44) will give the position and the orientation of the dumbbell. Finally, integrating $u_7,$ and u_8 results in γ_1 and γ_2.

3.3 Two degree-of-freedom manipulator

This section will develop kinematics of a two degree-of-freedom manipulator as shown in Figure 3.4. The objective is the design of a haptic display in which a closed kinematic relationship between the robot end effector and the end effector of the virtual manipulator is enforced.

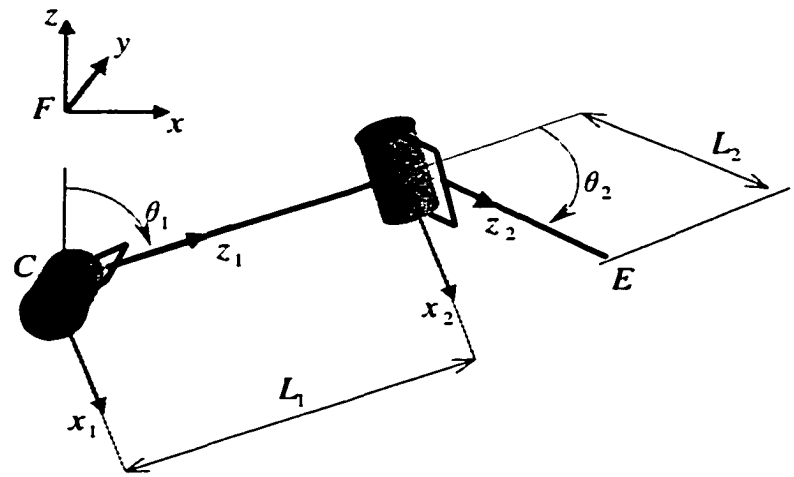

Figure 3.4 Two Degree-of-Freedom Manipulator

$F(x, y, z)$ is the fixed coordinate frame. The rotation θ_1 is described in the frame $C(x_1, y_1, z_1)$, and the rotation θ_2 is described in the frame $D(x_2, y_2, z_2)$.

The position of the virtual manipulator end effector end point, E, with respect to the fixed coordinate frame, F, is given by

$$^F P^E = x_E \vec{i} + y_E \vec{j} + z_E \vec{k} \tag{3.114}$$

where

$$\begin{aligned} x_E &= s\theta_1(L_1 + L_2 c\theta_2) + x_C \\ y_E &= -L_2 s\theta_2 + y_C \\ z_E &= c\theta_1(L_1 + L_2 c\theta_2) + z_C \end{aligned} \tag{3.115}$$

where $C(x_C, y_C, z_C)$ describes the position of the base with respect to the fixed reference frame.

Equations (3.115) form a taurus shape. The taurus function can be expressed by the points defined by

$$T = x_E \vec{i} + y_E \vec{j} + z_E \vec{k} \tag{3.116}$$

Then,

$$dT = \frac{\partial T}{\partial \theta_1} d\theta_1 + \frac{\partial T}{\partial \theta_2} d\theta_2 \tag{3.117}$$

where $\frac{\partial T}{\partial \theta_1}$ and $\frac{\partial T}{\partial \theta_2}$ define the unit vectors tangent to θ_1 and θ_2 curves.

The unit vectors tangent to θ_1 and θ_2 curves are then

$$\vec{i}_2 = c\theta_1 \vec{i} - s\theta_1 \vec{k} \tag{3.118}$$

$$\vec{j}_2 = s\theta_1 s\theta_2 \vec{i} + c\theta_2 \vec{j} + c\theta_1 s\theta_2 \vec{k} \tag{3.119}$$

The unit vector normal to the surface that θ_1 and θ_2 define is given by

$$\vec{k}_2 = \vec{i}_2 \times \vec{j}_2 = s\theta_1 c\theta_2 \vec{i} - s\theta_2 \vec{j} + c\theta_1 c\theta_2 \vec{k} \tag{3.120}$$

These three unit vectors define the rotation matrix R_v such that

$$\begin{bmatrix} \vec{i} \\ \vec{j} \\ \vec{k} \end{bmatrix} = R_v \begin{bmatrix} \vec{i}_2 \\ \vec{j}_2 \\ \vec{z}_2 \end{bmatrix} = \begin{bmatrix} c\theta_1 & s\theta_1 s\theta_2 & s\theta_1 c\theta_2 \\ 0 & c\theta_2 & -s\theta_2 \\ -s\theta_1 & c\theta_1 s\theta_2 & c\theta_1 c\theta_2 \end{bmatrix} \begin{bmatrix} \vec{i}_2 \\ \vec{j}_2 \\ \vec{z}_2 \end{bmatrix} \tag{3.121}$$

The virtual manipulator end effector angular velocity is given by

$${}^F\vec{w}^D = \dot{\theta}_2 \vec{i}_2 + \dot{\theta}_1 \vec{j} = \dot{\theta}_2 \vec{i}_2 + \dot{\theta}_1 c\theta_2 \vec{j}_2 - \dot{\theta}_2 s\theta_2 \vec{k}_2 = w_x \vec{i}_2 + w_y \vec{j}_2 + w_z \vec{k}_2 \tag{3.122}$$

where

$$w_x = \dot{\theta}_2, \; w_y = \dot{\theta}_1 c\theta_2, \; w_z = -\dot{\theta}_2 s\theta_2 \tag{3.123}$$

The Cartesian velocity of point E is obtained by the time differential of the position vector as

$${}^F\vec{V}^E = \dot{x}_E \vec{i} + \dot{y}_E \vec{j} + \dot{z}_E \vec{k} = (L_1 + L_2 c\theta_2)\dot{\theta}_1 \vec{i}_2 - L_2 \dot{\theta}_2 \vec{j}_2 = v_x \vec{i}_2 + v_y \vec{j}_2 + v_z \vec{k}_2 \tag{3.124}$$

where

$$v_x = (L_1 + L_2 c\theta_2)\dot{\theta}_1, \; v_y = -L_2 \dot{\theta}_2, \; v_z = 0 \tag{3.125}$$

A Jacobian matrix, J_v, can now be defined to express a relationship between the total velocity vector of point and the joint angular velocity vector E written in the end effector frame. Thus,

$${}^D\dot{x}_v = J_v \dot{\theta} \tag{3.126}$$

where

$${}^D\dot{x}_v = \begin{bmatrix} v_x & v_y & v_z & w_x & w_y & w_z \end{bmatrix}^T \tag{3.127}$$

$$\dot{\theta} = \begin{bmatrix} \dot{\theta}_1 & \dot{\theta}_2 \end{bmatrix}^T \tag{3.128}$$

and

$$J_v = \begin{bmatrix} L_1 + L_2 c\theta_2 & 0 & 0 & 0 & c\theta_2 & -s\theta_2 \\ 0 & -L_2 & 0 & 1 & 0 & 0 \end{bmatrix}^T \tag{3.129}$$

The following analysis is aimed at reconfiguring the virtual manipulator to achieve closest distance from point E to an arbitrary point in space. The results will be later used to help design the haptic interactions.

The unit vector along the line between any point in space, $R(x_r, y_r, z_r)$, and an arbitrary point on the surface that θ_1 and θ_2 define can be expressed by

$$\vec{u} = \frac{(x_E - x_r)\vec{i} + (y_E - y_r)\vec{j} + (z_E - z_r)\vec{k}}{\sqrt{(x_E - x_r)^2 + (y_E - y_r)^2 + (z_E - z_r)^2}} \tag{3.130}$$

The find a point on the surface that θ_1 and θ_2 define that has the shortest distance to R, the condition to realize is

$$\vec{u} \times \vec{k}_v = 0 \tag{3.131}$$

which leads to

$$(y_C - y_r)c\theta_1 c\theta_2 + (z_C - z_r)s\theta_2 + L_1 c\theta_1 s\theta_2 = 0 \tag{3.132}$$

$$(z_C - z_r)s\theta_1 c\theta_2 - (x_C - x_r)c\theta_1 c\theta_2 = 0 \tag{3.133}$$

$$(x_C - x_r)s\theta_2 + (y_C - y_r)s\theta_1 c\theta_2 + L_1 s\theta_1 s\theta_2 = 0 \tag{3.134}$$

The unique solutions for θ_1 and θ_2 are then found to be

$$\begin{aligned} \theta_1 &= \arctan2(x_r - x_C, z_r - z_C) \\ \theta_2 &= \arctan2((y_C - y_r)c\theta_1, z_r - z_C - L_1 c\theta_1) \end{aligned} \tag{3.135}$$

Thus, the joint angles, $\theta = [\theta_1 \quad \theta_2]^T$, locate the virtual manipulator at a configuration which achieves the closest distance from point E to point R.

Since θ_1 and θ_2 are functions of x_r, y_r and z_r only, it is easy to derive the equation

$$\dot{\theta} = [\dot{\theta}_1 \quad \dot{\theta}_2]^T = J_{vr} \cdot {}^F\dot{x} \tag{3.136}$$

where

$${}^F\dot{x} = [\dot{x}_r \quad \dot{y}_r \quad \dot{z}_r]^T \tag{3.137}$$

The jacobian matrix is derived to be

$$J_{vr} = \begin{bmatrix} J_{vr11} & 0 & J_{vr13} \\ J_{vr21} & J_{vr22} & J_{vr23} \end{bmatrix} \tag{3.138}$$

where the non zero terms are obtained to be

$$J_{vr11} = \frac{z_r - z_C}{(x_r - x_C)^2 + (z_r - z_C)^2} \tag{3.139}$$

$$J_{vr13} = \frac{-(x_r - x_C)}{(x_r - x_C)^2 + (z_r - z_C)^2} \tag{3.140}$$

$$J_{vr21} = \frac{1}{(z_r - z_C - L_1 c\theta_1)^2 + (y_r - y_C)^2 c^2\theta_1} \frac{(y_r - y_C)(z_r - z_C)^2 s\theta_1}{(x_r - x_C)^2 + (z_r - z_C)^2} \tag{3.141}$$

$$J_{vr22} = \frac{-(z_r - z_C - L_1 c\theta_1)c\theta_1}{(z_r - z_C - L_1 c\theta_1)^2 + (y_r - y_C)^2 c^2\theta_1} \tag{3.142}$$

$$J_{vr23} = \frac{y_r - y_C}{(z_r - z_C - L_1 c\theta_1)^2 + (y_r - y_C)^2 c^2\theta_1} \left(c\theta_1 - \frac{(x_r - x_C)(z_r - z_C)s\theta_1}{(x_r - x_C)^2 + (z_r - z_C)^2} \right) \tag{3.143}$$

4. HAPTIC INTERACTIONS

Haptic interactions between a human and the virtual environment are experienced as forces and torques from the haptic interface device using an in-hand the robotic device. The user holds a handle at the end effector of the manipulator, and the user-applied forces and torques are used to create changes in the virtual environment. The dynamic response of the environment is felt by the user as forces and torques which are reflected from the virtual environment to the user hand. The performance of the haptic interaction depends not only on the quality of the virtual environment simulation but also on the dynamics of the interface device with which the user is connected. Stablility, of course, is an essential requirement in haptic display in order to import a sense of realistic immersion. Equally important is that the motion and forces feel natural and are consistent with the expected response.

In this chapter, the focus will be on the implementation of the haptic interactions between the user and the virtual object. The virtual object will be, in the first case, a multibody dynamical system (Dumbbell) and, in the second case, a two-degree of freedom manipulator. Two approaches to simulation will be used to develop the haptic simulations here, the first is an admittance controlled implementation of a multibody dynamical system and the second is an impedance controlled implementation of a two degree-of-freedom virtual manipulator. The admittance control example will be used to show the use of Kane's method for implementing nonlinear nonholonomic constraints. The impedance control example will show the use of a haptic device for simulating specific kinematic force relationships in the virtual environment.

4.1 Multibody haptic interface

The dumbbell is oriented in such a way that the axle is coincident with the end effector of the robot manipulator as shown in Figure 4.1. In order to interact with the virtual dynamical system, the user grasps the end effector at the handle or the axle of the dumbbell. The forces and torques applied at the end effector by the user are measured via a force transducer and used as the input to the numerical dynamic simulation of the dumbell. These forces and torques are exerted on the dumbell in the computer model to generate desired position and orientation of the dumbbell, which is then defined to be coincident with the robot end effector handle. A computed torque controller is used to calculate desired joint angles, q_d. The error that the controller drives to zero is

$$e_v = q_d - q \tag{4.1}$$

The desired velocity of the robot end effector and the dumbbell are given in equations (3.4) and (3.19). Thus,

$$^R\dot{x}_{rd} = J_r\dot{q}_d = J_v u \tag{4.2}$$

Then the desired angular velocities of robot joints are calculated by

$$\dot{q}_d = J_r^{-1}\cdot{}^R\dot{x}_{rd} \tag{4.3}$$

Equation (4.2) is used to derive

$$^R\ddot{x}_{rd} = \dot{J}_r\dot{q}_d + J_r\bar{q}_d = \dot{J}_v u + J_v\dot{u} \tag{4.4}$$

The desired joint accelerations are then

$$\ddot{q}_d = J_r^{-1}(^R\ddot{x}_{rd} - \dot{J}_r\dot{q}_d) \tag{4.5}$$

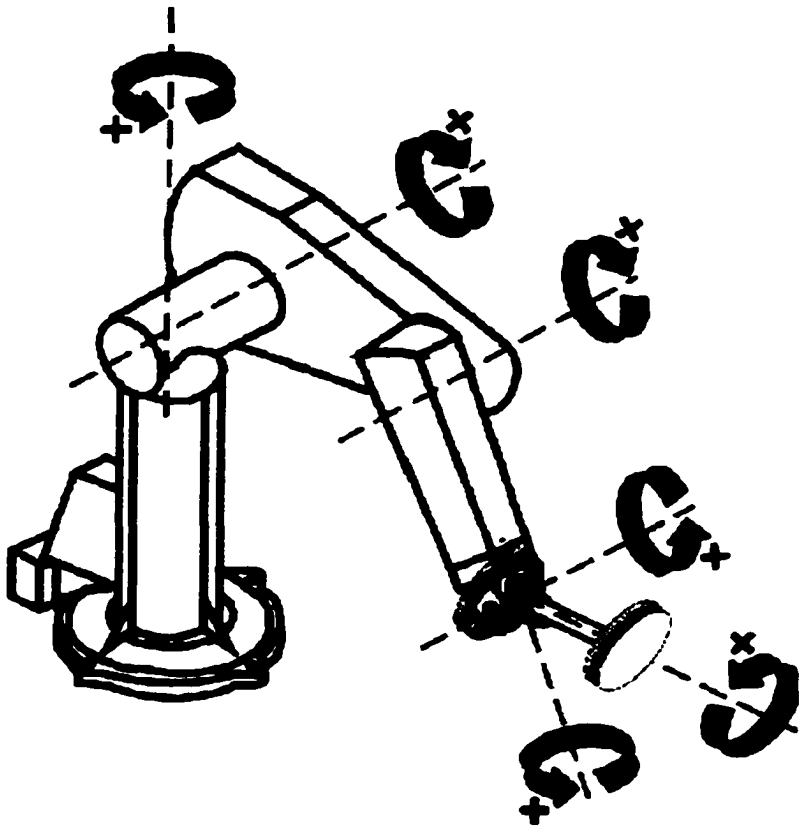

Figure 4.1 PUMA 560 Schematic and Dumbbell

The dynamics in the joint space is given by equation (3.5) as

$$H(q)\ddot{q} + C(q,\dot{q})\dot{q} + f_r\dot{q} + g(q) = \tau - J_r^T \cdot {}^R F_r \tag{4.6}$$

A computed torque with outer loop PD control scheme is used

$$\tau = H(\ddot{\theta}_d + K_p e_\theta + K_v \dot{e}_\theta) + \hat{C} + \hat{f}_r \dot{q} + \hat{g} + J_r^T \cdot {}^R F_r \tag{4.7}$$

where the gravity and friction compensation terms are $\hat{g}(q)$ and $\hat{f}_r$. It is assumed that $g(q) \approx \hat{g}(q)$ and $f_r = \hat{f}_r$.

Equation (4.7) is substituted into the robot equation (4.6). Noting that the inertia matrix $H(q)$ is a symmetric positive definite matrix, the error dynamics can be seen as

$$\ddot{e} + K_v \dot{e} + K_p e = 0 \tag{4.8}$$

which implies that the system is stable as long as K_p and K_v are positive definite.

4.2 Virtual Manipulator Optimal position control

This section presents the development of an approach in which a six degree-of-freedom conventional industrial manipulator, PUMA 560 robotic manipulator, is used as the interface device. The interface provides the user with haptic feedback, from a virtual mechanism with a specific kinematic configuration. A virtual manipulator concept is developed that couples the actual robot kinematics with the constraints of the simulated manipulator. This is shown schematically in Figure 4.2, where a virtual manipulator configuration is developed with kinematics that constrains the motion in a specific manner. Combining the PUMA 560 kinematics and the virtual manipulator kinematics results in a controller that moves as if the robot motions are constrained by the virtual manipulator. As in the case of the dumbbell simulator, the user grasps the PUMA 560 end effector that is coincident with the virtual simulator handle. The position and velocity error terms are used to design a virtual manipulator optimal position controller which constraints the robot end effector motions in all directions that are orthogonal to the allowable motions of the virtual manipulator.

Let us assume that the two degree-of-freedom virtual manipulator described in section 3.3 is located inside the reachable workspace of the robot manipulator. Given an arbitrary position of the PUMA 560 robot manipulator end effector, the shortest distance from $R(x_r, y_r, z_r)$ to the surface of the manifold describing possible virtual manipulator positions can be calculated by using equations (3.115) and equation (3.135). The goal of the optimal position of the virtual manipulator controller is to drive the robot end effector to this desired position.

The surface formed by the motions of the virtual manipulator end effector end point, E, is shown in Figure 4.3. The objective is to have the robot end effector constraint to move on this Taurus shape.

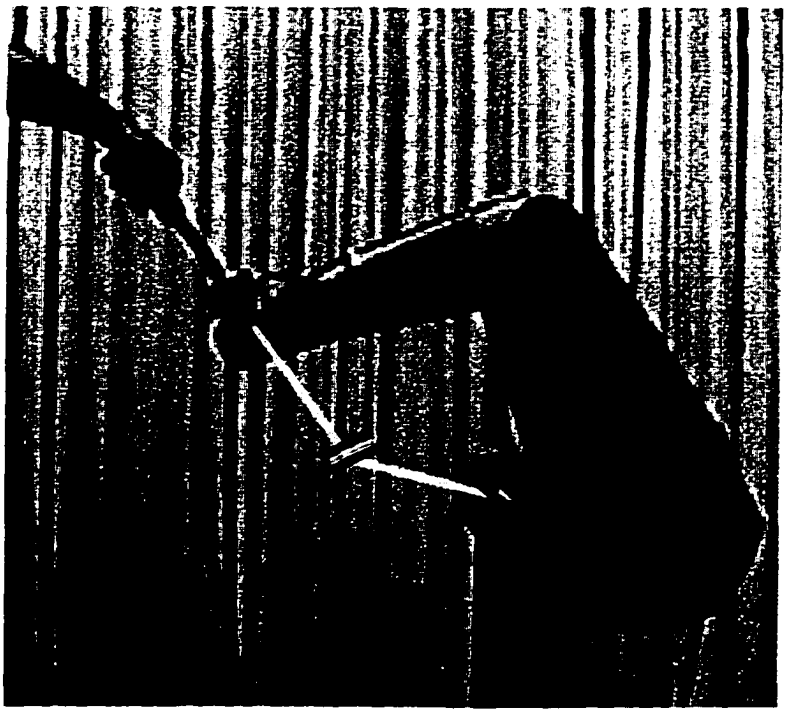

Figure 4.2 Coupled Motion

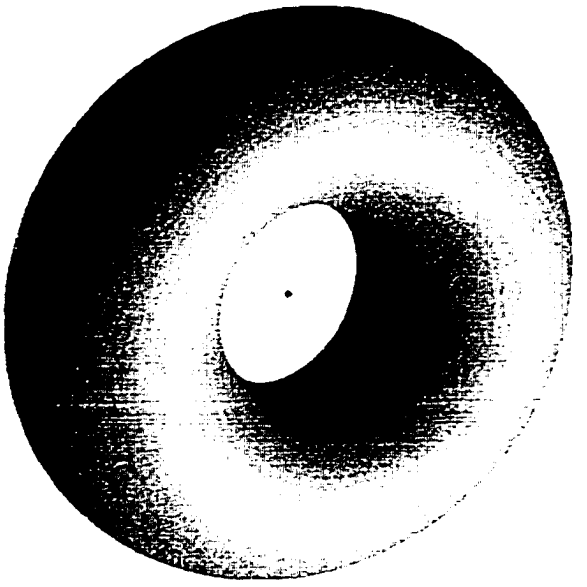

Figure 4.3 Taurus Shape

The total velocity of the robot manipulator end effector is given in equation (3.4) by

$$^{R}\dot{x}_r = J_r\dot{q} \tag{4.9}$$

which can also be expressed in the virtual manipulator end effector frame by

$$^{D}\dot{x}_r = \begin{bmatrix} R_v^T & 0 \\ 0 & R_v^T \end{bmatrix} \cdot {}^{F}\dot{x}_r = \begin{bmatrix} R_v^T & 0 \\ 0 & R_v^T \end{bmatrix} \begin{bmatrix} R_r & 0 \\ 0 & R_r \end{bmatrix} \cdot {}^{R}\dot{x}_r \tag{4.10}$$

where the rotation matrix, R_r, is given in equation (3.3) and it describes the robot end effector frame with respect to the base frame. Similarly, R_v, is given in equation (3.117) and it describes the virtual manipulator end effector frame with respect to a fixed reference frame. In this work, the virtual manipulator fixed reference frame is assumed to coincide with the base frame of the robotic manipulator, although it is possible that the virtual manipulator base moves relative to the base of the haptic display manipulator.

Note that the total velocity of the virtual manipulator end effector end point was defined in equation (3.124) as

$$^{D}\dot{x}_{v} = J_{v}\dot{\theta} \tag{4.11}$$

and the joint angular velocities were given in equation (3.134) by

$$\dot{\theta} = J_{vr}\cdot^{F}\dot{x}_{r} \tag{4.12}$$

where $^{F}\dot{x}_{r}$ is now the robot end effector total Cartesian velocity written in the base frame of the robotic manipulator.

By substituting equation (4.12) into equation (4.11), the desired virtual manipulator velocity is obtained and given by

$$^{D}\dot{x}_{vd} = J_{v}\dot{\theta} = J_{v}\left[J_{vr} \quad 0\right]^{F}\dot{x}_{r} \tag{4.13}$$

Note that the robotic manipulator end effector angular velocity terms have no determinant effect on the virtual manipulator velocities. This is because the optimal position of the virtual manipulator is a function of the position of the haptic display end effector, and not the orientation. The virtual manipulator joint angular velocity, $\dot{\theta}$, is calculated by differentiating this position relationship. Thus, the virtual manipulator desired velocity $,^{D}\dot{x}_{vd} = J_{v}\dot{\theta}$, is not a function of the haptic display robot end effector angular velocity. Equation (4.13) can also be written as

$$^{D}\dot{x}_{vd} = J_{v}\left[J_{vr} \quad 0\right]\begin{bmatrix} R_{v} & 0 \\ 0 & R_{v} \end{bmatrix}\cdot^{D}\dot{x}_{r} \tag{4.14}$$

Here, R_{v} is again the rotation matrix to describe the virtual manipulator end effector frame with respect to a fixed reference frame.

If the position error is described by

$$^{D}e = {}^{D}x_{vd} - {}^{D}x_{r} \tag{4.15}$$

Then,

$$^{D}\dot{e} = {}^{D}\dot{x}_{vd} - {}^{D}\dot{x}_{r} = (J_{v}\begin{bmatrix} J_{vr} & 0 \end{bmatrix}\begin{bmatrix} R_{v} & 0 \\ 0 & R_{v} \end{bmatrix} - I) \cdot {}^{D}\dot{x}_{r} = J_{e} \cdot {}^{D}\dot{x}_{r} \tag{4.16}$$

where

$$J_{e} = J_{v}\begin{bmatrix} J_{vr} & 0 \end{bmatrix}\begin{bmatrix} R_{v} & 0 \\ 0 & R_{v} \end{bmatrix} - I \tag{4.17}$$

When the user grasps the virtual manipulator and applies external forces/torques, $^{D}F_{v}$, to the end effector a set of joint torques, τ_{v}, for the virtual manipulator are calculated using the relationship

$$\tau_{v} = J_{v}^{T} \cdot {}^{D}F_{v} \tag{4.18}$$

Suppose that the control system is used to apply a set of external forces and torques modeled by a massless spring-damper system such that

$$^{D}F_{v} = K_{p} \cdot {}^{D}e + K_{d} \cdot {}^{D}\dot{e} \tag{4.19}$$

and the user applied forces and torques at the handle attached to the robot end effector are assumed to be the same. Then,

$$^{R}F_{r} = {}^{R}F_{v} = \begin{bmatrix} R_{r}^{T} & 0 \\ 0 & R_{r}^{T} \end{bmatrix}\begin{bmatrix} R_{v} & 0 \\ 0 & R_{v} \end{bmatrix}(K_{p} \cdot {}^{D}e + K_{d} \cdot {}^{D}\dot{e}) \tag{4.20}$$

where K_{p} is a positive definite matrix of spring constants and K_{d} is a positive definite matrix of damping coefficients.

The controller chosen is chosen as

$$\tau = J_r^T \cdot {}^R F_{vf} + \hat{f}_r \dot{q} + \hat{g}(q) + J_r^T \cdot {}^R F_r \tag{4.21}$$

where

$${}^R F_{vf} = \begin{bmatrix} R_r^T & 0 \\ 0 & R_r^T \end{bmatrix} \begin{bmatrix} R_v & 0 \\ 0 & R_v \end{bmatrix} S(K_p \cdot {}^D e + K_d \cdot {}^D \dot{e}) \tag{4.22}$$

${}^R F_{vf}$ is a representative of filtered forces and torques applied by the user. S represents a null space filter. The definition of the null space filter, S, and the filtered force, ${}^R F_{vf}$, are developed in the next chapter, where the stability of the system will be studied. Using the filtered control command ensures that the robot motion matches the virtual manipulator motions. Using this filtered control law, the robot will resist components of the user-applied forces and torques that would be constrained by the kinematics of the virtual manipulator. Note that this controller does not require user-applied force and torque measurements. Therefore, a force transducer is not needed to implement this control scheme.

The design and stability of this controller will be studied in the next chapter in detail. A proof of asymptotic stability for the overall system will be presented to satisfy the safety and performance requirements for the use of this approach.

3.3 Shift mechanism

One advantage of the use of impedance based control is the ease with which unilateral constraints can be implemented. These constraints are best implemented using the concepts of virtual walls. Past research exploring the use of virtual walls has been very extensive [1]

[17] [19] [46] [61]. Virtual walls are traditionally created by allowing the motion along a direction until a unilateral constraint is encountered. When the constraint is encountered, the model is modified to include the constraint. Although the haptic display system is stable in free space, the use of unilateral constraints have been shown [17] [19] to generate instability. This undesired phenomenon is partly due to digitizing the controller which presents a time lag between the input motion by the end effector and the output force generation by the virtual wall. Therefore, in the implementation of a virtual wall, this system may gain energy because of the sampled data nature of the haptic display. This energy must be dissipated by the system to guarantee stability.

Research in this area [17] [19] has shown that, for sampled data passivity, there must exist some inherent damping in the haptic display. This requirement limits how stiff a virtual wall can be made. Although increasing the inherent damping of the haptic display results in a sampled-data passive system, it reduces the performance of the haptic interactions. Because of the additional control force necessary to overcome the physical damping, the transparency of the haptic interface device is reduced unless controller terms are added to overcome the damping. The stiffest wall effect can be created if the controller is designed to use position and velocity gains as large as possible without sacrificing the sampled data passivity requirement. An alternative is using faster sample rates to reduce the sampled data nature of the controller.

Because the virtual stiffness is determined by the physical characteristics of the haptic device, the work presented here does not aim at solving this problem. Our motivation is to extend the virtual wall implementation to create complex shapes in the virtual environment.

The objective of this work is to implement a virtual shift mechanism by the use of a PUMA 560 industrial manipulator. The motions of the robot end effector are restricted to form stick shift motion as shown in Figure 4.4. In effect, motion of the virtual mechanism is constrained using impedance walls along the border of the desired pattern.

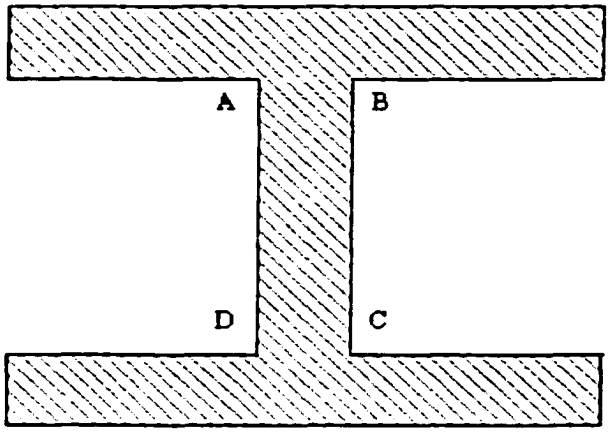

Figure 4.4 Virtual Shift Pattern

When the actual robot end effector is moved along a trajectory that encounters a unilateral constraint, the controller is designed to apply forces to create a stiff wall effect. In Figure 4.4, wall effects are created by the controller when the robot end effector moves outside the shaded area.

One major problem is observed when the end effector is forced to move around sharp corners, which are represented by points A, B, C and D in Figure 4.4. In a sampled data system, it is possible that the end effector switches between two sides of a corner between time samples without noticing a wall. Another problem is that after the penetration, the controller must be able to determine to which side of the corner the wall effect should push

the end effector. Very sharp corners in the virtual constraints can create instability in the vicinity of the corner. One solution to this problem is to use a function that is continuous at the corners.

In order to avoid instability, a continuous analytical representation of the motion constraints becomes an important part of this problem. Although, the search for a mathematical equation to represent rounded corners can lead to several alternatives, a Lame curve [?] is used in this study. The Lame curve is used to create a very good representation of a rounded corner, and can be coupled with the impedance algorithms to effectively implement corners in the constraints.

A Lame curve, $L(a,b)$, is described by

$$\left(\frac{x-x_0}{a}\right)^n+\left(\frac{y-y_0}{b}\right)^n=1 \tag{4.23}$$

Here (x_0, y_0) locates the origin of the Lame curve, and a and b are parameters defining the size of the Lame curve as shown in Figure 4.5, two Lame curves, $L_1(a_1,b_1)$ and $L_2(a_2,b_2)$, are shown. The curve parameter $n = 12$ is used to allow stable operation. Larger n values result in sharper corners, which cause instabilities at the corners. The largest n value for stable operation may be identified experimentally.

Let us assume that the motion is constrained to be outside the Lame curve L_2. Assume also that a penetration to a point $P(x_p, y_p)$ on the Lame curve L_1 occurs. Thus,

$$\left(\frac{x_p-x_0}{a_2}\right)^n+\left(\frac{y_p-y_0}{b_2}\right)^n<1 \tag{4.24}$$

Note also that

$$\frac{a_1}{b_1} = \frac{a_2}{b_2} \tag{4.25}$$

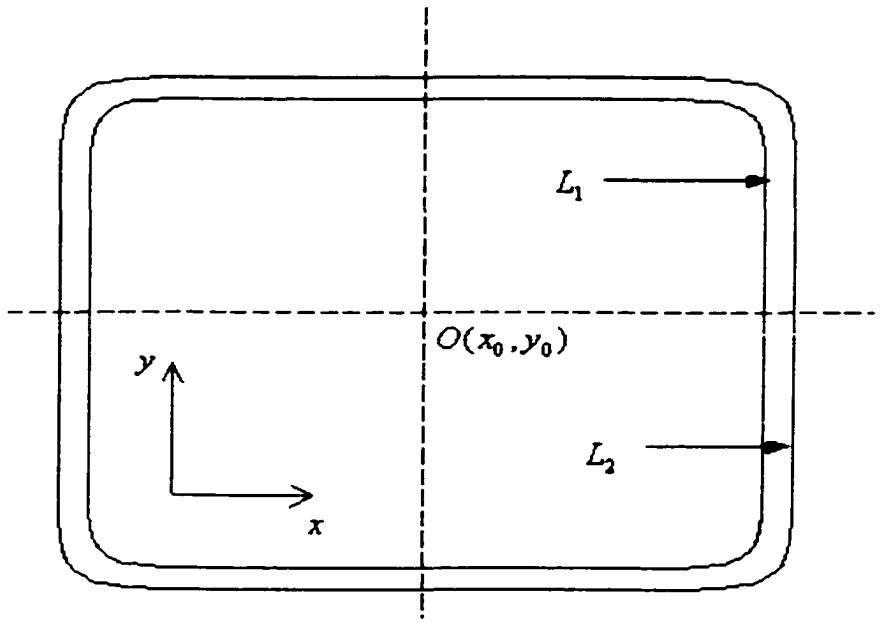

Figure 4.5 Lame Curve

To implement a wall effect, point $P(x_p, y_p)$ should be forced back to a point on the Lame curve L_2. To find the desired position on L_2, the slope at $P(x_p, y_p)$ on the Lame curve L_1 is computed

$$m = \frac{dy}{dx} = -\left(\frac{b_1}{a_1}\right)^n \left(\frac{x_p - x_0}{y_p - y_0}\right)^{n-1} \tag{4.26}$$

Point $P(x_p, y_p)$ is then pushed back to a desired location, (x_{pd}, y_{pd}), on L_2 which has the same slope value. Thus,

$$m = \frac{dy}{dx} = -\left(\frac{b_1}{a_1}\right)^n \left(\frac{x_p - x_0}{y_p - y_0}\right)^{n-1} = -\left(\frac{b_2}{a_2}\right)^n \left(\frac{x_{pd} - x_0}{y_{pd} - y_0}\right)^{n-1} \tag{4.27}$$

Using equation (4.25), this equation reduces to

$$\frac{x_p - x_0}{y_p - y_0} = \frac{x_{pd} - x_0}{y_{pd} - y_0} \tag{4.28}$$

The desired location, $P(x_{pd}, y_{pd})$, is then calculated and given by

$$\begin{aligned} y_{pd} &= y_0 + \frac{a_2 b_2 (y_p - y_0)}{(b_2^n (x_p - x_0)^n + a_2^n (y_p - y_0)^n)^{n^{-1}}} \\ x_{pd} &= x_0 + (y_{pd} - y_0)\frac{x_p - x_0}{y_p - y_0} \end{aligned} \tag{4.29}$$

Now that the algorithm to handle corners is developed, the shift mechanism can be generated using Lame curves. An H pattern shift is created by using two Lame curves as shown in Figure 4.6. This shift mechanism is implemented on the surface of the Taurus descibed in section 4.2 as shown in Figure 4.7.

The robotic manipulator end effector motions are first restricted to trace the surface of the Taurus. The optimal impedance controller described in the previous section is employed to achieve this. Then, the motions are further constrained to a small part of the Taurus to present a shift pattern as shown in Figure 4.6. The robotic manipulator end effector is constrained to move inside the shaded area. The unilateral constraints are not created along a line, but along a curve on a skewed surface. Thus, in this implementation, (θ_2, θ_1) are the Lame constraint parameters, and the algorithm developed above is easily applied.

The overall mechanism constraint can be applied using the virtual manipulator and Lame curves to impose impedance limits on the haptic display robot. These limits guide the motion of the robot end effector along the defined pattern. Thus, the user's hand can push

the manipulator anywhere with the allowable pattern, but will encounter resistance when pushed outside of the allowable motion pattern.

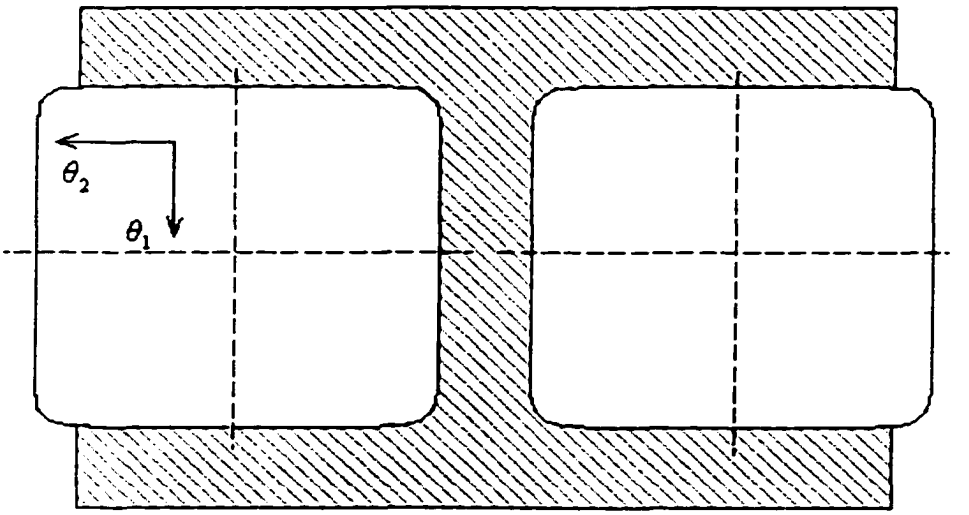

Figure 4.6 Shift Pattern on a Taurus

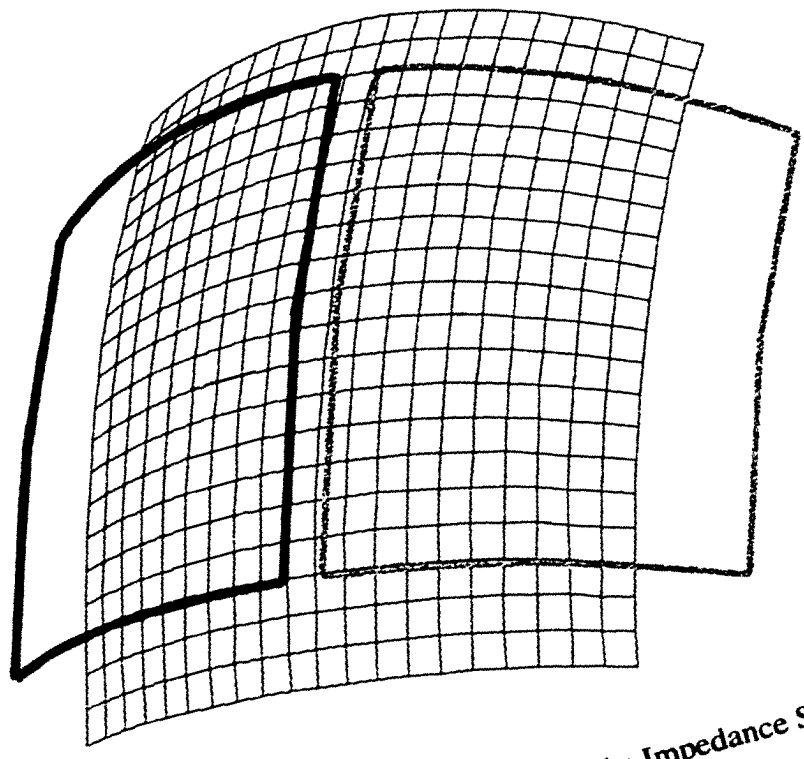

Figure 4.7 H Pattern Constraint Superimposed on the Impedance Surface of the Virtual Manipulator

5. STABILITY AND PROOF

This chapter studies the stability of a robotic manipulator when it is constrained to mimic the behavior of a virtual manipulator. The stability of the overall system will be proven by showing that the position error between the end effector of the haptic display and the virtual manipulator end effector tends towards zero over time.

The user applies forces and torques at a handle attached at the robot end effector in order to interact with or manipulate the virtual manipulator. Using the impedance constraints, the controller is designed to resist applied forces in all directions that are orthogonal to the allowable motions of the virtual manipulator. Thus, the external forces create motions only in directions that move the haptic simulation in directions allowed by the constraints.

5.1 Force generation

When an external force, ${}^{D}F_{v}$, is applied at the end effector of the virtual manipulator from the user's hand, a set of joint torques that resist this motion, τ_{v}, for the virtual manipulator can be computed using the well-known relationship

$$\tau_{v} = J_{v}^{T} \cdot {}^{D}F_{v} \tag{5.1}$$

Here the superscript D is used to denote forces expressed in the end effector coordinate frame of the virtual manipulator. J_{v}^{T} is the transpose of the virtual manipulator Jacobian. It

defines a relationship between the virtual manipulator end effector end point velocity and the virtual manipulator joint angles.

Equation (5.1) shows that any choice for the vector ${}^{D}F_v$ produces a corresponding vector τ_v that is always in the column space of J_v^T. In general, the virtual manipulator Jacobian is not square, because the motion of the end effector is constrained to a subspace defined by the kinematics of the virtual manipulator. The Jacobian J_v^T is therefore an $m \times n$ matrix, where m is the degree-of-freedom of the virtual manipulator and n is the degree-of-freedom of the robotic manipulator or the interface device. Since this study uses a PUMA 560 robot, n is 6. When there are constraints imposed by the virtual manipulator, the maximum degrees-of-freedom of a virtual manipulator is 5, thus $m \prec 6$. Because the Jacobian relationship, $\tau_v = J_v^T \cdot {}^{D}F_v$, is under constrained, there are an infinite number of 6×1 vector ${}^{D}F_v$ combinations that result in a given $m \times 1$ vector of τ_v.

Euation (5.1) has the following general solution

$$ {}^{D}F_v = (J_v^T)^{+} \tau_v + (I - (J_v^T)^{+} J_v^T) y_2 \tag{5.2} $$

where y_2 is any 6×1 vector and $(J_v^T)^{+} = (J_v^{+})^T$ is the transpose of the pseudoinverse [Strang 1980] of the matrix J_v. The pseudoinverse of J_v is

$$ J_v^{+} = (J_v^T J_v)^{-1} J_v^T \tag{5.3} $$

which implies

$$ (J_v^T)^{+} = J_v (J_v^T J_v)^{-T} = J_v (J_v^T J_v)^{-1} \tag{5.4} $$

Using equation (5.1), all vectors ${}^{D}F_v$ can also be expressed by

$$ {}^{D}F_v = (J_v^T)^{+} \cdot J_v^T \cdot {}^{D}F_v + (I - (J_v^T)^{+} \cdot J_v^T) \cdot {}^{D}F_v \tag{5.5} $$

where

$$I-(J_v^T)^+ \cdot J_v^T = I - J_v(J_v^T J_v)^{-1} J_v^T = S \tag{5.6}$$

The 6×6 matrix S is called the projection of ${}^D F_v$ on the null space of J_v. This projection matrix has the following properties [30]

1. Indempotent, $S^2 = S$,
2. Symmetric, $S^T = S$,
3. Positive semi definite (i.e., $v^T S v \geq 0$ for all vectors $v \in \mathrm{R}^n$),
4. Bounded, (i.e., $\|Sv\| \leq \|v\|$ for all vectors $v \in \mathrm{R}^n$),

Now, since $(J_v^T)^+ \cdot J_v^T \cdot {}^D F_v$ is orthogonal to $(I-(J_v^T)^+ \cdot J_v^T)\cdot {}^D F_v$, the torque required to constrain the motion will also be $(I-(J_v^T)^+ \cdot J_v^T)\cdot {}^D F_v = S \cdot {}^D F_v$. The filtered force required to constrain the virtual manipulator motion is then given by

$${}^D F_{vf} = S \cdot {}^D F_v \tag{5.7}$$

It is important to realize that user-applied forces and torques are partly responsible in the generation of the external force ${}^D F_v$. There might be other unavoidable effects that play a part in the force generation.

The haptic display objective is to enforce the robotic manipulator end effector to follow the motions of the virtual manipulator end effector end point. If there is some initial position or velocity error, the control force is partly generated by this difference. Although they do not affect stability, imperfect gravity and friction compensation of the haptic interface device may be another cause for position and velocity errors.

Because the external force ${}^{D}F_{v}$ is generated as a result of both the position and the velocity errors, ${}^{D}F_{v}$ can be easily modeled by a spring-damper system. Thus,

$$ {}^{D}F_{v} = K_{p} \cdot {}^{D}e + K_{d} \cdot {}^{D}\dot{e} \tag{5.8} $$

where ${}^{D}e$ is a 6×1 position error vector and ${}^{D}\dot{e}$ is a 6×1 vector of velocity error. K_{p} is a 6×6 symmetric positive definite matrix of spring constants and K_{d} is a symmetric 6×6 positive definite matrix of damping coefficients.

The position error ${}^{D}e$ is defined by

$$ {}^{D}e = {}^{D}x_{vd} - {}^{D}x_{r} \tag{5.9} $$

where ${}^{D}x_{r}$ is the 6×1 position vector of the robot end effector written in a coordinate frame attached at the end effector of the virtual manipulator. ${}^{D}x_{vd}$ is also a 6×1 position vector, and it is the desired position of the virtual manipulator end effector end point written in the same coordinate frame.

The time differential of the position error is the velocity error, which is

$$ {}^{D}\dot{e} = {}^{D}\dot{x}_{vd} - {}^{D}\dot{x}_{r} \tag{5.10} $$

where ${}^{D}\dot{x}_{r}$ is the 6×1 velocity vector of the robot end effector, and ${}^{D}\dot{x}_{vd}$ is the 6×1 vector of virtual manipulator end effector end point velocity.

Substitution of equation (5.8) into equation (5.7) results in

$$ {}^{D}F_{vf} = S \cdot {}^{D}F_{v} = S(K_{p} \cdot {}^{D}e + K_{d} \cdot {}^{D}\dot{e}) \tag{5.11} $$

The force vector, ${}^{D}F_{vf}$, in a fixed coordinate frame is

$$ {}^{F}F_{vf} = \begin{bmatrix} R_{v} & 0 \\ 0 & R_{v} \end{bmatrix} S(K_{p} \cdot {}^{D}e + K_{d} \cdot {}^{D}\dot{e}) \tag{5.12} $$

where R_v, is a3×3 rotation matrix which describes the virtual manipulator end effector frame with respect to the fixed reference frame. The control system applied external force is expressed in the robot end effector frame by

$$ {}^{R}F_{vf} = \begin{bmatrix} R_r^T & 0 \\ 0 & R_r^T \end{bmatrix} \begin{bmatrix} R_v & 0 \\ 0 & R_v \end{bmatrix} S(K_p \cdot {}^{D}e + K_d \cdot {}^{D}\dot{e}) \tag{5.13} $$

where the rotation matrix, R_r, is given in equation (3.3) and it describes the robot end effector frame with respect to the fixed reference frame, or the base frame of the robot.

If the external forces and torques applied at the end effector of the robotic manipulator, ${}^{R}F_r$, are assumed to be the same as the forces and torques applied at the virtual manipulator end effector, ${}^{R}F_v$, the forces and torques that the user exerts on the robot can be expressed by

$$ {}^{R}F_r = {}^{R}F_v = \begin{bmatrix} R_r^T & 0 \\ 0 & R_r^T \end{bmatrix} \begin{bmatrix} R_v & 0 \\ 0 & R_v \end{bmatrix} (K_p \cdot {}^{D}e + K_d \cdot {}^{D}\dot{e}) \tag{5.14} $$

5.2 General robot dynamics

The kinematics and the dynamics of a six degree-of-freedom manipulator have been summarized in section 3.1. The dynamics in the joint space is given by

$$ H(q)\ddot{q} + C(q,\dot{q})\dot{q} + f_r\dot{q} + g(q) = \tau - J_r^T \cdot {}^{R}F_r \tag{5.15} $$

where $H(q)$ is the symmetric positive definite inertia matrix, $C(q,\dot{q})\dot{q}$ the vector of coriolis and centrifugal terms, f_r the frictional terms, $g(q)$ the vector of gravitational terms, ${}^{R}F_r$ the external Cartesian force and torque vector, and finally τ is the joint actuator torque vector.

In the stability analysis, the first assumption will be that the gravitational terms can be fully compensated. The gravitational terms can be modeled analytically or experimental data can be collected to compensate $g(q)$. The gravity compensation term will be defined by $\hat{g}(q)$. Thus, the assumption is $g(q) \approx \hat{g}(q)$. The second assumption that will be made is that the frictional terms can be fully compensated. This is usually done experimentally. Thus, $f_r = \hat{f}_r$.

The inertia matrix $H(q)$ is a symmetric positive definite matrix, and it is continuously differentiable. The inertia matrix and the elements of the matrix $C(q,\dot{q})$ are related and this relation is given in terms of the Christoffel symbols of the first kind [6]. It is also shown that $\dot{H}(q) - 2C(q,\dot{q})$ is a skew symmetric matrix. The matrix $C(q,\dot{q})$ has the property such that $\|C(q,\dot{q})\| = a_1\|\dot{q}\|$ where α_1 is a positive constant.

5.3 Control law

The control law is used to constrain the robot end effector to follow the end effector of the virtual manipulator. Therefore the robot does not need to resist all components of the end effector force, only those components that would have been resisted by kinematics of the

virtual manipulator. This means that the controller should be chosen so that the robot will be free to move along the end effector trajectory defined by the virtual manipulator, but will resist any motion in all other directions. The designed controller is

$$\tau = J_r^T \cdot {}^R F_{vf} + \hat{f}_r \dot{q} + \hat{g}(q) + J_r^T \cdot {}^R F_r \tag{5.16}$$

If (5.16) is substituted into equation (5.15), the joint space dynamics of the Puma 560 manipulator can then be expressed by

$$H(q)\ddot{q} + C(q,\dot{q})\dot{q} = J_r^T \cdot {}^R F_{vf} \tag{5.17}$$

Then, the robot dynamic equation in conjunction with the filtered force definition given in equation (5.13) can be rewritten as

$$H(q)\ddot{q} + C(q,\dot{q})\dot{q} = J_r^T \begin{bmatrix} R_r^T & 0 \\ 0 & R_r^T \end{bmatrix} \begin{bmatrix} R_v & 0 \\ 0 & R_v \end{bmatrix} S(K_p \cdot {}^D e + K_d \cdot {}^D \dot{e}) \tag{5.18}$$

5.4. Stability

To carry out the stability analysis, the following Lyapunov candidate function will be chosen

$$V = \frac{1}{2}\dot{q}^T H \dot{q} + \int \left(SK_p \cdot {}^D e\right)^T d\left({}^D e\right) \tag{5.19}$$

V is a valid Lyapunov function if it is positive except at the equilibrium where

$${}^D e = {}^D \dot{e} = \dot{q} = 0 \tag{5.20}$$

The first term in the Lyapunov function V is an expression of the system's total kinetic energy, which is zero if $\dot{q} = 0$. Because the inertia matrix H is positive definite, this first term is always greater than or equal to zero. The function V is therefore positive definite if the second term is positive definite. For that, the following condition should hold

$$F(e_x) = \int \left(SK_p \cdot {}^D e\right)^T d\left({}^D e\right) \succ 0 \tag{5.21}$$

The function F is positive definite if the following convex function conditions are satisfied.

1. $F(0) = 0$

2. $\left.\dfrac{\partial F}{\partial\left({}^D e\right)}\right|_{{}^D e=0} = 0$

3. $\dfrac{\partial}{\partial\left({}^D e\right)}\dfrac{\partial F}{\partial\left({}^D e\right)^T}$ is positive definite

Thus,

1. $F(0) = 0$

2. $\left.\dfrac{\partial F}{\partial\left({}^D e\right)}\right|_{e=0} = SK_p \cdot {}^D e\big|_{{}^D e=0} = 0$

3. $G = \dfrac{\partial}{\partial\left({}^D e\right)}\dfrac{\partial F}{\partial\left({}^D e\right)^T} = SK_p + N$

where the element in the ith row and jth column of the matrix of N is given by

$$N_{(i,j)} = \frac{\partial S_{(i)}}{\partial\left({}^D e_{(j)}\right)} K_p \cdot {}^D e \tag{5.22}$$

where $S_{(i)}$ is the ith row vector of S and ${}^D e_{(j)}$ is the jth element of ${}^D e$.

The matrix N is zero at the equilibrium ${}^{D}e = 0$, but it may otherwise be negative definite. It caries information of the virtual manipulator's second order kinematics. N is very small near equilibrium, and $G = \frac{\partial}{\partial({}^{D}e)}\frac{\partial F}{\partial({}^{D}e)^{T}} \approx SK_{p} \geq 0$. This fact is proven in [26].

This result means that even if we just consider local stability, the matrix G may be zero. Thus, the Lyapunov function is not always positive.

Let us analyze this problem more carefully by taking another look at the error term given in equation (5.9),

${}^{D}e = {}^{D}x_{vd} - {}^{D}x_{r}$

By studying the kinematics of the virtual manipulator, the velocity of the end effector end point and the joint angular velocities can be easily related. This relationship is given by

$${}^{D}\dot{x}_{v} = J_{v}\dot{\theta} \tag{5.23}$$

where J_{v} is the $6\times m$ Jacobian matrix written in the end effector frame. The angular velocity of the joint angles may be defined by

$$\dot{\theta} = \begin{bmatrix} J_{vr} & 0 \end{bmatrix}{}^{F}\dot{x}_{r} \tag{5.24}$$

where J_{vr} is an $m\times 3$ Jacobian matrix, and ${}^{F}\dot{x}_{r}$ the 6×1 velocity vector of the robot end effector written in a fixed reference frame, which is chosen as the base frame of the robot.

The process of computing the elements of the matrix J_{vr} is based on the idea that the optimal location of the virtual manipulator end effector is a function of the position of the robot end effector, and not the orientation of the end effector. The desired position vector ${}^{D}x_{vd}$ is therefore the optimal location reachable by the robot manipulator that eliminates the position error. The desired position vector was calculated for a two degree-of-freedom virtual

manipulator described in section 3.3. Equation (3.135) calculates the desired joint angles in this case, and the desired position is given by equation (3.115). By differentiating this realationship with respect to time, the elements of the Jacobian in equation (5.23) are easily identified. The process is also illustrated by the same example in section (3.3). By substituting equation (5.24) into (5.23), the desired velocity of the virtual manipulator end effector end point is obtained.

The desired velocity of the virtual manipulator end effector end point is then given by

$$ {}^{D}\dot{x}_{vd} = J_v\dot{\theta} = J_v\begin{bmatrix} J_{vr} & 0 \end{bmatrix}{}^{F}\dot{x}_r \tag{5.25} $$

$$ {}^{D}\dot{x}_{vd} = J_v\begin{bmatrix} J_{vr} & 0 \end{bmatrix}\begin{bmatrix} R_v & 0 \\ 0 & R_v \end{bmatrix}\cdot{}^{D}\dot{x}_r \tag{5.26} $$

The velocity error equation can now be expressed by

$$ {}^{D}\dot{e} = {}^{D}\dot{x}_{vd} - {}^{D}\dot{x}_r = \left(J_v\begin{bmatrix} J_{vr} & 0 \end{bmatrix}\begin{bmatrix} R_v & 0 \\ 0 & R_v \end{bmatrix} - I\right)\cdot{}^{D}\dot{x}_r = J_e\cdot{}^{D}\dot{x}_r \tag{5.27} $$

where

$$ J_e = J_v\begin{bmatrix} J_{vr} & 0 \end{bmatrix}\begin{bmatrix} R_v & 0 \\ 0 & R_v \end{bmatrix} - I \tag{5.28} $$

The haptic display robot end effector angular velocity has no determinant effect on the virtual manipulator desired velocity. This is because the optimal position of the virtual manipulator is a function of the position of the haptic display end effector, and the virtual manipulator joint angular velocity, $\dot{\theta}$, is calculated by differentiating this relationship. Thus, the virtual manipulator desired velocity, ${}^{D}\dot{x}_{vd} = J_v\dot{\theta}$, is not a function of the haptic display robot end effector angular velocity. Therefore, the position and velocity error terms that

generate the force ${}^{D}F_{v}$ do not carry any orientation components. Therefore, the desired position is not a function of the robot end effector orientation. Thus,

$${}^{D}e={}^{D}x_{vd}-{}^{D}x_{r}=\begin{bmatrix}{}^{D}e_{x} & 0 & 0 & 0\end{bmatrix}^{T} \tag{5.29}$$

where the Cartesian position error in the $X, Y,$ and Z directions in the virtual manipulator end effector frame is

$${}^{D}e_{x}=\begin{bmatrix}e_{x} & e_{y} & e_{z}\end{bmatrix}^{T} \tag{5.30}$$

The Cartesian velocity error is then

$${}^{D}\dot{e}={}^{D}\dot{x}_{vd}-{}^{D}\dot{x}_{r}=\begin{bmatrix}{}^{D}\dot{e}_{x} & 0 & 0 & 0\end{bmatrix}^{T} \tag{5.31}$$

where

$${}^{D}\dot{e}_{x}=\begin{bmatrix}\dot{e}_{x} & \dot{e}_{y} & \dot{e}_{z}\end{bmatrix}^{T} \tag{5.32}$$

Note that the projection matrix S, given in equation (5.6), may also be expressed by

$$S=\begin{bmatrix}S_{x} & S_{xw}\\ S_{xw} & S_{w}\end{bmatrix} \tag{5.33}$$

where S_{x}, S_{w}, and S_{xw} are 3×3 matrices. Since $\text{rank}(S)+m=6$, for position control, $\text{rank}(S_{x})=3$ when $m\le3$. In this case, the Lyapunov function may be expressed by

$$V=\frac{1}{2}\dot{q}^{T}H\dot{q}+\int\left(SK_{p}\cdot{}^{D}e\right)^{T}d\left({}^{D}e\right)=\frac{1}{2}\dot{q}^{T}H\dot{q}+\int\left(S_{x}K_{px}\cdot{}^{D}e_{x}\right)^{T}d\left({}^{D}e_{x}\right) \tag{5.34}$$

where the matrix S_{x} is symmetric positive definite and the 3×3 stiffness matrix K_{Px} may be chosen as

$$K_{px}=k_{p}I \tag{5.35}$$

Then,

$$V = \frac{1}{2}\dot{q}^T H\dot{q} + k_p \int \left(S_x \cdot {}^D e_x\right)^T d\left({}^D e_x\right) \tag{5.36}$$

The Lyapunov function is always positive definite if and only if

$$F(e_x) = k_p \int \left(S_x \cdot {}^D e_x\right)^T d\left({}^D e_x\right) \succ 0 \tag{5.37}$$

or

$$G = \frac{\partial}{\partial\left({}^D e\right)} \frac{\partial F}{\partial\left({}^D e\right)^T} = S_x + N \succ 0 \tag{5.38}$$

where the element in the ith row and jth column of the matrix of N is again given by

$$N_{(i,j)} = \frac{\partial S_{x(i)}}{\partial\left({}^D e_{x(j)}\right)} \cdot {}^D e_x \tag{5.39}$$

The matrix N caries information of the virtual manipulator's second order kinematics, and it is zero at the equilibrium ${}^D e = 0$. Because N is very small near equilibrium,

$$G = \frac{\partial}{\partial\left({}^D e\right)} \frac{\partial F}{\partial\left({}^D e\right)^T} = S_x \succ 0 \tag{5.40}$$

This result means that the Lyapunov function is always positive near equilibrium. It may or may not be positive away from the equilibrium. The second order should be studied for the particular virtual manipulator to resolve this question.

The time derivative of the Lyapunov function must be decreasing to prove stability. If V decreases to zero, then the system is asymptotically stable. In order to show that V is a decrescent function of time, the time derivative of the Lyapunov candidate function is first obtained.

$$\dot{V} = \dot{q}^T \left(-C\dot{q} + J_r^T \begin{bmatrix} R_r^T & 0 \\ 0 & R_r^T \end{bmatrix} \begin{bmatrix} R_v & 0 \\ 0 & R_v \end{bmatrix} S\left(K_p \cdot {}^D e + K_d \cdot {}^D \dot{e}\right) + \frac{\dot{H}}{2}\dot{q}\right) + \left({}^D \dot{e}\right)^T S K_p \cdot {}^D e \tag{5.41}$$

where $(\dot{H}-2C)$ is skew symmetric which implies $\dot{q}^T(-C\dot{q}+\frac{\dot{H}}{2}\dot{q})=0$. Then,

$$\dot{V}=\dot{q}^T J_r^T\begin{bmatrix} R_r^T & 0 \\ 0 & R_r^T \end{bmatrix}\begin{bmatrix} R_v & 0 \\ 0 & R_v \end{bmatrix}S(K_p\cdot^D e+K_d\cdot^D \dot{e})+\left({}^D\dot{e}\right)^T SK_p\cdot^D e \tag{5.42}$$

If we rewrite equation (7),

$${}^D\dot{e}={}^D\dot{x}_{vd}-{}^D\dot{x}_r=J_e\cdot^D\dot{x}_r \tag{5.43}$$

Using equation (6), we get

$${}^D\dot{e}=J_e\cdot^D\dot{x}_r=J_e\begin{bmatrix} R_v^T & 0 \\ 0 & R_v^T \end{bmatrix}\begin{bmatrix} R_r & 0 \\ 0 & R_r \end{bmatrix}\cdot^R\dot{x}_r \tag{5.44}$$

or

$$\dot{q}^T J_r^T={}^R\dot{x}_r^T=\left({}^D\dot{e}\right)^T J_e^{-T}\begin{bmatrix} R_v^T & 0 \\ 0 & R_v^T \end{bmatrix}\begin{bmatrix} R_r & 0 \\ 0 & R_r \end{bmatrix} \tag{5.45}$$

By substituting this equation in (13), we get

$$\dot{V}=\left({}^D\dot{e}\right)^T J_e^{-T}S(K_p\cdot^D e+K_d\cdot^D \dot{e})+\left({}^D\dot{e}\right)^T SK_p\cdot^D e \tag{5.46}$$

Here, we will make use of the fact that

$$S+SJ_e=0 \tag{5.47}$$

which can be proven by writing

$$S=I-J_v(J_v^T J_v)^{-1}J_v^T \tag{5.48}$$

$$J_e=J_v\left(\begin{bmatrix} J_{vr} & 0 \end{bmatrix}\begin{bmatrix} R_v & 0 \\ 0 & R_v \end{bmatrix}-I\right) \tag{5.49}$$

$$S+SJ_e=(I-J_v(J_v^T J_v)^{-1}J_v^T)J_v\left(\begin{bmatrix} J_{vr} & 0 \end{bmatrix}\begin{bmatrix} R_v & 0 \\ 0 & R_v \end{bmatrix}-I\right) \tag{5.50}$$

$$S + SJ_e = J_v([J_{vr} \quad 0]\begin{bmatrix} R_v & 0 \\ 0 & R_v \end{bmatrix} - I) - J_v(J_v^T J_v)^{-1} J_v^T J_v([J_{vr} \quad 0]\begin{bmatrix} R_v & 0 \\ 0 & R_v \end{bmatrix} - I) \tag{5.51}$$

$$S + SJ_e = J_v([J_{vr} \quad 0]\begin{bmatrix} R_v & 0 \\ 0 & R_v \end{bmatrix} - I) - J_v([J_{vr} \quad 0]\begin{bmatrix} R_v & 0 \\ 0 & R_v \end{bmatrix} - I) \tag{5.52}$$

$$S + SJ_e = 0 \tag{5.53}$$

which implies the fact that

$$S + J_e^T S = 0, \; S + J_e^{-T} S = 0 \tag{5.54}$$

then, equation (14) becomes

$$\dot{V} = -\left({}^D\dot{e}\right)^T S(K_p \cdot {}^D e + K_d \cdot {}^D \dot{e}) + \left({}^D\dot{e}\right)^T S K_p \cdot {}^D e \tag{5.55}$$

$$\dot{V} = -\left({}^D\dot{e}\right)^T S K_d \cdot {}^D \dot{e} \tag{5.56}$$

Noting again that the velocity error given in equation (5.30) does not carry any angular velocity components, this equation can then be rewritten as

$$\dot{V} = -\left({}^D\dot{e}_x\right)^T S_x K_{dx} \cdot {}^D \dot{e}_x \tag{5.57}$$

where the damping matrix K_{dx} is a 3×3 symmetric matrix, and it may be chosen as

$$K_{dx} = k_d I \tag{5.58}$$

Then,

$$\dot{V} = -k_d \left({}^D\dot{e}_x\right)^T S_x \cdot {}^D \dot{e}_x \tag{5.59}$$

Since S_x is a 3×3 symmetric positive definite matrix, $\dot{V}$ is always negative unless ${}^D\dot{e}_x = 0$. This is also the only case the Lyapunov function is not positive, but positive semi definite. If we rewrite equation (11) for this case, we get

$$H(q)\ddot{q} = J_r^T \begin{bmatrix} R_r^T & 0 \\ 0 & R_r^T \end{bmatrix} \begin{bmatrix} R_v & 0 \\ 0 & R_v \end{bmatrix} SK_p \cdot {}^D e \tag{5.60}$$

For end effector position control, this equation reduces to

$$H(q)\ddot{q} = k_p J_r^T \begin{bmatrix} R_r^T & 0 \\ 0 & R_r^T \end{bmatrix} \begin{bmatrix} R_v & 0 \\ 0 & R_v \end{bmatrix} \begin{bmatrix} S_x & S_{xw} \\ S_{xw} & S_w \end{bmatrix} \cdot {}^D e \tag{5.61}$$

$$H(q)\ddot{q} = k_p J_r^T \begin{bmatrix} R_r^T R_v S_x & 0 \\ 0 & 0 \end{bmatrix} \begin{bmatrix} {}^D e_x \\ 0 \end{bmatrix} \tag{5.62}$$

This equation implies that as long as S_x is symmetric positive definite, the system is asymptotically stable.

$$\dot{V} = 0 \Rightarrow {}^D \dot{e}_x = 0 = \dot{q} \Rightarrow {}^D e_x = 0 \tag{5.63}$$

Note that with this optimal impedance type controller the orientation of the robotic manipulator is not actuated at all. Therefore, a conventional PD controller is employed to control the orientation of the end effector. The end effector orientation must be controlled because the user grabs a handle attached to it and manipulates the virtual manipulator. The desired position of the haptic display is already calculated by the optimal position controller. The desired orientation of the haptic display may then be chosen the same as the orientation of the virtual manipulator end effector. Thus, $R_v = R_r$. Solving the inverse kinematics of the haptic display then gives the desired orientation.

A conventional PD controller is expressed by

$$\tau = K_P e + K_D \dot{e} + \hat{f}_r \dot{q} + \hat{g}(q) \tag{5.64}$$

where K_P and K_D are the constant positive definite diagonal matrices of the stiffness and damping. The robot joint angular position and the angular velocity errors are

$$e = q_d - q$$
$$\dot{e} = \dot{q}_d - \dot{q} \tag{5.65}$$

To show stability, a Lyapunov candidate function is chosen.

$$V = \frac{1}{2}\dot{q}^T H\dot{q} + \frac{1}{2}e^T K_P e \tag{5.66}$$

which is always positive except at the equilibrium. The time derivative of V can be easily shown to be

$$\dot{V} = \dot{q}^T(-C\dot{q} + K_P e + K_D\dot{e} + \frac{\dot{H}}{2}\dot{q} - J_r^T \cdot {}^R F_r) + \dot{e}^T K_P e \tag{5.67}$$

Since $(\dot{H} - 2C)$ is skew symmetric, this equation becomes

$$\dot{V} = \dot{q}^T(K_P e + K_D\dot{e} - J_r^T \cdot {}^R F_r) + \dot{e}^T K_P e \tag{5.68}$$

If we choose $\dot{q}_d = \ddot{q}_d = 0$, then

$$\dot{V} = \dot{q}^T(K_P e - K_D\dot{q} - J_r^T \cdot {}^R F_r) - \dot{q}^T K_P e \tag{5.69}$$

$$\dot{V} = -\dot{q}^T K_D\dot{q} - \dot{q}^T J_r^T \cdot {}^R F_r \tag{5.70}$$

$\dot{V}$ is negative as long as ${}^R F_r$ is bounded, except when $\dot{q} = 0$. Note that $\dot{q} = 0$ implies $\dot{e} = 0 \Rightarrow e = 0$. Therefore, $\dot{V}$ is always negative except at the equilibrium. Thus, the system is stable.

A final note is that the virtual manipulator joint angles can also obtained by first setting the rotation matrix of the robot manipulator to that of the virtual manipulator. In this case, the desired position is a function of the robot joint angles, which define the orientation of the end effector. This relationship can be expressed by

$${}^D x_{vd} = f(R_r) \tag{5.71}$$

The time differential of this equation is

$$ {}^{D}\dot{x}_{vd} = \frac{\partial f}{\partial q}\dot{q} = \frac{\partial f}{\partial q} J_r^{-1} \cdot {}^{R}\dot{x} \tag{5.72} $$

which implies that the desired velocity carry the information of both the Cartesian velocity and the angular velocity of the robot end effector. Thus, the positive semi-definite matrix S can not be divided into its components, which was done earlier to prove stability. Proving asymptotic stability in this case becomes more difficult. This system is not stable unless there exists a minimum amount of environmental stiffness, which adds to the term SK_p and makes the sum a positive definite matrix. Both the first and the second order kinematics of the virtual manipulator also become more detrimental in the stability problem.

6. EXPERIMENTAL TESTBED

The control laws described in the previous chapter guarantee the stability of the haptic interaction when using the control approach outlined. These controllers couple the virtual simulator dynamics to that of the robotic manipulator. The hardware implementation of the haptic display algorithms mentioned earlier requires a haptic interface (robotic manipulator), control interface and a force/torque-measuring device. This chapter will describe these devices and briefly address the safety precautions taken.

6.1 Robotic manipulator

The robotic manipulator to be used is a PUMA 560 manipulator, shown in Figure 3.1. The selection of this device is mainly due to the availability of this common device and the widespread use in both industry and research laboratories. The research accomplished by this dissertation can therefore be easily reproduced and extended. Because the PUMA 560 is a six-degree of freedom robotic manipulator, the algorithms developed in this research can be easily incorporated with a different type of manipulator.

6.2 Control interface

The manufacturer of the PUMA 560 manipulator has used a Unimation LSI/11 Val industrial computer and servo control cards as the control interface. Control of joint torques and encoder readings were not possible. Therefore, control cards associated with the Val computer were replaced by a Trident Robotics TRC004 servo control card. This card enables joint level control by means of a personal computer. TRC004 servo card is used to apply analog output voltages to the DC servomotors of the manipulator to control each joint torque. It provides encoder readings, which are used to calculate the joint angles. The angular velocity of each joint is obtained by differentiating the corresponding joint angle.

A TRC006 interface card that is equipped by a microprocessor is installed in the port memory of the personal computer. This card maintains the input output data access between the TRC004 card and the port memory of the personal computer. The data flow from TRC006 card to the port memory determines the angular position of each joint of the manipulator. The data flow from the port memory to the TRC004 card controls the joint torques of the robot. A C program is written to simulate the virtual tool motions and to access the port memory of the computer.

6.3 Force transducer

A force transducer is used to measure forces applied by the user on the handle attached to the end effector of the manipulator. The force torque-measuring device used in this research is a six axis ATI force/torque transducer which is mounted between the end effector and the handle. This particular transducer is able to sense forces up to 133 N in the x and y directions and 266 N in the z direction. The maximum measurable torque in all directions is 11.3 N-m. The transducer connects by means of a cable to a parallel interface card in the port memory of the personal computer. The same C program also reads the force data from the port memory. The noise in the force data and the force torque resolutions reduce the performance and limit the achievable transparency of the haptic display. In order to minimize the noise in the force data, a first order digital filter is employed prior to the use of the data for virtual tool simulations.

6.4 Safety considerations

Robotic manipulators pose safety concerns in haptic display applications because the user has to be in close proximity to them to grab a handle and manipulate them. They are usually big in size and can push back with great forces against the user. Thus, it is very important to design the interaction between the robot and the user so that the user feels in control and safe in case the robot should start acting in an erratic way.

During operation, stability of the robot is not an easy task to assure. Even with a stable digital controller, variations in the control cycle can drive the system unstable. In the design of a stable digital controller, the control cycle is expected to remain a constant. However, this sampling time varies slightly in a 32-bit Windows 95/NT operating environment. For this reason, these variations are recorded by means of the system clock measurements. The robot power is shut down when the variations become too large. Another concern is if the computer stops functioning. A watchdog timer is implemented to observe the data flow between the computer and the robot. Whenever data flow stops, the power to the robot is turned off. Although these precautions takes care of many safety concerns, situations might arise in which the robot starts acting in an unstable behavior. For this reason a dead-man switch is wired to the control interface and is carried by the user. When the robot starts acting in an erratic way, the user releases the switch to stop the robot from moving. Impedance fields are also designed to prevent the robot from singular configurations where the controller is not stable.

When a force transducer is used in measuring the user-applied forces, another safety concern arises. The force transducer has upper limits of forces and torques. If the user-applied forces or torques is larger than these limits, the software must be able to detect this by producing an error message that eventually stops the robot from moving. This precaution is designed to prevent any damage to the strain gages of the force transducer.

7. EXPERIMENTAL RESULTS

This chapter presents experimental results using the two haptic simulations together with the PUMA 560 robotic manipulator as the haptic display device. The dumbbell simulation demonstrates the use of dynamic modeling for display of multibody systems including switching constraints and nonholonomic motion. The virtual mechanism simulation shows the application of virtual kinematic constraints for use in evaluating a specific mechanism motion in the virtual environment. The chapter is divided into three major sections. The first section illustrates the use of a multibody dynamical system to create user interactions in a virtual environment. The second section studies the interactions when the robot manipulator is coupled kinematically with a two degree-of-freedom manipulator. The third section illustrates the implementation of a stick shift mechanism, which is generated by constraining the motions of the two degree-of-freedom virtual manipulator to form a shift pattern.

7.1 Dumbbell

The application shows the ability of the PUMA 560 robot manipulator to accurately simulate dynamic characteristics of a multibody system. The dumbbell can be translated and rotated in any desired direction in free space motion. During free space motion, the user can manipulate and bring both wheels in contact with a flat surface to experience the dynamic

effects in rolling. The user may then push the dumbbell away from this surface, so the rolling contact motion is stopped. Although, the wheels are not rolling, they continue rotating in free space at a constant angular velocity. If the user chooses to experience the rolling constraint, the wheels will have this initial velocity. This means that the user will feel the dynamics of the additional degrees of freedom created by the rotations of the wheels. In this application, the dumbbell is constrained to move in a virtual box to escape from motion singularities and to provide a safe workspace.

The first case studied is the one where the user applies forces in X, Y and Z directions to manipulate the dumbbell in free space. This case shows tracking along three linear axes. Any parameter of the dumbbell can be changed to allow investigation of that effect. For example, the weight of the dumbbell can be changed by varying the gravitational constant. The gravitational forces are set to zero for all simulations presented.

The forces applied by the human in the X, Y, and Z directions of the robot end effector frame are shown in Figure 7.1(a), Figure 7.2(a), and Figure 7.3(a). A 10-kg mass is manipulated in free space, which results in the X, Y, and Z positions of the end effector as shown in Figure 7.1(c), Figure 7.2(c), and Figure 7.3(c). The velocity of the end effector is shown in Figure 7.1(b), Figure 7.2(b), and Figure 7.3(b). The experimental data measured from the robot sensors are shown using thicker lines and solid lines represent the simulation values. This application shows the stable behavior of the PUMA 560 manipulation as a haptic display in a multibody system, dumbbell. Force feedback is employed using a computed torque controller described in chapter 4. The position error in the X, Y, and Z directions stays less than 0.005 meter.

In the second case, the user is allowed to apply torques in X, Y, or Z directions of the robot base frame only. This case shows the tracking ability of the PUMA 560 along three rotational axes. Thus, only torque feedback is possible. The amount of rotations in each directions are limited to prevent hitting system singularities. The motion characteristics are shown in Figure 7.4, Figure 7.5, and Figure 7.6. This application allows the user to feel inertia of an object resulting from dimensional effects.

In the third case, both force and torque feedback is accomplished. The user grabs the dumbbell and can manipulate it in free space in any way he or she desires. The motion characteristics are again illustrated in Figures 7.7 through Figure 7.12. The position error in the X, Y, and the Z-direction is less than 0.005m. The spikes that show in the angular velocity error as shown in Figures 7.10(d), 7.11(d), and 7.12(d) are because the angular travel in these directions are forced to stay within certain values. Whenever, these limits are hit, a wall effect is created.

The simulations performed in simulating the free space motion of the dumbbell show that a multibody system can be easily interacted virtually using a robotic haptic interface device. It should also be noted that simulation of small masses and inertias cause stability problems. Although digitizing the controller is the main reason for this, part of the problem is the difficulty to perform numerical integration. The use of small mass or inertia results in a very large acceleration, and the integration with varying large accelerations results in unstable system response.

The dumbbell can also be used to feel non-holonomic constraints. In this case, rolling constraints are demonstrated. As the user manipulates the dumbbell in free space, he or she may bring it in contact with a surface. As soon as the surface is hit, contact with the vertical

surface constrains the vertical position of the dumbbell and the wheels are allowed to roll. During the rolling contact, the dumbbell can be steered by applying forces and torques.

In this case study, the user applies forces at the dumbbell center of gravity. The simulation starts with free space manipulation. The dumbbell is oriented in such a way that the dumbbell shaft is parallel to the horizontal direction. Then, the dumbbell is pushed against a surface in the z-plane. The surface is located at z=0.21 m. As the wheels come in contact with this surface, the motion along the z-direction is constrained. The z-position, velocity and the accelerations of the dumbbell are all set to zero. This wall effect is shown in Figure 7.15 (b) and (c). The force applied in this direction is shown Figure 7.15(a), which is resisted to prevent the dumbbell from penetrating the surface. As the rolling motion starts in the global Y-direction, the wheels rotate at the same angular velocity. The motion characteristics in this direction are shown Figure 7.14. The point of contact between the wheels and the surface present a trajectory that is always parallel to the global X-axis. Thus, the motion in the X-direction is not permitted as seen in Figure 7.13(b) and (c). A torque in the vertical direction may be applied that allows the user to change rolling direction of the dumbbell. This case is illustrated in Figure 7.16 through Figure 7.19. The moment applied and the angular velocity attained in the vertical direction are shown in Figure 7.19(a) and (b). The spike in the angular velocity in Figure 7.19(c) is again the effect of enforcing an angular position constraint. The choice in constraining the angular motion inside a region is arbitrary and can be easily removed. In this work, the joint angles of the PUMA 560 were constrained for safety concerns. The application shows how a virtual dynamic model can be used to create both a virtual wall effect and nonholonomic (rolling) constraint motions.

Although, the user interacts in the virtual environment using a six degree-of-freedom manipulator, he or she can achieve additional degrees-of-freedom. If the user rolls the dumbbell on the flat surface and then lifts it up, the rolling constraint is then removed from the dynamic system. The user may choose to first move away from the contact surface and then come back to experience the rolling motion again. Note that the wheels keep their angular velocities at a constant value during the free space motion. When the next contact with the surface occurs, the dumbbell will accelerate its motion, even though the user is not creating this particular motion. This case is illustrated in Figure 7.20 through Figure 7.23. Note how after the second contact, there is a sudden change in the Y-direction velocity as shown in Figure 7.21(b). Although the user-applied forces are very small, especially in the Y-direction, he or she feels an acceleration of the dumbbell due to the hidden dynamics of the wheels in free motion. In other words, the user feels the dynamics of these additional degrees-of-freedom only in the case of rolling contact motions.

7.2 Two degree-of-freedom manipulator

The virtual manipulator end effector end-point is shown to generate a basic taurus shape. The robot end effector is constrained to move on this taurus shape. This is done by creating a closed kinematic chain between the virtual mechanism and the robot. The impedance controller developed in section 5.2 is employed. The orientation of the robot end-effector is the same as that of the virtual manipulator end effector. The robot end effector position information is used to find the closest reachable location on the surface of the taurus.

The controller constantly directs the PUMA 560 end effector orientation to match the position and the orientation of the virtual manipulator end effector. The controller is optimal because the position error is minimized by solving the minimal distance problem, which is described in section 5.2.

The robot end effector position on this surface is shown in Figure 7.24. Figure 7.25(a) and Figure 7.25(b) are used to show the tangential forces (Ftheta1 and Ftheta2) as a function of the virtual manipulator joint angles. The normal force as a function of the position error is shown in Figure 7.25(c). The position error is defined as the distance between the robot end effector and the desired position on the surface of the virtual manipulator workspace. This distance is minimized by the optimal impedance controller to assure stable interactions. The position error is between 0.0018 and 0.007 meter, as shown in Figure 7.25(c).

7.3 Shift mechanism

The motions of the two-degree-of-freedom manipulator are further constrained to implement a stick shift mechanism. This application also uses the optimal position controller described in section 5.2. The impedance controller employed has the advantage of being easily modified by adding new, separate impedance fields to achieve other constraints. Two examples are shown in this section. The first adds constraints using the Lame fields, the second adds detent forces using an attractive field. The attractive field is created by accelerating the motion in certain directions. Haptic interactions in generating a shift

mechanism are explained in section 5.3. The model uses Lame curves to model motions around corners.

Figure 7.26 shows the robot end effector motion, as it is constraint to move on a taurus shape to present motions of a shift pattern. The forces tangential to the surface during motion are presented in Figure 7.27(a) and (b). Figure 7.27(c) shows the amount of position error in meters together with the surface normal force in Newton. The motion is stable and the error remains very small. The shift pattern is created by limiting the motion to present a shift pattern, shown in Figure 7.26.

In order to demonstrate the flexibility of the constraint approach, the same experiment is also performed using a very narrow shift pattern as illustrated in Figure 7.28. The forces and the position error are again shown (see Figure 7.29).

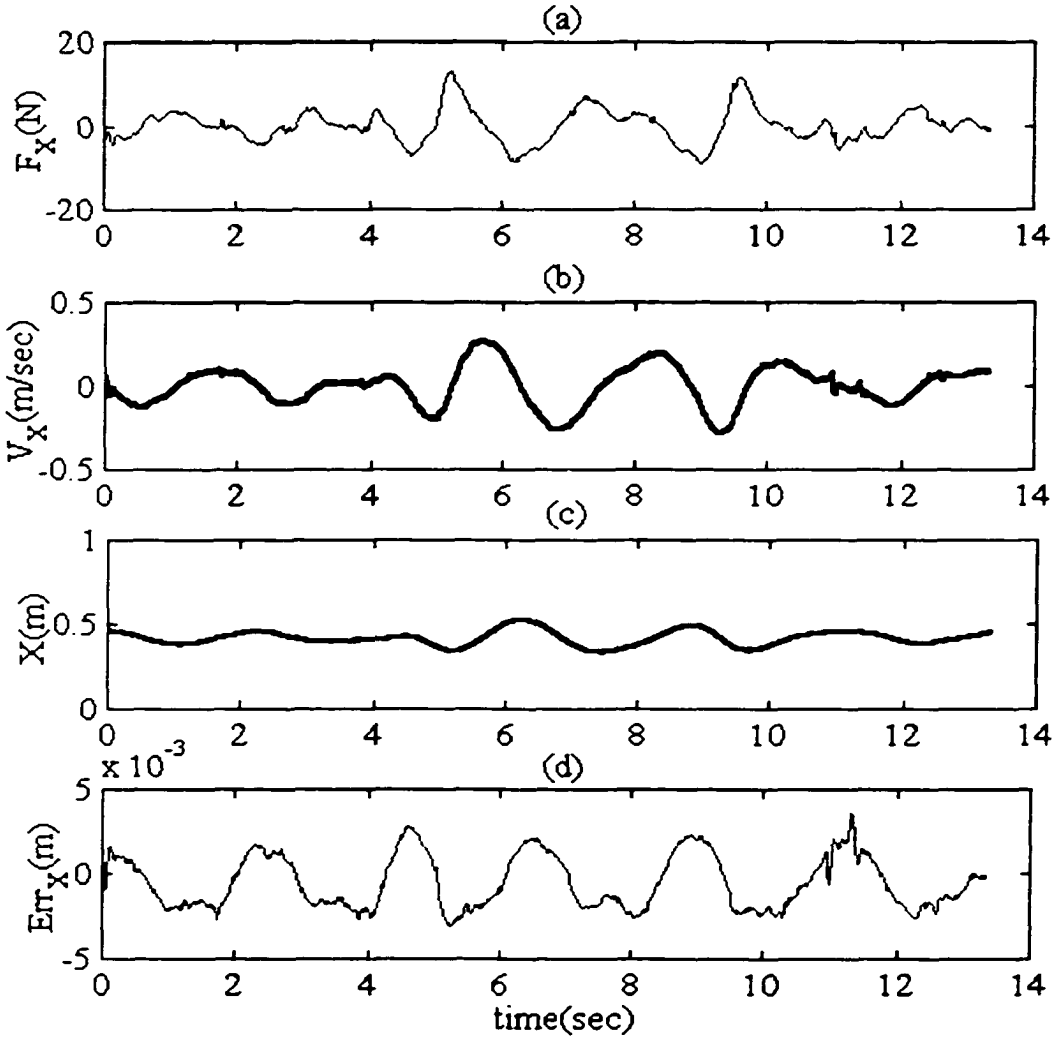

Figure 7.1 Dumbbell cartesian motion, X direction

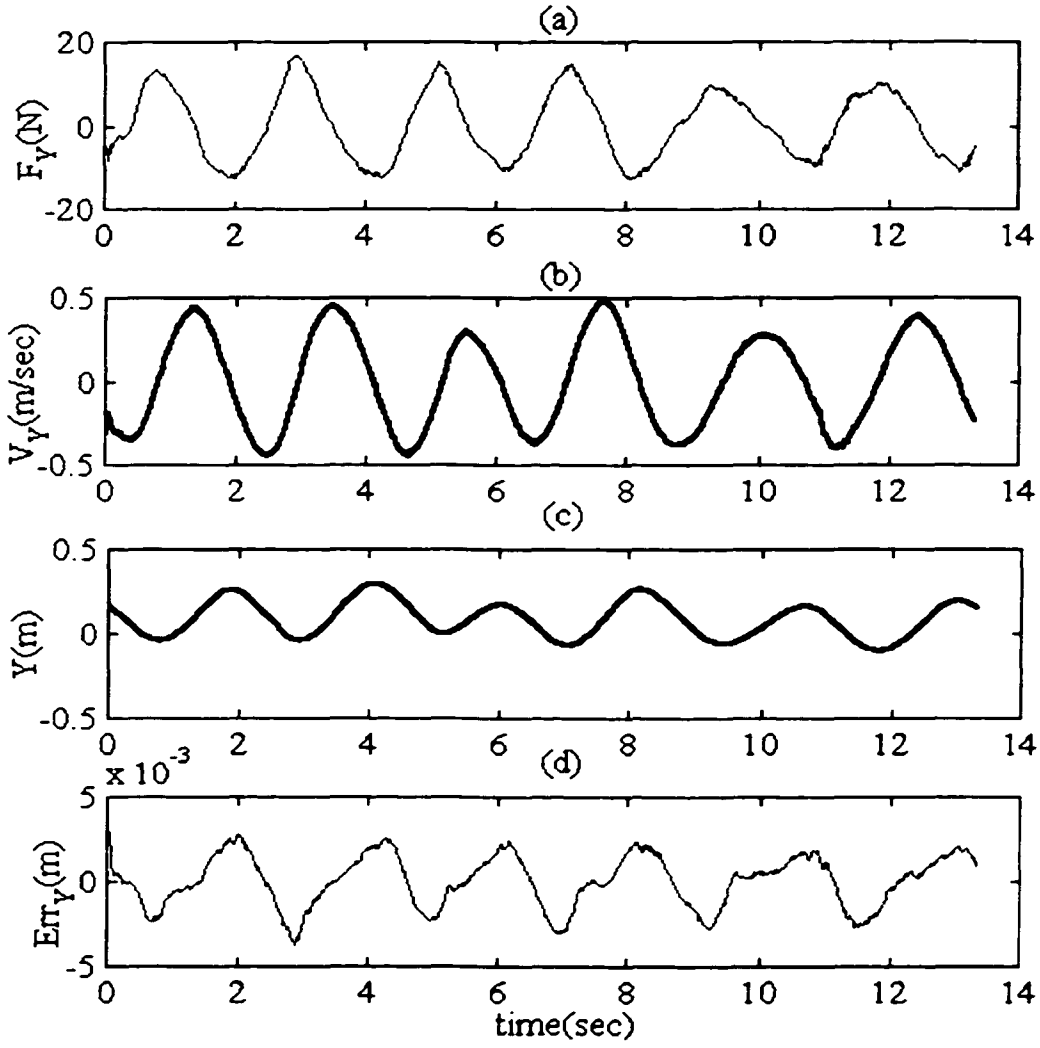

Figure 7.2 Dumbbell cartesian motion, Y direction

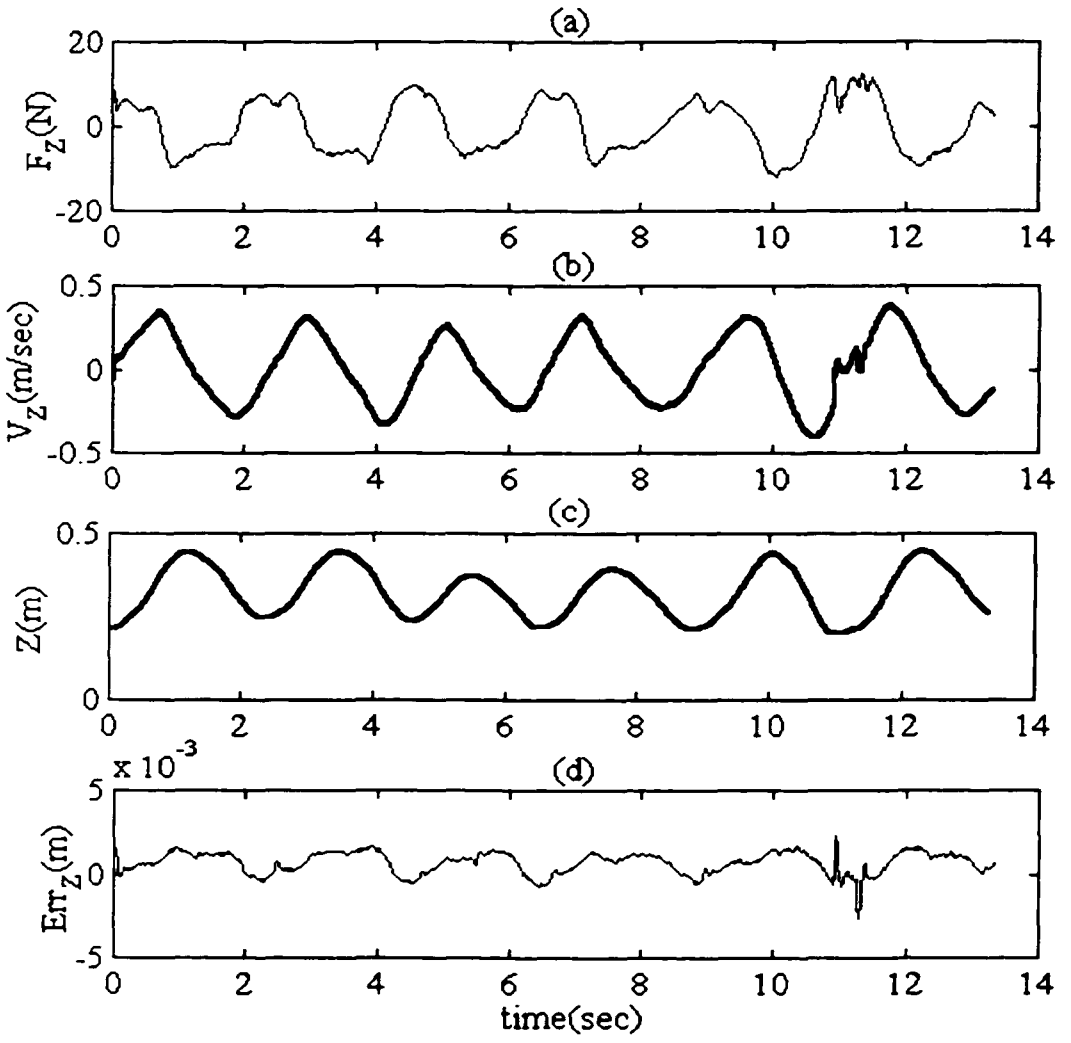

Figure 7.3 Dumbbell cartesian motion, Z direction

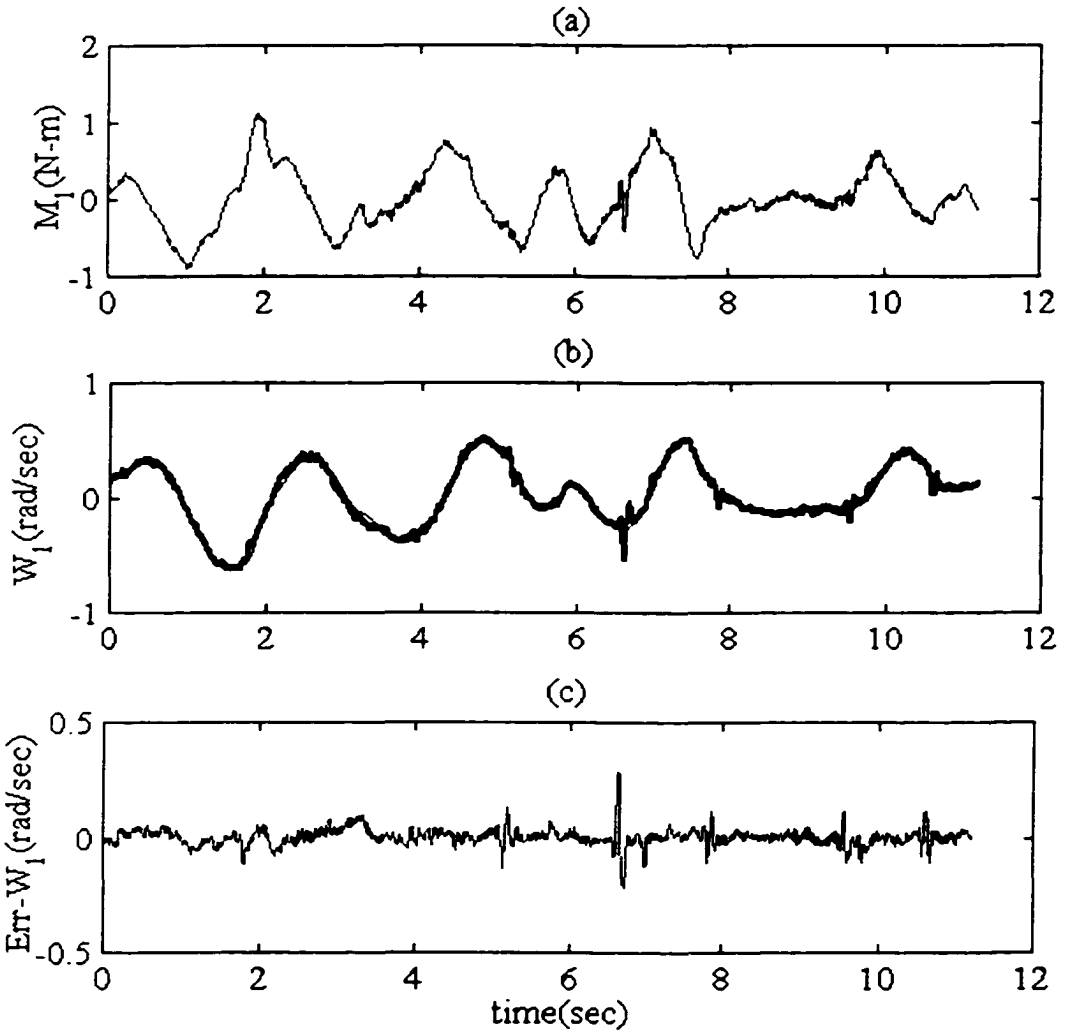

Figure 7.4 Dumbbell angular motion, X direction

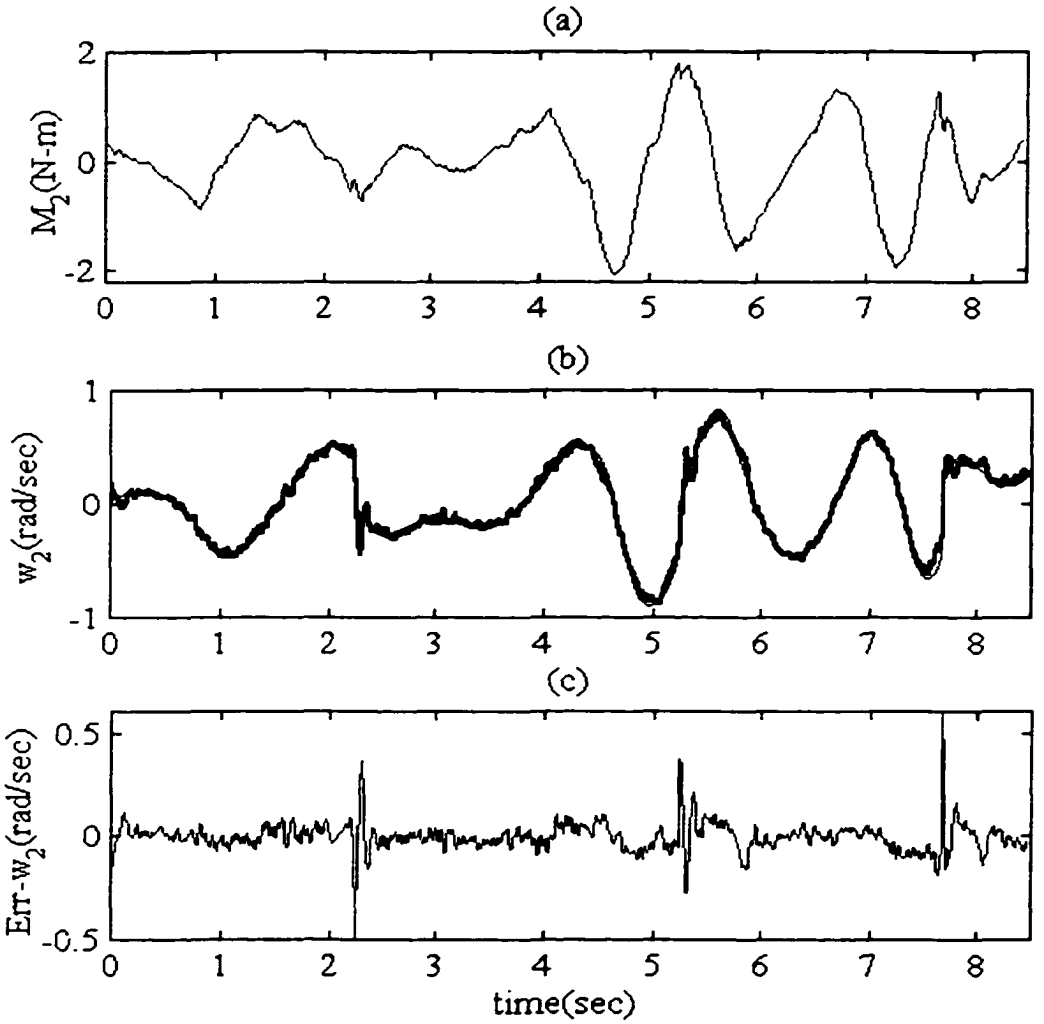

Figure 7.5 Dumbbell angular motion, Y direction

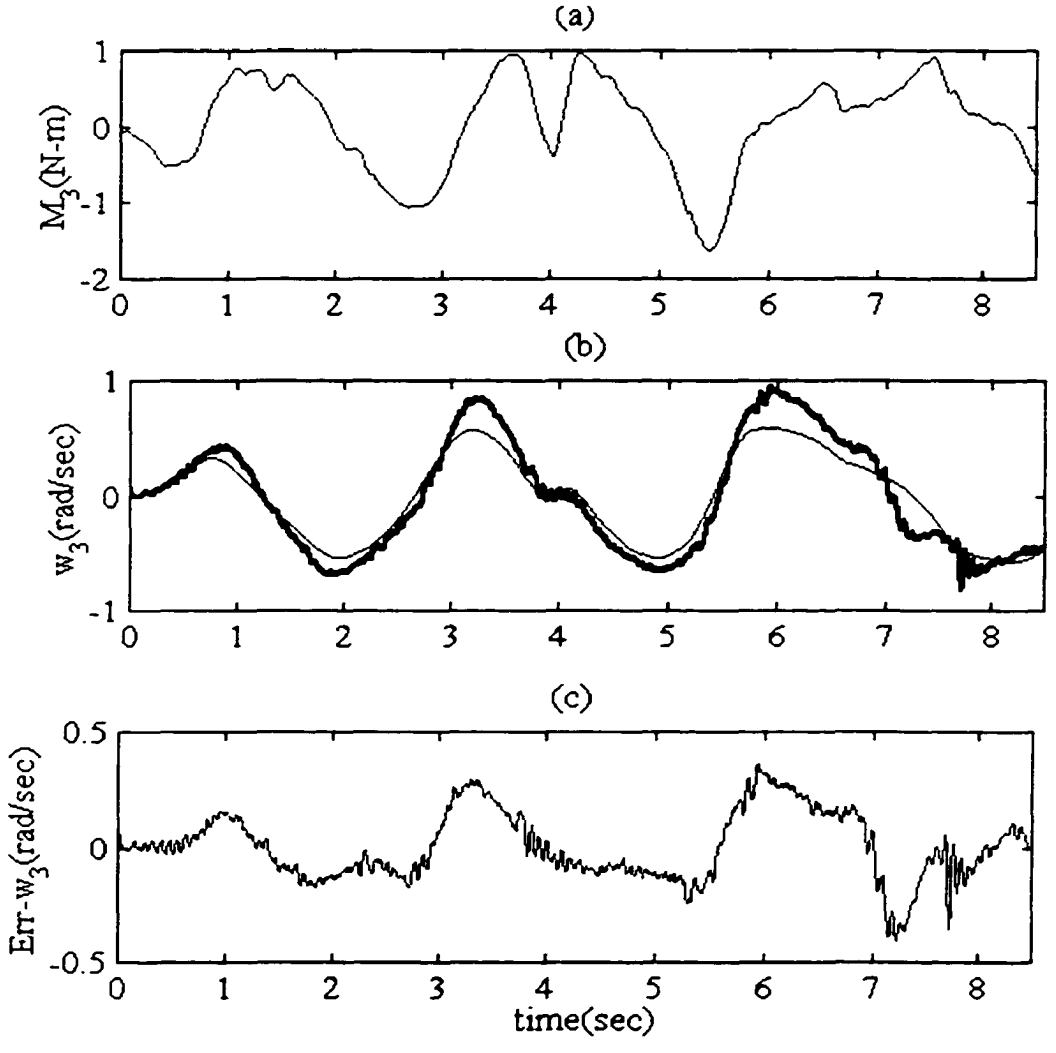

Figure 7.6 Dumbbell angular motion, Z direction

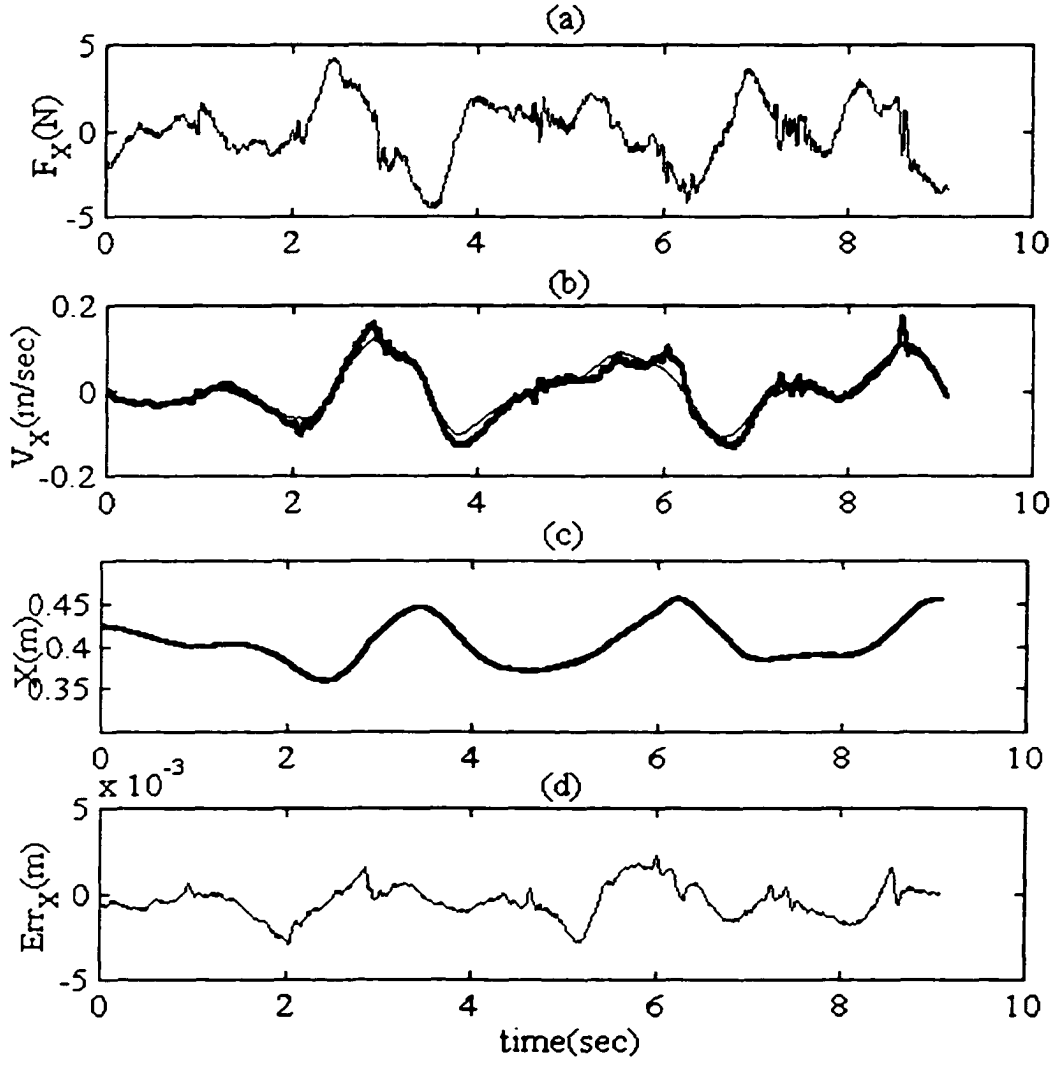

Figure 7.7 Dumbbell general motion, X direction

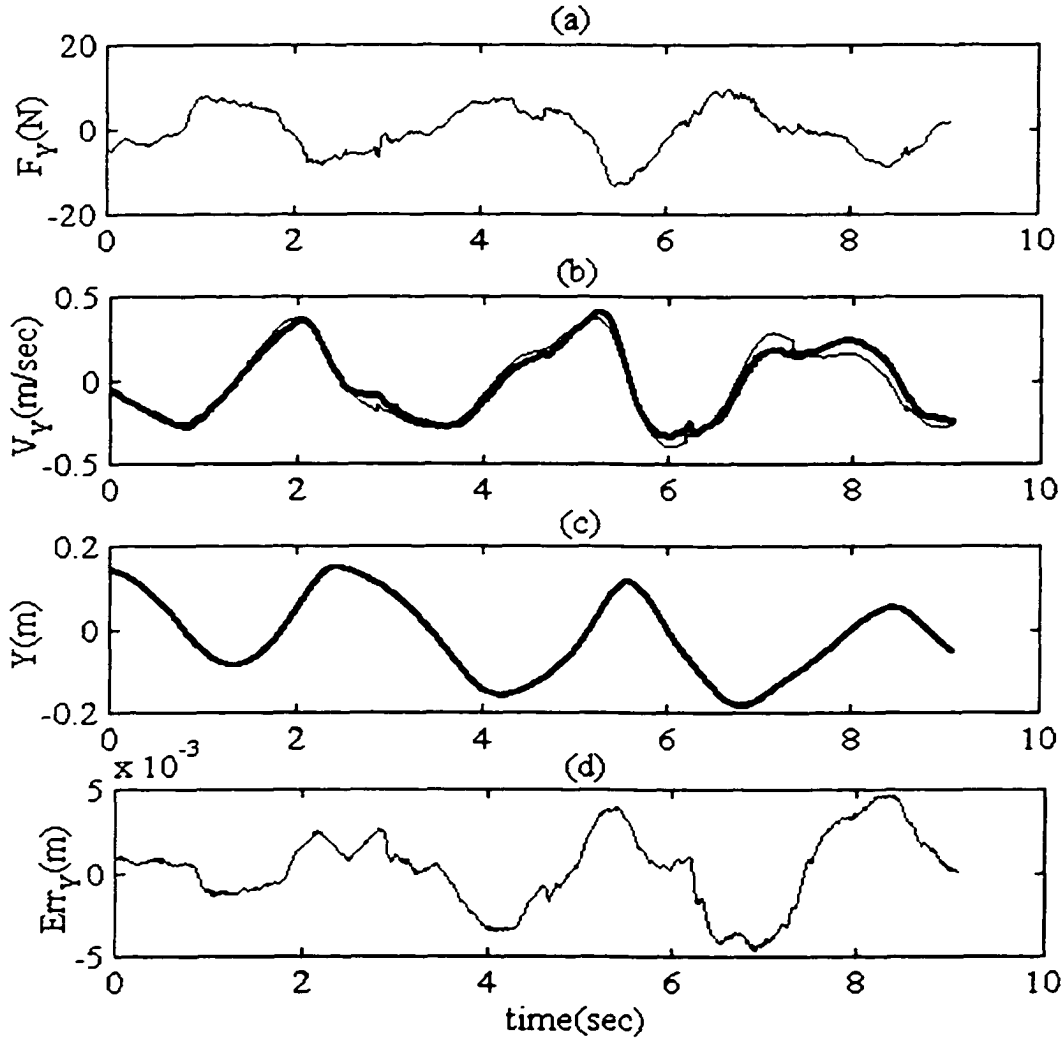

Figure 7.8 Dumbbell general motion, Y direction

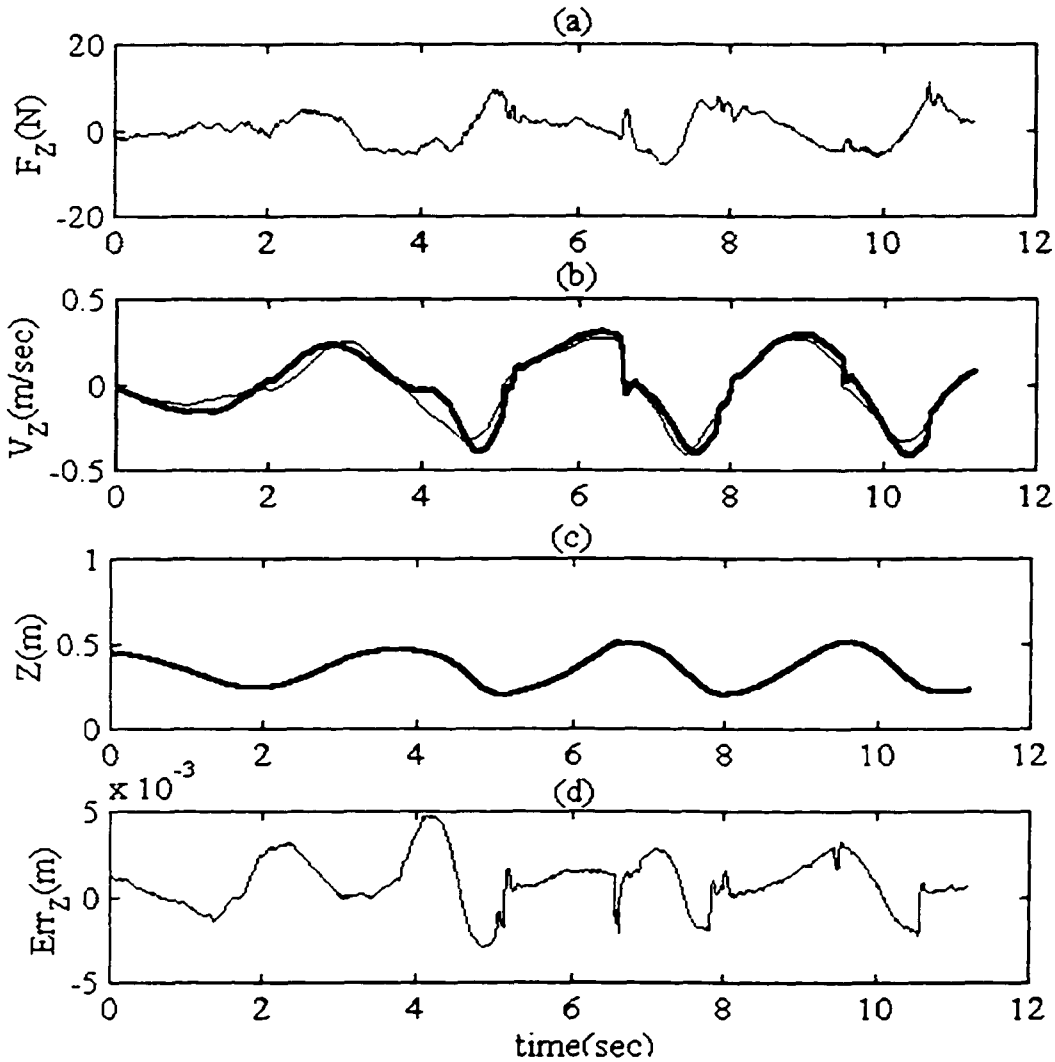

Figure 7.9 Dumbbell general motion, Z direction

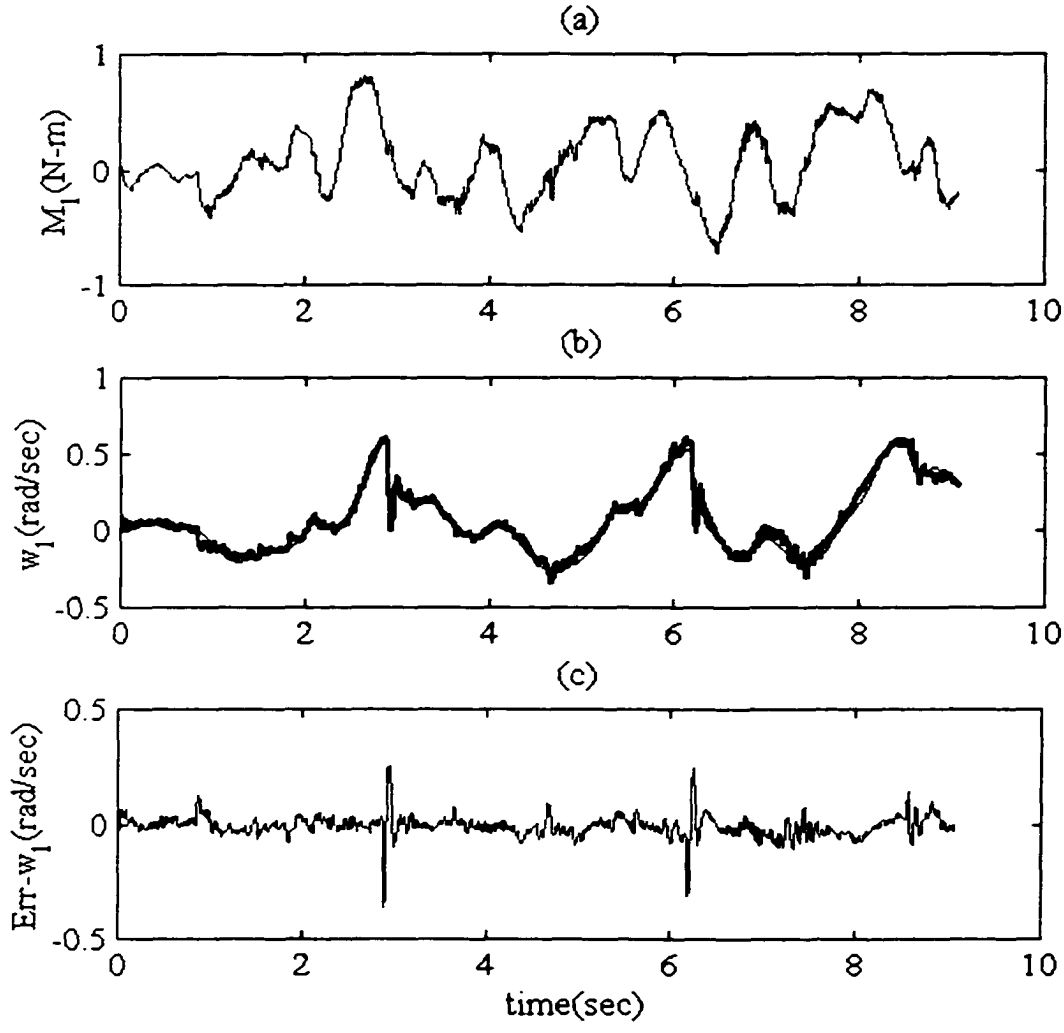

Figure 7.10 Dumbbell general angular motion, X direction

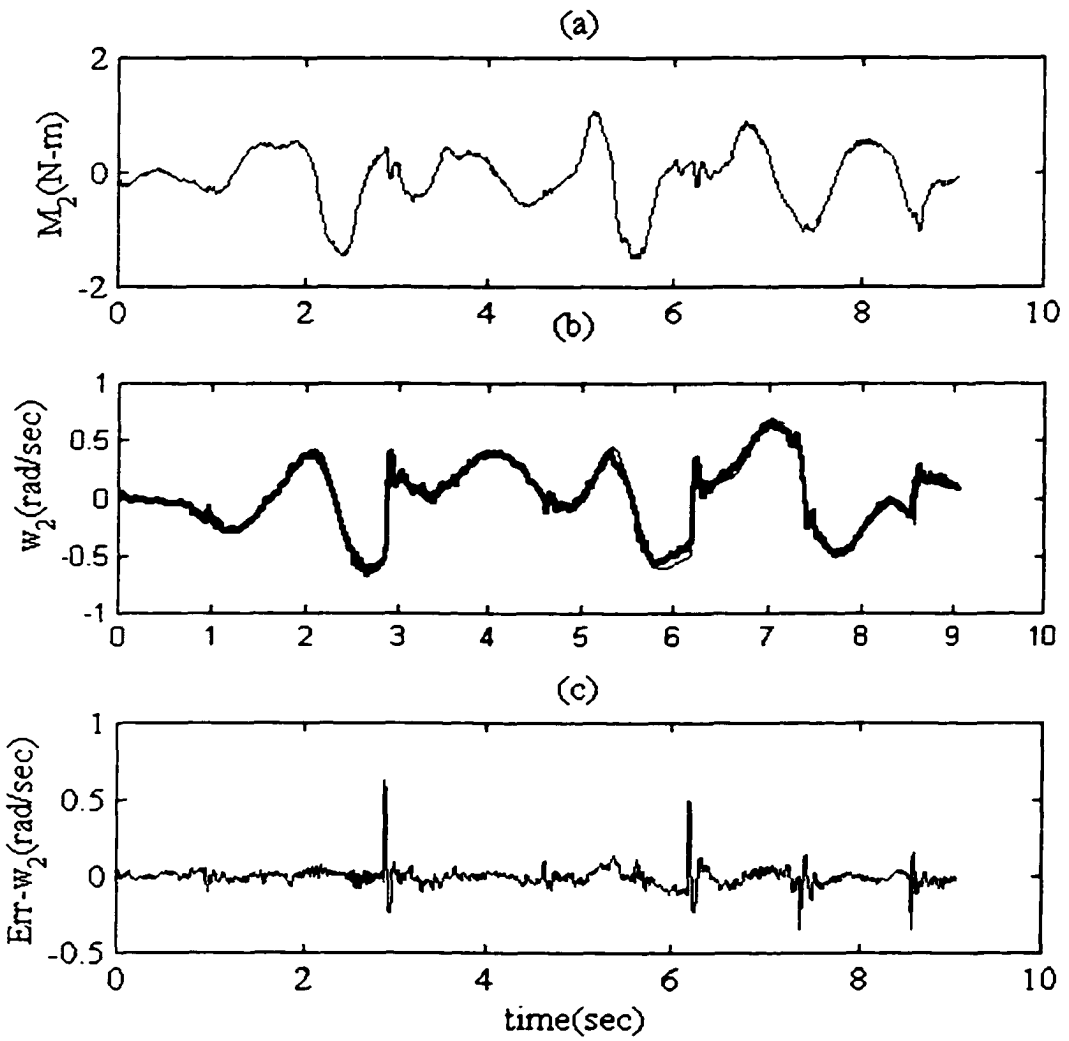

Figure 7.11 Dumbbell general angular motion, Y direction

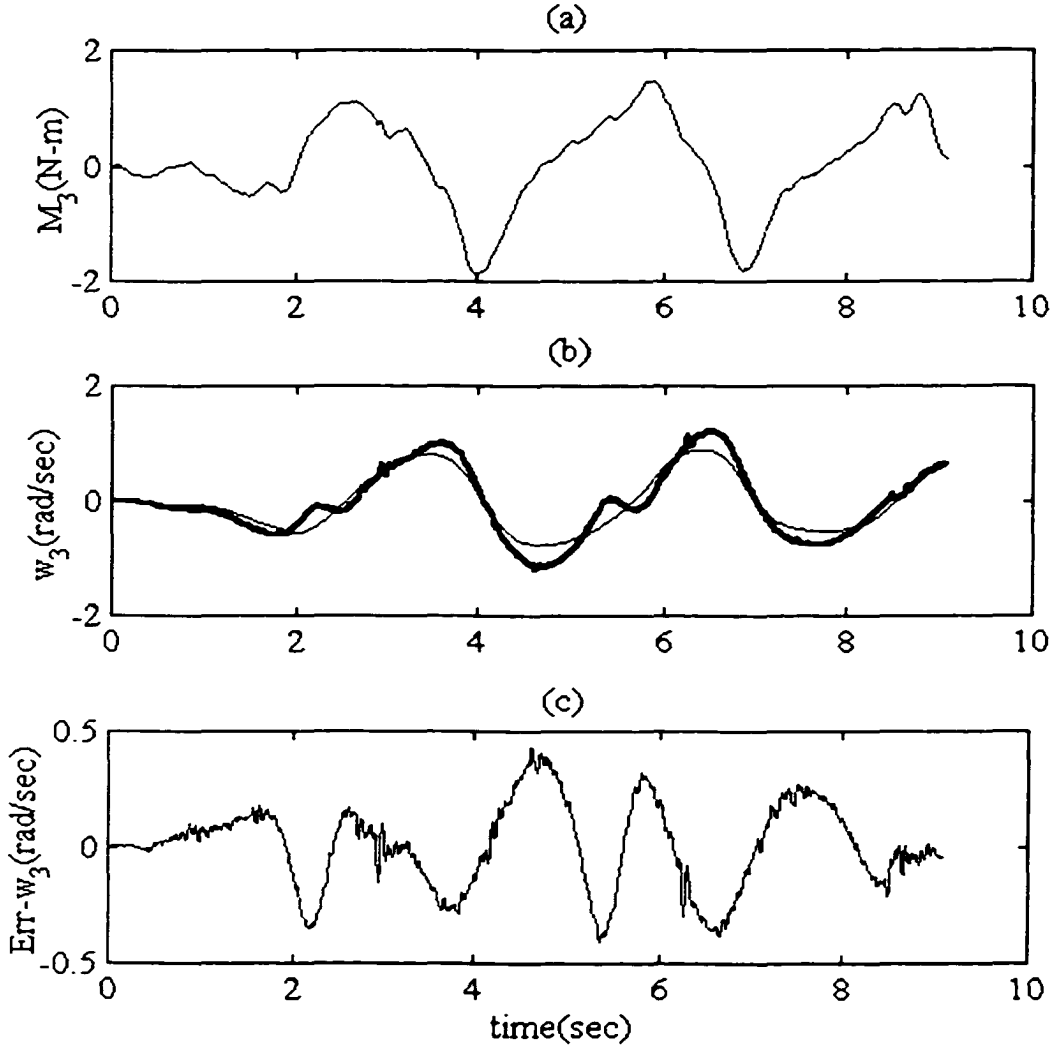

Figure 7.12 Dumbbell general angular motion, Z direction

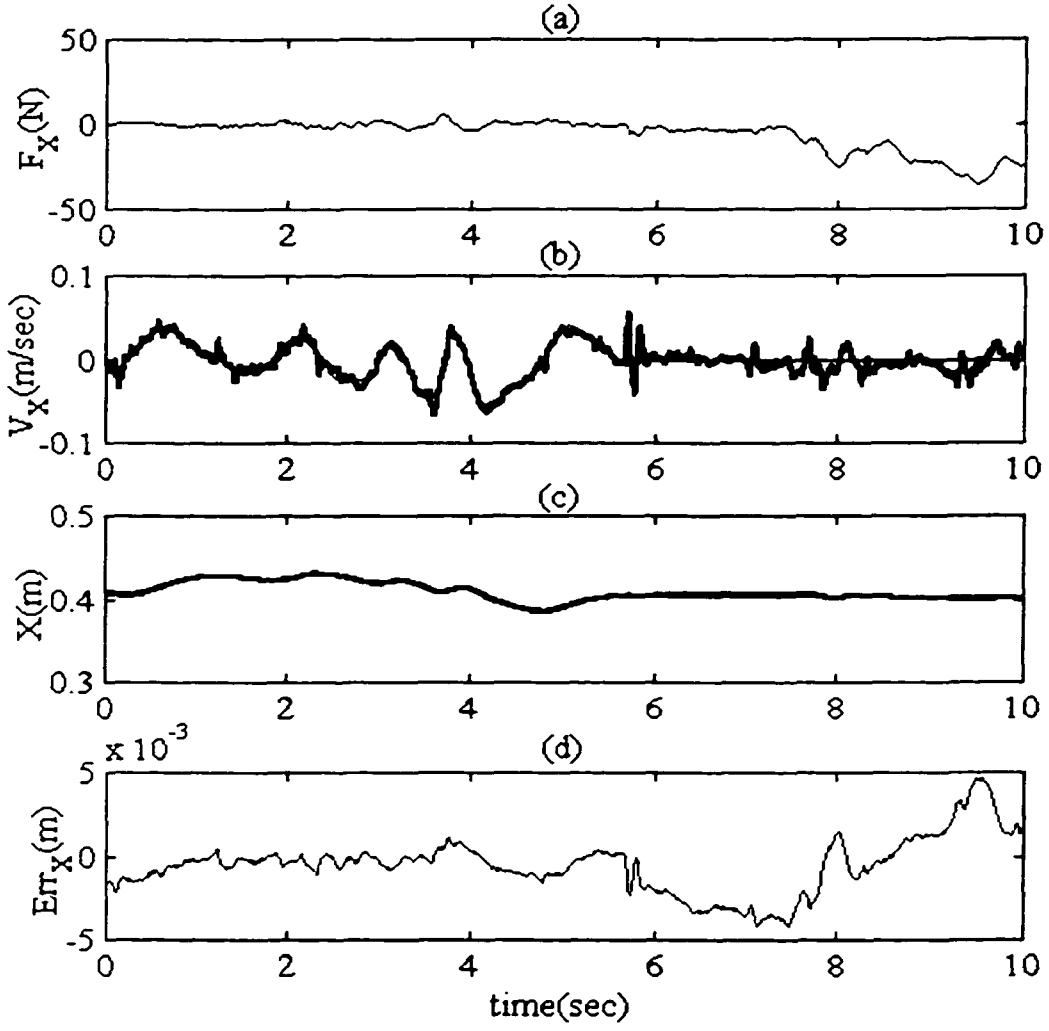

Figure 7.13 Dumbbell X-direction cartesian motion, rolling constraint

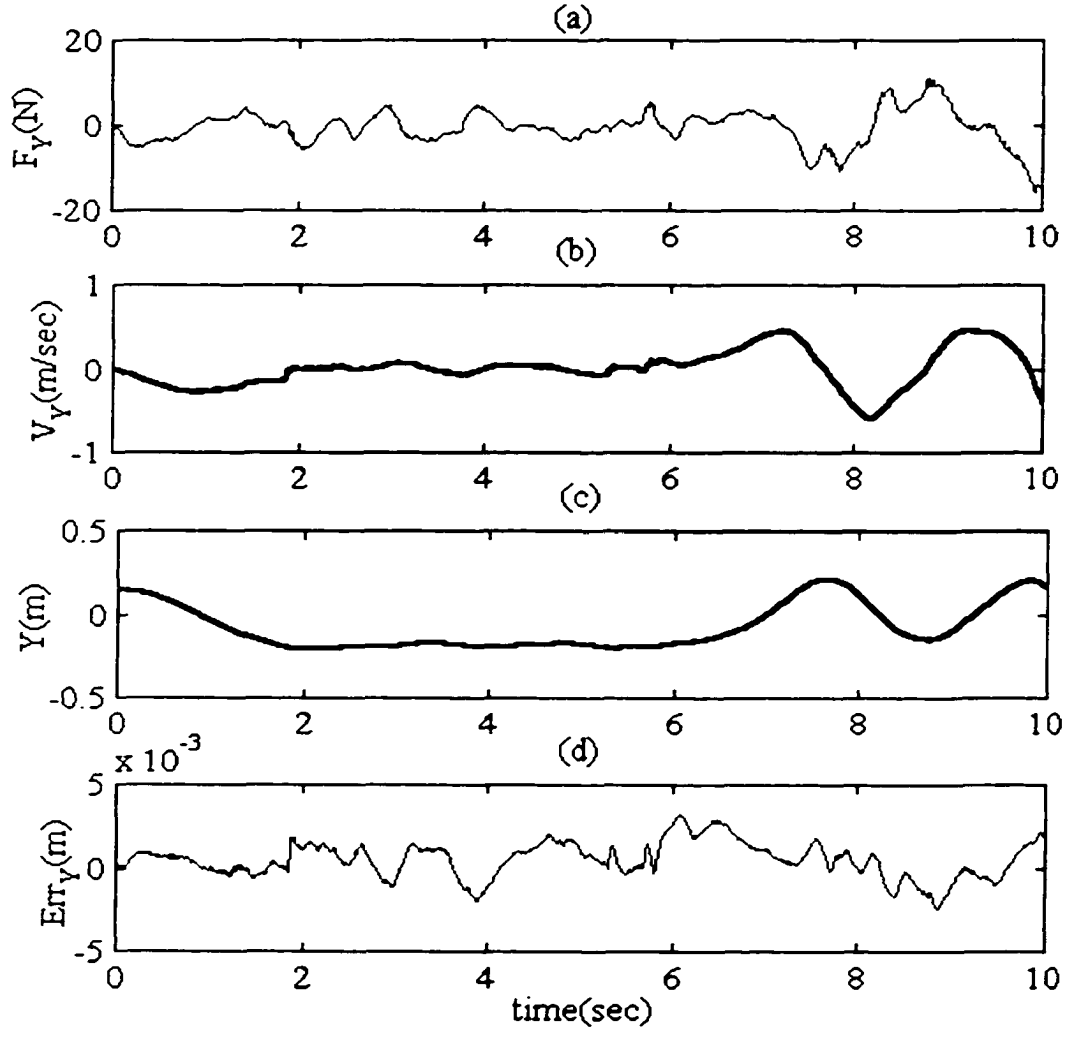

Figure 7.14 Dumbbell Y-direction cartesian motion, rolling constraint

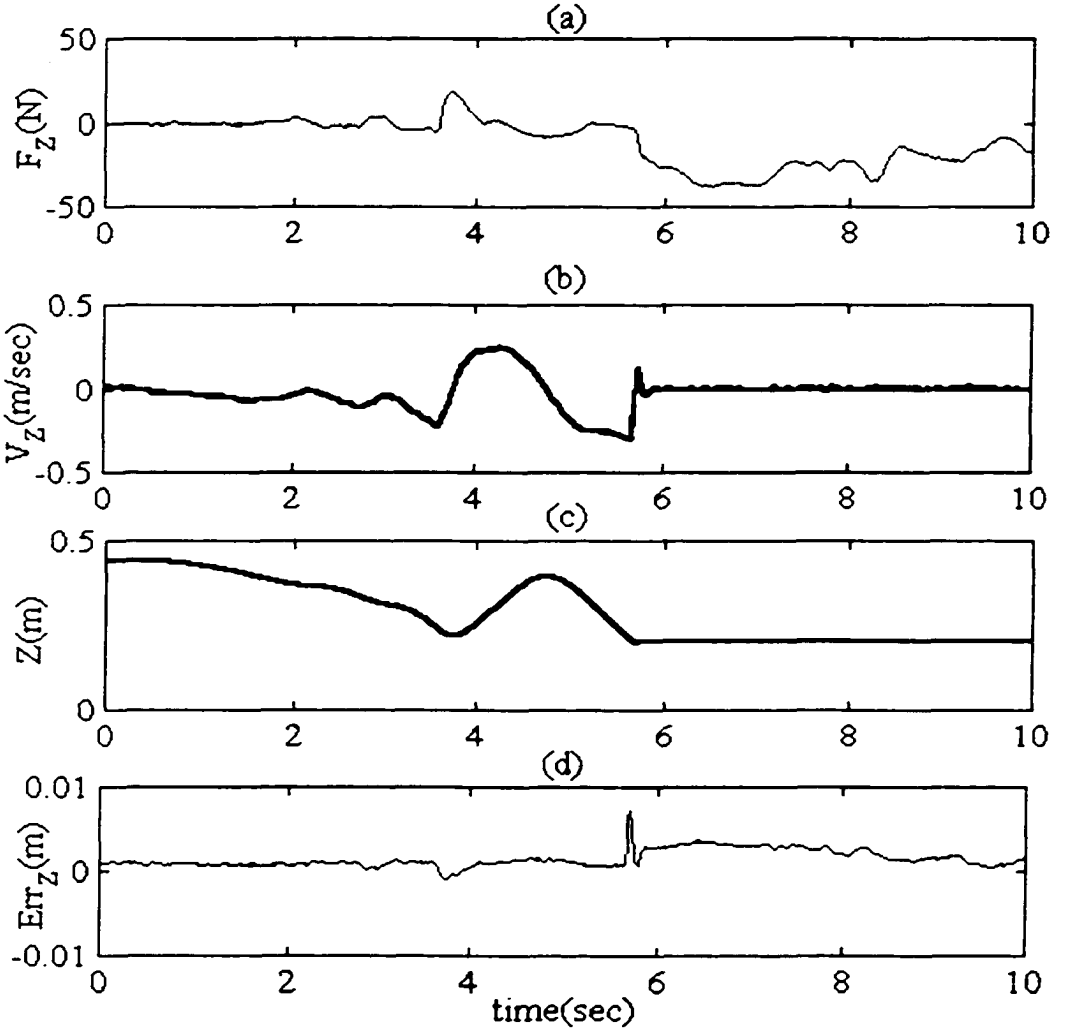

Figure 7.15 Dumbbell Z-direction cartesian motion, rolling constraint

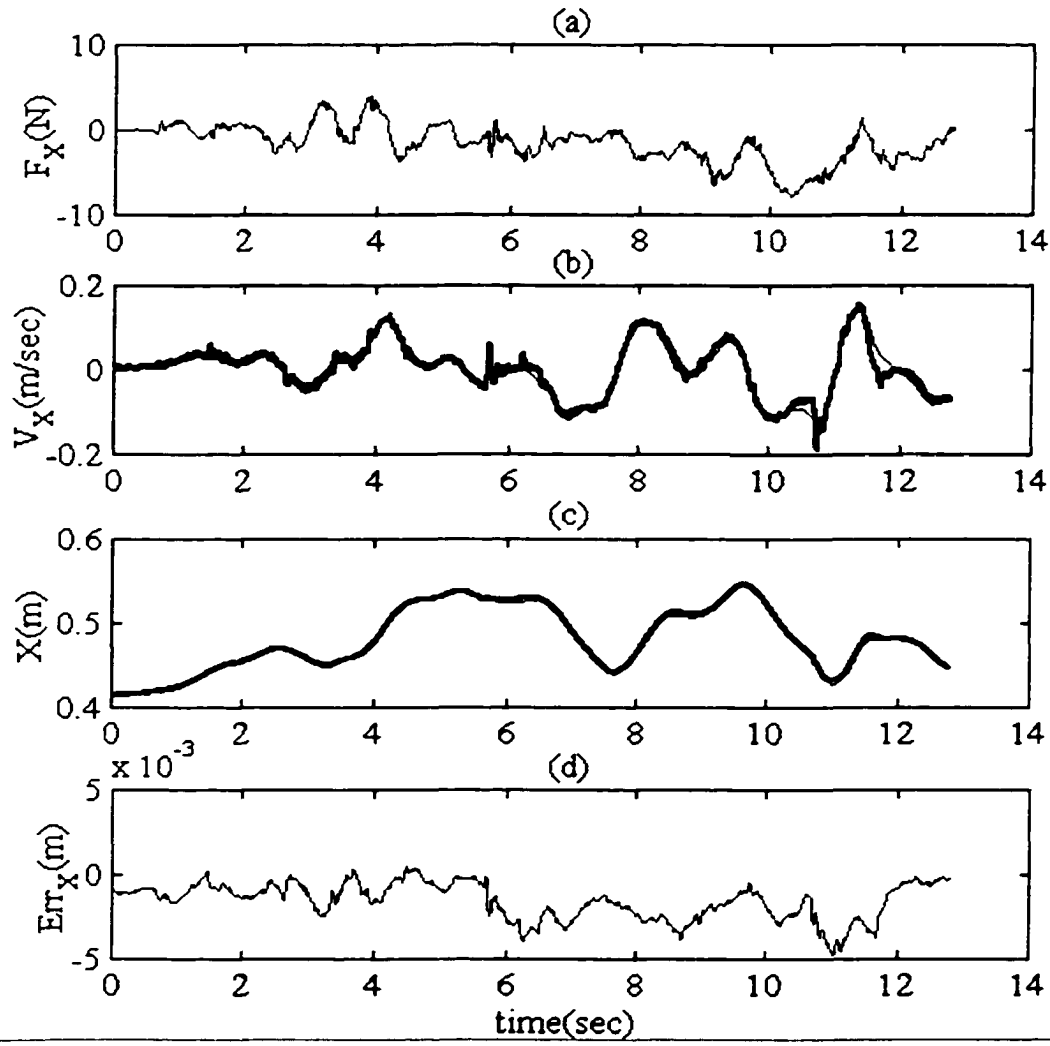

Figure 7.16 Dumbbell X-direction cartesian motion, rolling constraint

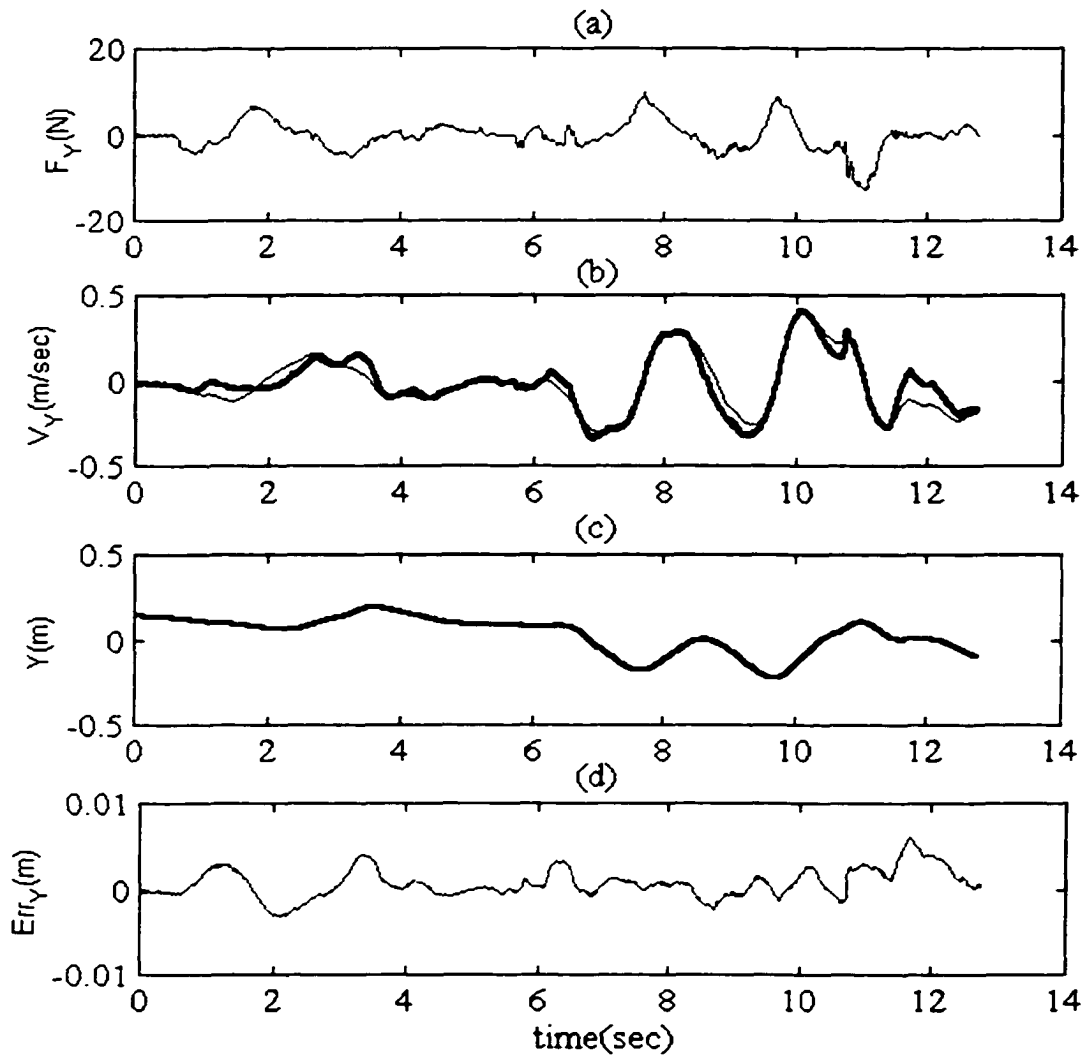

Figure 7.17 Dumbbell Y-direction cartesian motion, rolling constraint

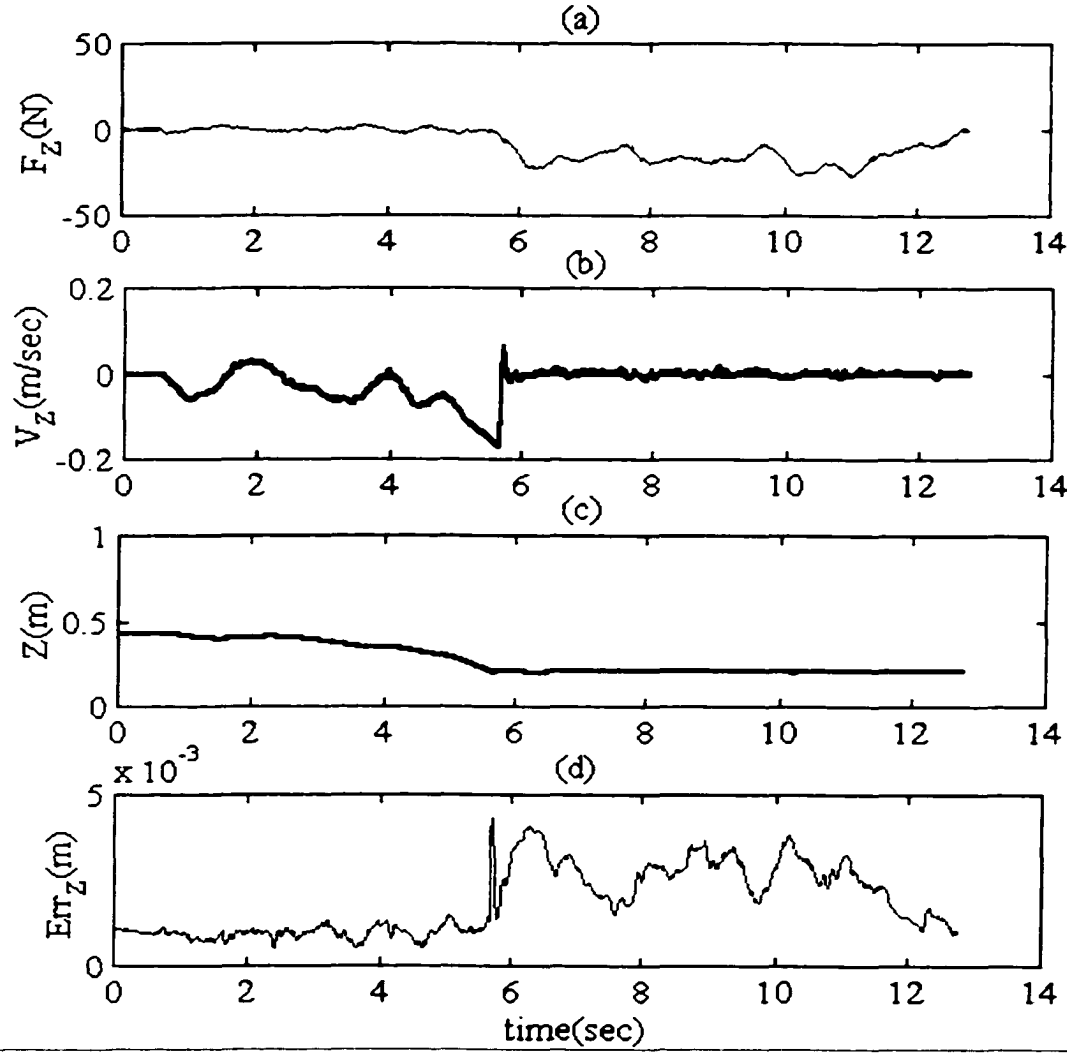

Figure 7.18 Dumbbell Z-direction cartesian motion, rolling constraint

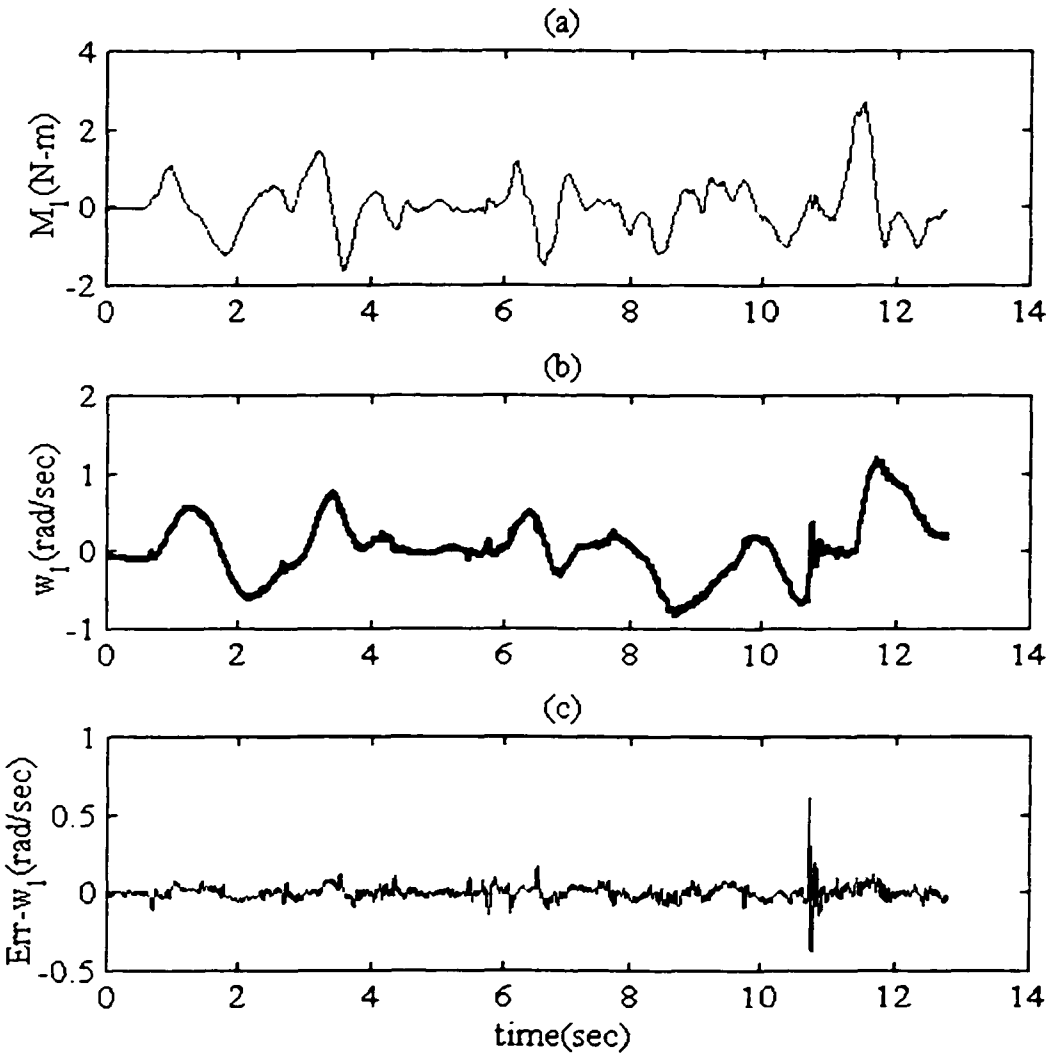

Figure 7.19 Dumbbell orientation, rolling constraint

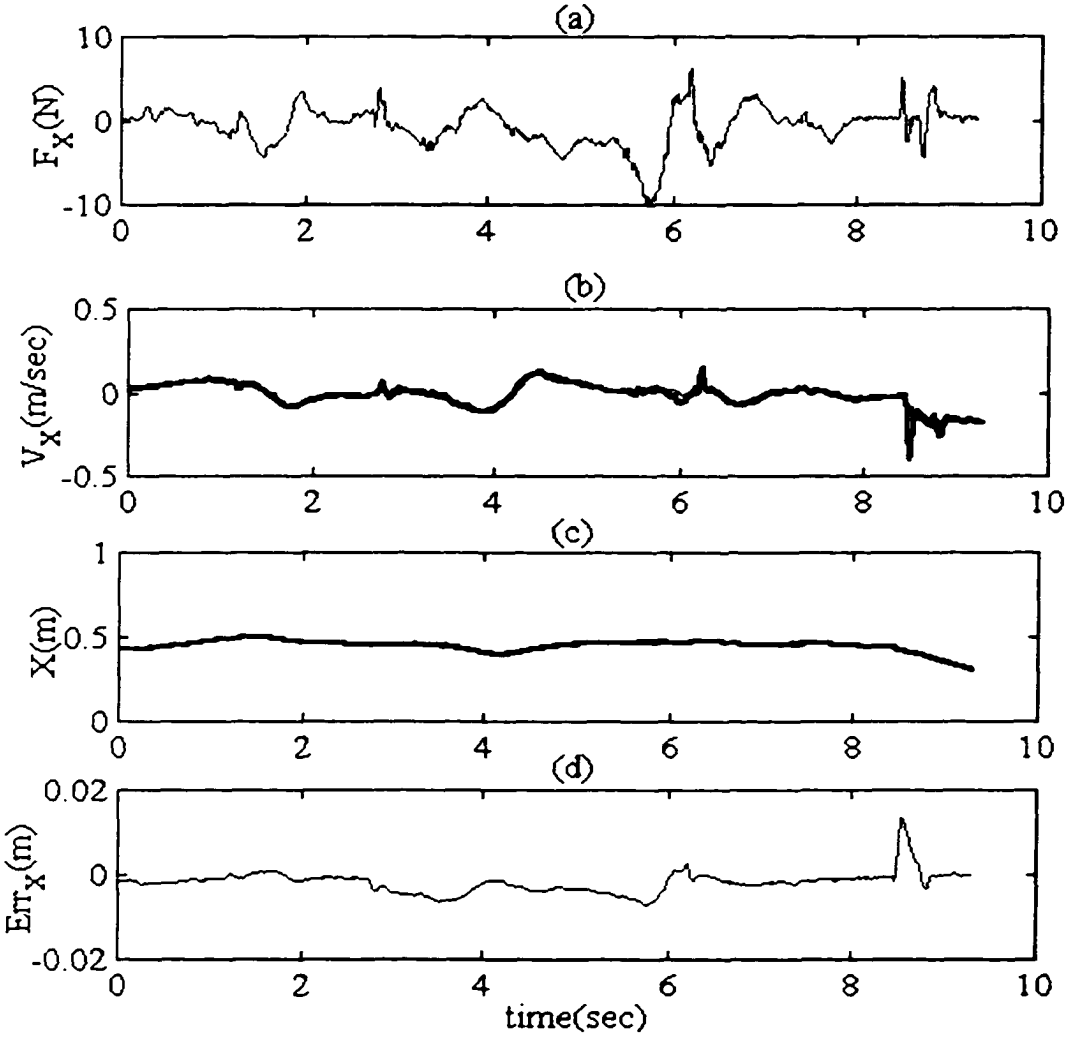

Figure 7.20 Dumbbell X-direction cartesian motion, rolling constraint

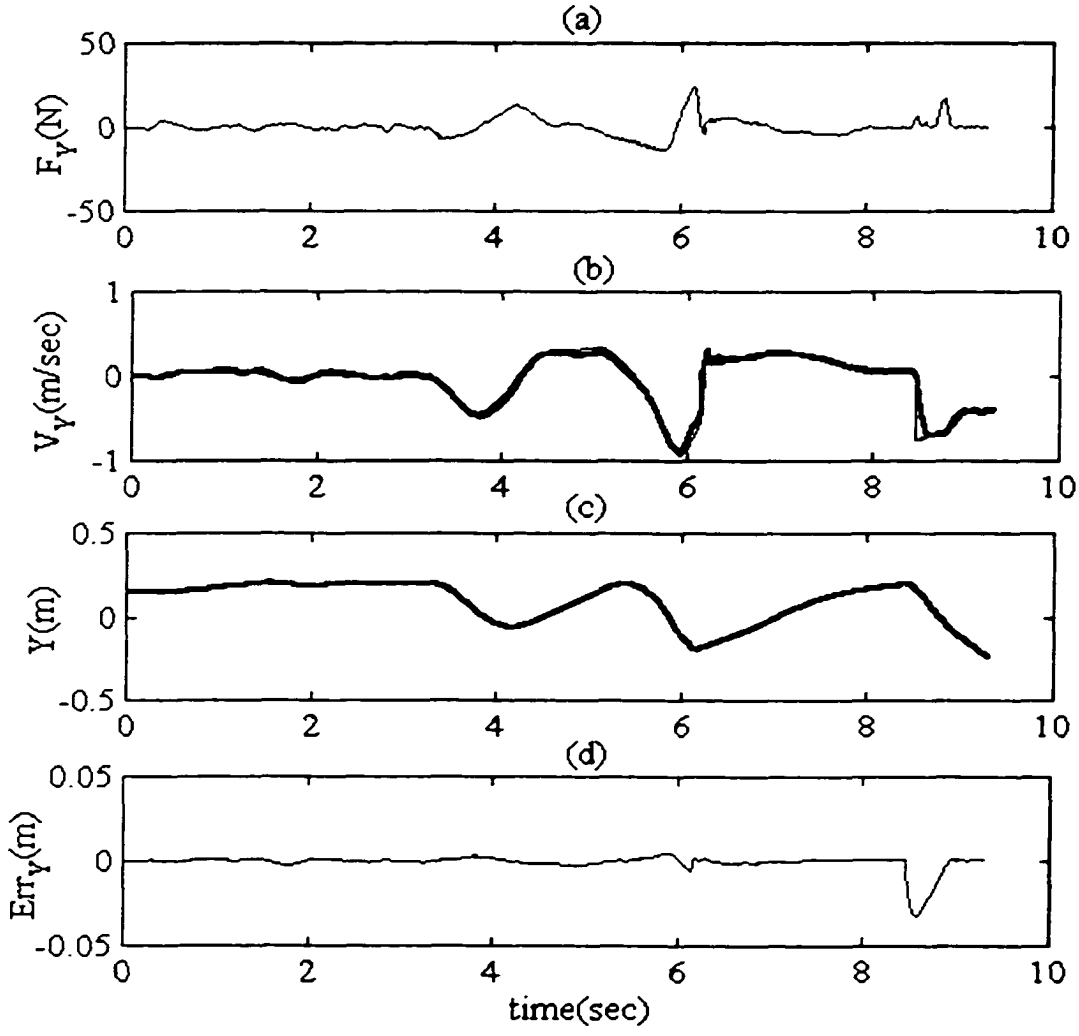

Figure 7.21 Dumbbell Y-direction cartesian motion, rolling constraint

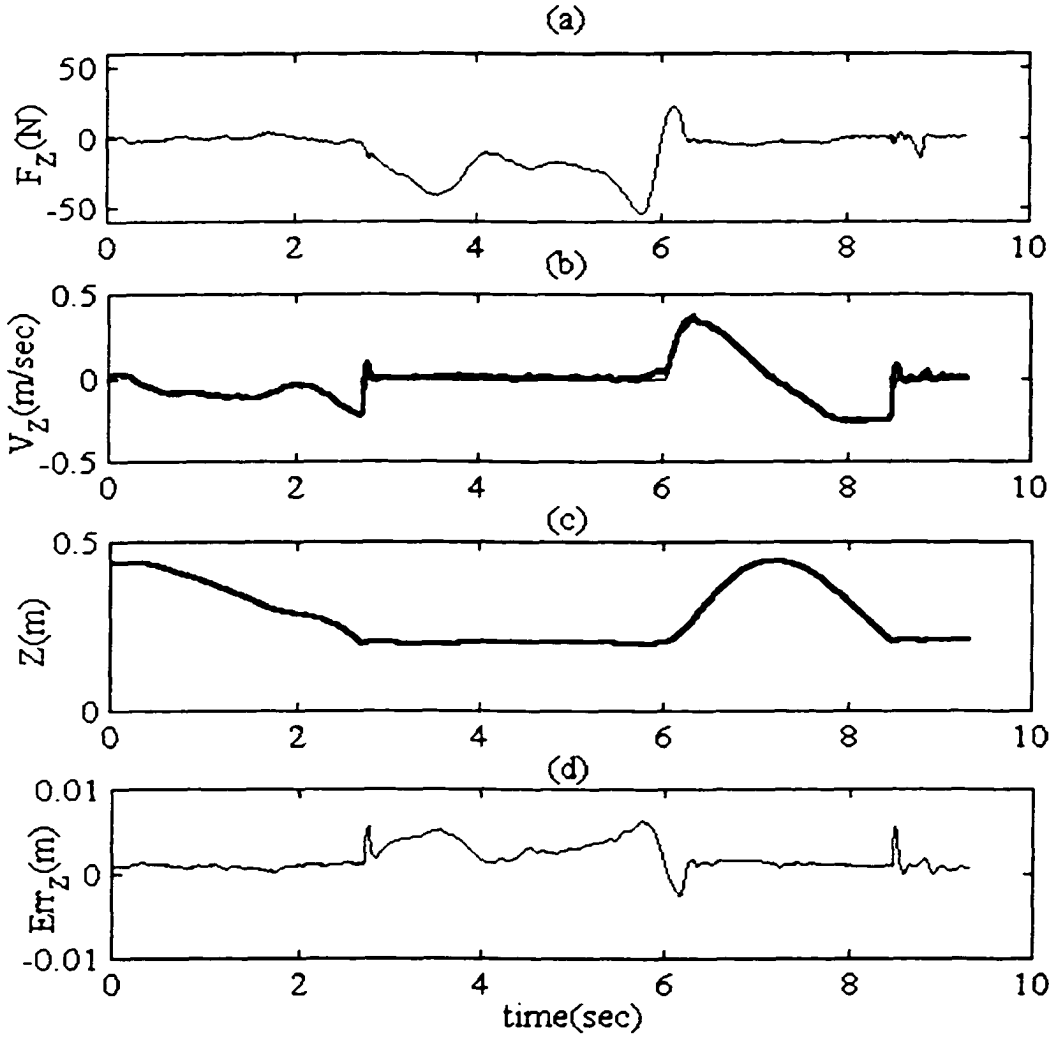

Figure 7.22 Dumbbell Z-direction cartesian motion, rolling constraint

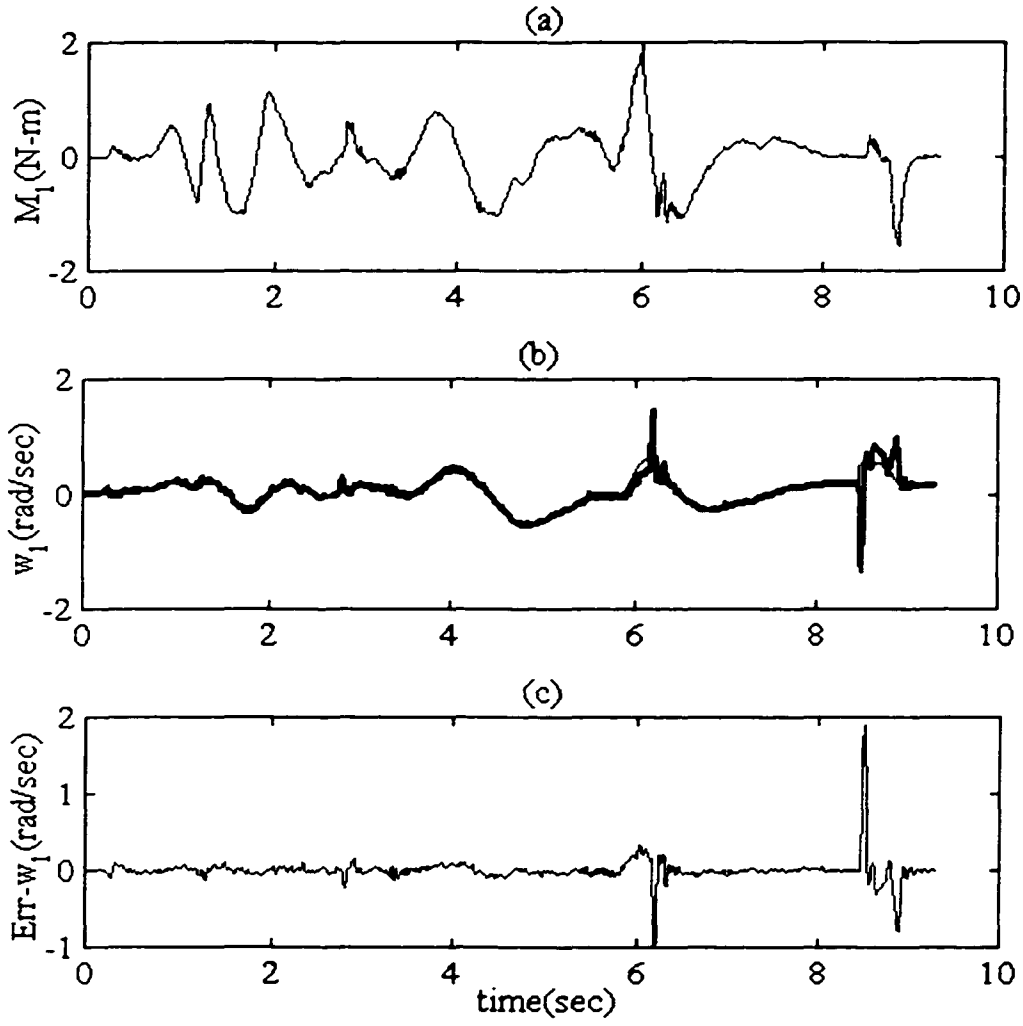

Figure 7.23 Dumbbell orientation, rolling constraint

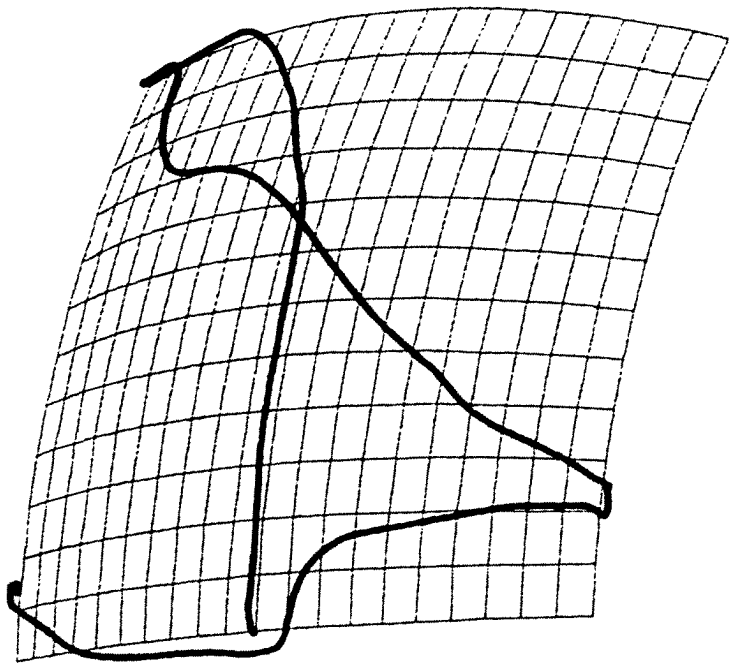

Figure 7.24 Constraint motion

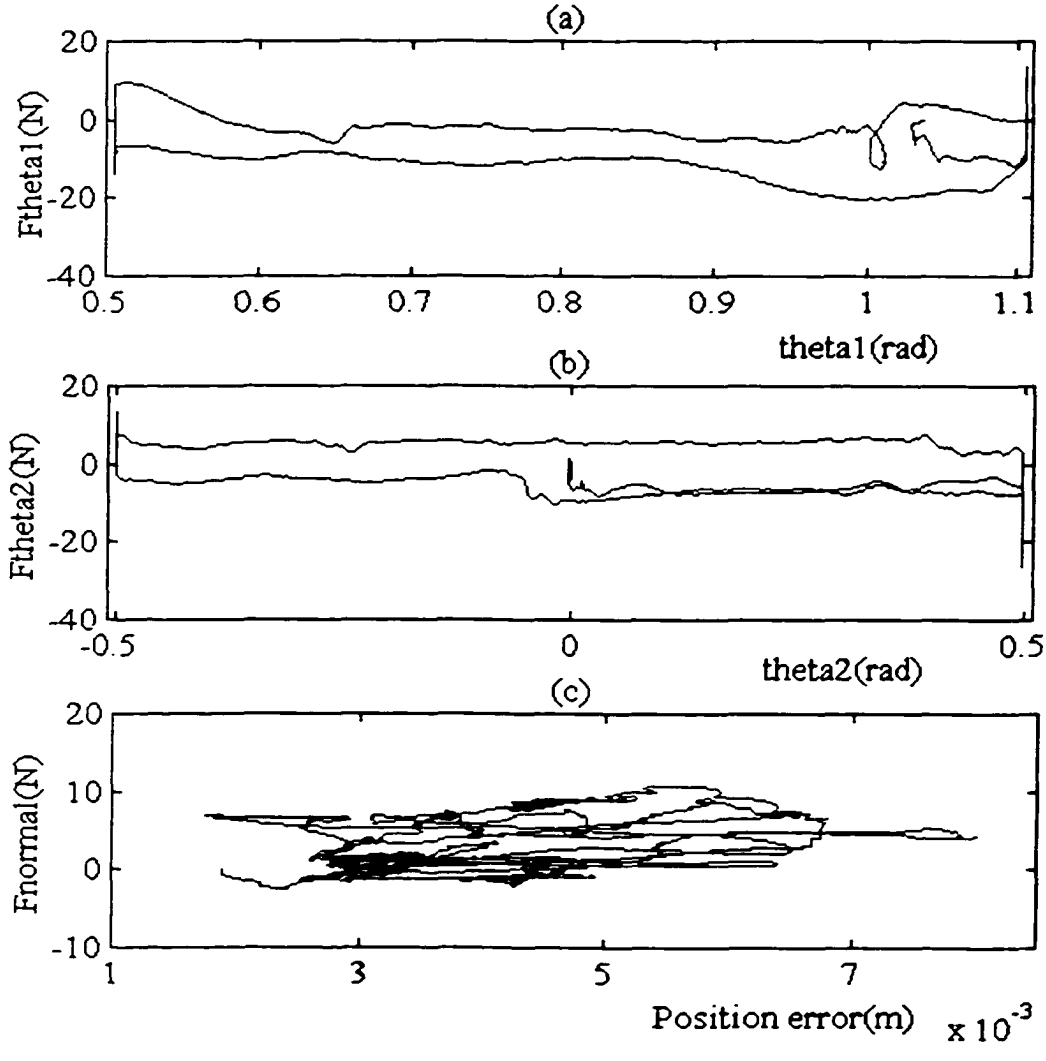

Figure 7.25 Total forces

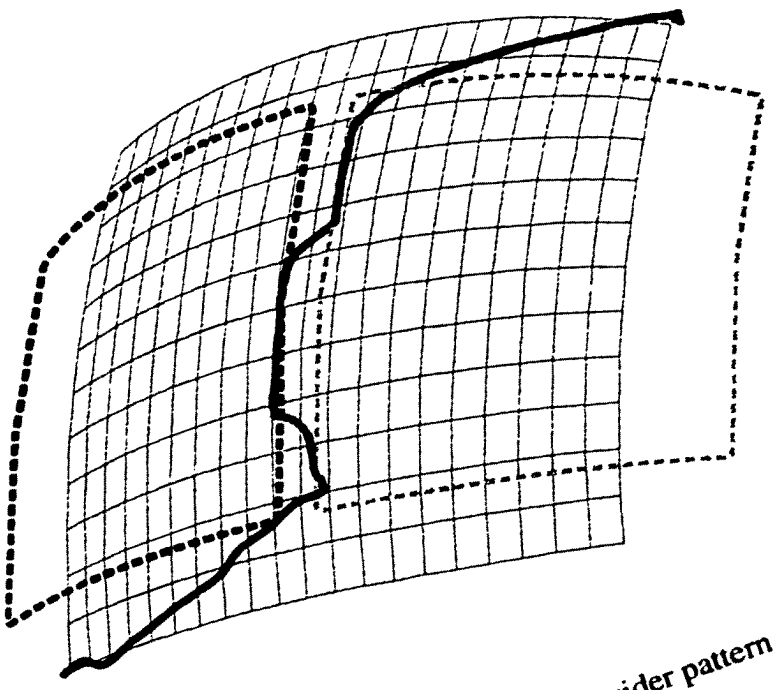

Figure 7.26 Shift mechanism, wider pattern

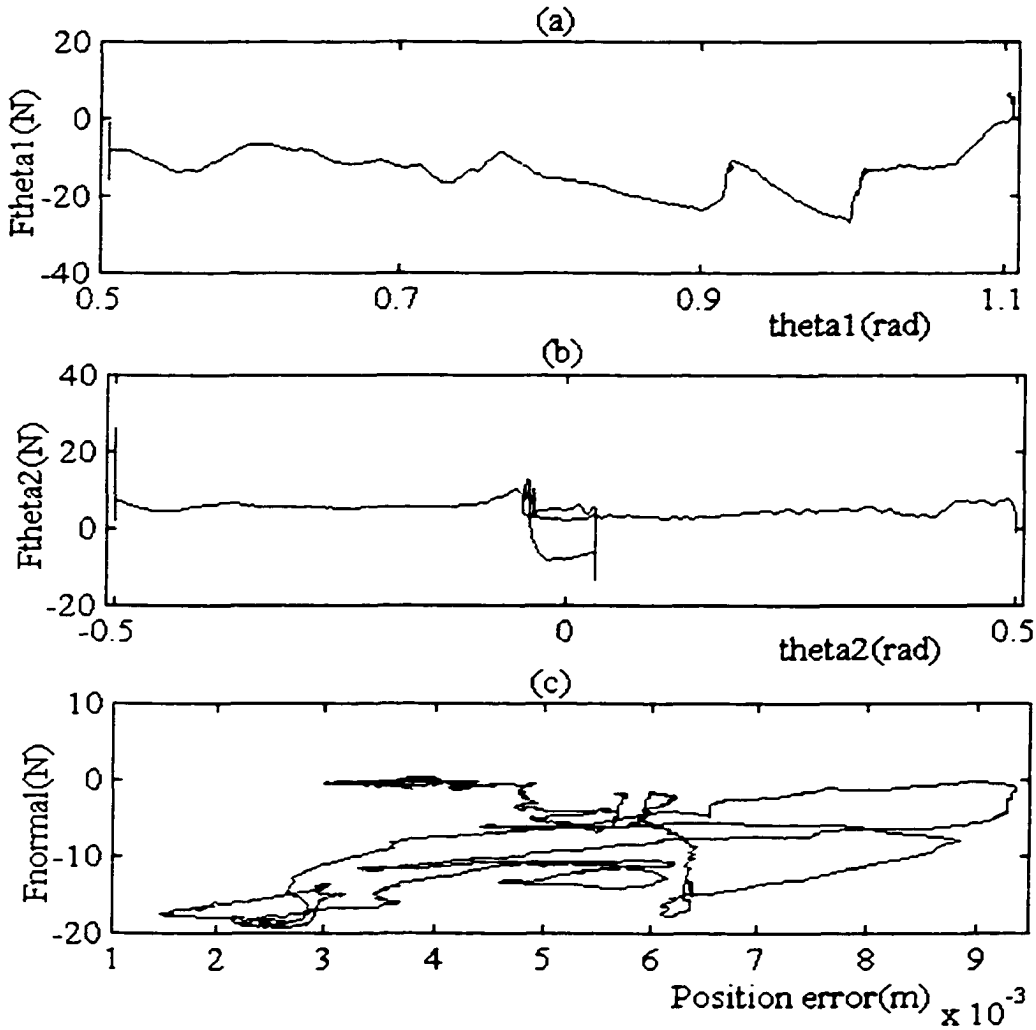

Figure 7.27 Total forces

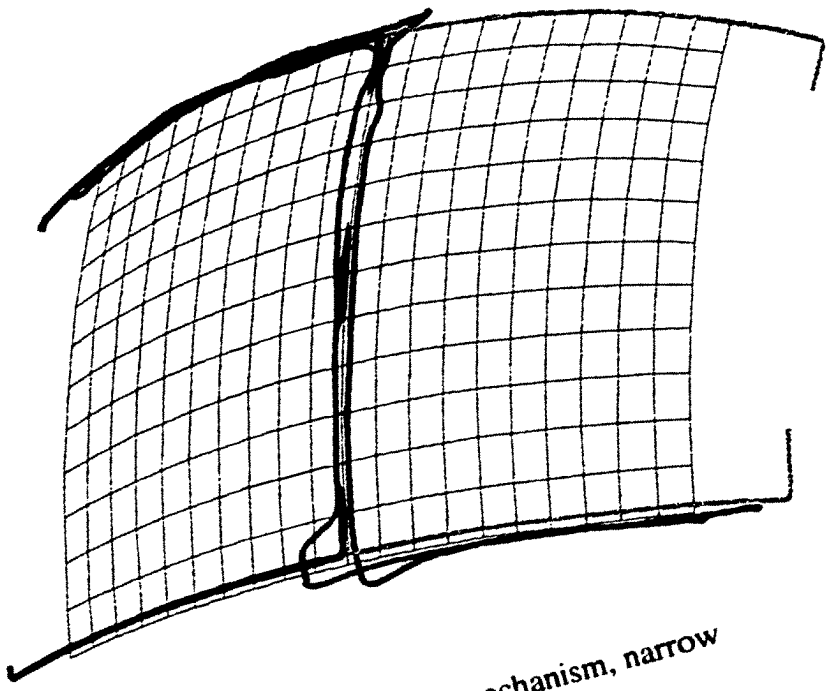

Figure 7.28 Shift mechanism, narrow

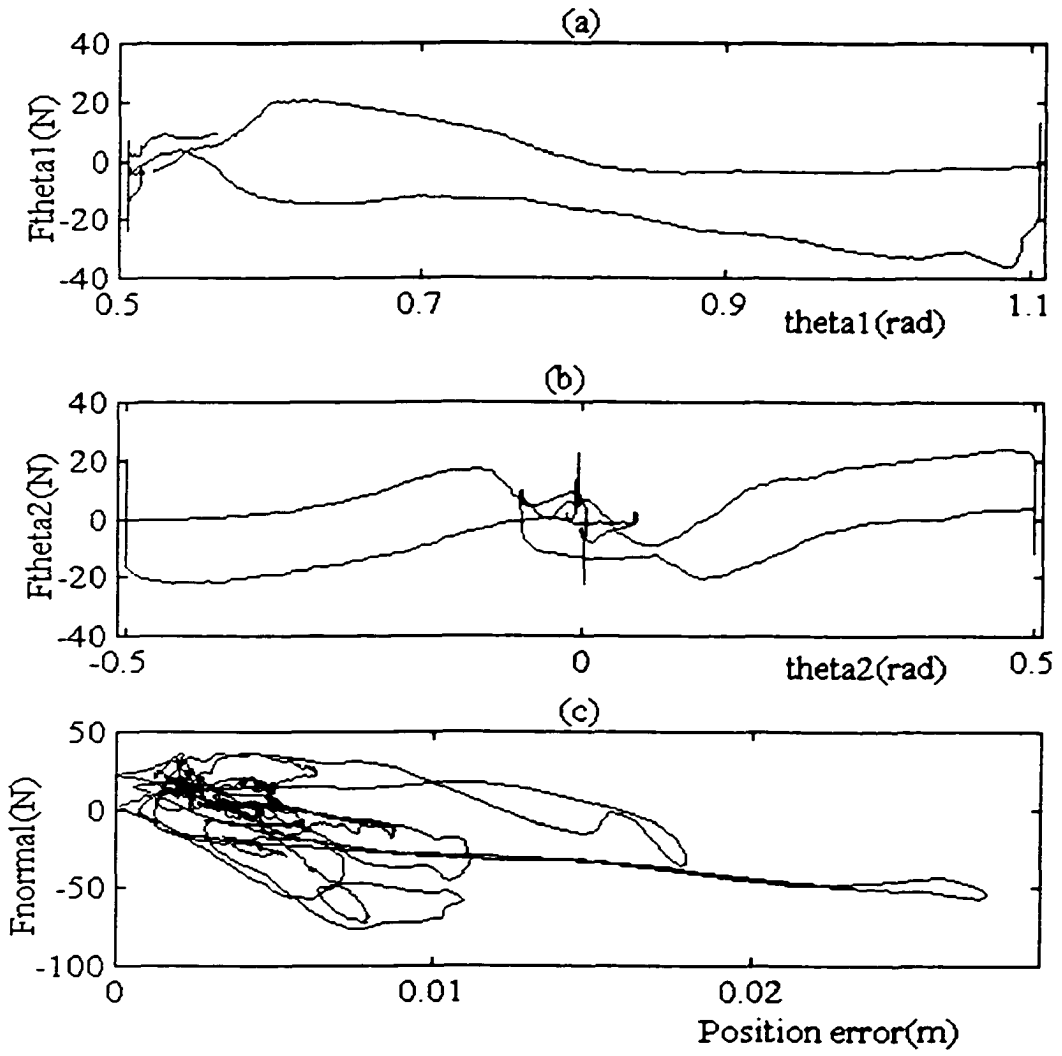

Figure 7.29 Total forces

8. CONCLUSIONS

The purpose of this dissertation is to demonstrate two approaches to design of haptic interactions for realistic and stable applications. This dissertation presents a study of both impedance based and admittance based virtual tools for haptic interactions. The impedance approach uses constraints based on a virtual mechanism to guide motion in the virtual environment. The admittance approach uses a dynamic model including nonholonomic constraints to predict motion in the virtual world. Both methods make use of a PUMA 560 industrial manipulator as the physical haptic display device. In both approaches, the user is able to physically touch and interact with the virtual environment in a realistic manner.

A general robotic manipulator has been shown to be an effective haptic interface device to design haptic interactions. The user is mechanically coupled with the robotic device by means of a handle so he or she may exert forces and torques to manipulate and interact with the virtual environment. The user is provided both force and torque feedback from the virtual environment to feel changes made as a result of the interaction.

A two degree-of-freedom virtual manipulator is chosen to demonstrate a solution for haptic interaction using kinematic redundancy. The coupling of a six degree-of-freedom robot with a two degree-of-freedom manipulator is studied in designing an optimal controller to accomplish stable interactions. The motion of the robot is constrained to present motions on a skewed three dimensional plane. The motion is also further constrained on this plane to study unilateral constraints.

The haptic interaction applications using dynamic systems that can provide both force and torque feedback to the user has been lacking in literature, and this study aims partly at providing a small effort in this direction.

8.1 Results

A dumbbell is modeled as a multibody system to design dynamic virtual interactions. Experimental results are presented to show both force and torque interactions. The dumbbell is used to present both stiff wall effects and rolling motion constraints. The rolling constraints are handled by employing non-holonomic constraints derived by the use of the Kane's method. The introduction of the Kane's method to design haptic interactions has been shown to be very effective, especially when dealing with non-holonomic constraints. Experimental results are shown to illustrate how the two wheels come in contact with a surface and the rolling motion suddenly starts. Then, the dumbbell is lifted to remove rolling motion constraints. The consecutive contact with the surface uses the initial velocity characteristics of the wheels to accelerate the motion.

An optimal impedance type controller is designed to handle system redundancies encountered when two manipulators with different number of degrees-of-freedom are kinematically coupled. The results include a proof of stability based on this newly developed optimal controller. A two degree-of-freedom manipulator is designed to test this controller. Experimental results show stable haptic interactions, thus the theoretical proof is justified.

A shift mechanism is employed using a two-degree-of-freedom virtual manipulator. The problems associated with motions around corners are studied and a method which uses Lame curves is designed to handle this problem. Experimental results show how the motions constrained on a skewed plane can be further constrained to present a shift pattern. The shift is designed to be the handle attached at the end effector of the robotic manipulator. Two case studies are presented. Experimental results show how the shift mechanism are used to present both a wide and a narrow shift pattern.

8.2 Major contributions

The work presented in this dissertation uses both kinematic and dynamic based virtual manipulators as virtual simulators to address problems associated in both free and constrained motions. The results are expected to improve on the current haptic display technology by a new type of optimal position controller and better algorithms to handle both holonomic and non-holonomic constraints.

Major contributions include:

- Development of an approach to dynamic simulation for use in interactive haptic display that include multibody systems and switching constraints,
- Development of a control system using kinematic coupling between a virtual manipulator and the haptic display device to impose motion constraints and the virtual interactions,
- Development of proof of stability for the kinematic approach that guides the details of the implementation of the control law,

- Implementation of both haptic display simulations in an experimental interaction system that allows for the evaluation of the performance of the haptic interaction. Both implementations are general enough to allow researchers with any six degree-of-freedom robot to apply the approaches and continue in this area of research.

8.3 Future research

The experimental and the theoretical results presented in this work provide many directions for future research in the design and the implementations of haptic interactions.

Future work includes the implementation of the admittance control to simulate interactions of multibody systems with other dynamic objects in the virtual environment. More complex and realistic collision detection algorithms must also be developed in this application. Friction may be added in designing the simulation of contact motions.

The optimal position controller developed in this work may be applied to higher degree-of-freedom virtual manipulators to generate forces that simulate kinematic constraints. Theoretical work in identifying general conditions for asymptotic stability of this controller is needed. Including friction or using a dynamic model of the virtual manipulator can improve the quality of the interaction by the user.

APPENDIX

PUMA 560 MANIPULATOR KINEMATICS AND DYNAMICS:

The transformation describing the end effector frame with respect to the base frame is

$$ {}^{0}_{6}T = \begin{bmatrix} r_{11} & r_{12} & r_{13} & x_1 \\ r_{21} & r_{22} & r_{23} & x_2 \\ r_{31} & r_{32} & r_{33} & x_3 \\ 0 & 0 & 0 & 1 \end{bmatrix} $$

where

$$ x_1 = (s_{23}l_4 + c_2l_1 + c_{23}l_3)c_1 - s_1l_2 $$
$$ x_2 = (s_{23}l_4 + c_2l_1 + c_{23}l_3)s_1 + c_1l_2 $$
$$ x_3 = -s_{23}l_3 + c_{23}l_4 - s_2l_1 $$

$$ r_{11} = (-c_{23}s_4s_6 - s_{23}s_5c_6 + c_{23}c_4c_5c_6)c_1 - s_1c_4s_6 - s_1s_4c_5c_6 $$
$$ r_{12} = (-c_{23}s_4c_6 + s_{23}s_5s_6 - c_{23}c_4c_5s_6)c_1 - s_1c_4c_6 + s_1s_4c_5s_6 $$
$$ r_{13} = (c_{23}c_4s_5 + s_{23}c_5)c1 - s_1s_4s_5 $$
$$ r_{21} = (-c_{23}s_4s_6 - s_{23}s_5c_6 + c_{23}c_4c_5c_6)s_1 + c_1s_4c_5c_6 + c_1c_4s_6 $$
$$ r_{22} = (-c_{23}s_4c_6 + s_{23}s_5s_6 - c_{23}c_4c_5s_6)s_1 - c_1s_4c_5s_6 + c_1c_4c_6 $$
$$ r_{23} = (c_{23}c_4s_5 + s_{23}c_5)s_1 + c_1s_4s_5 $$
$$ r_{31} = -s_{23}c_4c_5c_6 + s_{23}s_4s_6 - c_{23}s_5c_6 $$
$$ r_{32} = s_{23}c_4c_5s_6 + s_{23}s_4c_6 + c_{23}s_5s_6 $$
$$ r_{33} = -s_{23}c_4s_5 + c_{23}c_5 $$

where $s_i = \sin(q_i)$ and $c_i = \cos(q_i)$ for $i = 1,2,3,4,5,6$.

The total velocity of the end effector in the end effector frame is given by

$$ {}^{R}\dot{x}_r = J_r\dot{\theta} $$

where the nonzero elements of J_r are

$$
\begin{aligned}
J_{r11} &= c_5 * c_6 * [-c_{23} * c_4 * l_2 + (c_2 * l_1 + c_{23} * l_3 + s_{23} * l_4) * s_4] \\
&\quad + s_6 * [c_{23} * s_4 * l_2 + (c_2 * l_1 + c_{23} * l_3 + s_{23} * l_4) * c_4] + s_5 * c_6 * s_{23} * l_2 \\
J_{r12} &= (c_4 * c_5 * c_6 - s_4 * s_6) * (s_3 * l_1 + l_4) + s_5 * c_6 * (c_3 * l_1 + l_3) \\
J_{r13} &= (c_4 * c_5 * c_6 - s_4 * s_6) * l_4 + s_5 * c_6 * l_3
\end{aligned}
$$

$$
\begin{aligned}
J_{r21} &= -c_5 s_6 \left(- c_{23} c_4 l_2 + (c_2 l_1 + c_{23} l_3 + s_{23} l_4) s_4\right) + c_6 \left(c_{23} s_4 l_2 + (c_2 l_1 + c_{23} l_3 + s_{23} l_4) c_4\right) - s_5 s_6 s_{23} l_2 \\
J_{r22} &= -(c_4 c_5 s_6 + s_4 c_6)(s_3 l_1 + l_4) - s_5 s_6 (c_3 l_1 + l_3) \\
J_{r23} &= -(c_4 c_5 s_6 + s_4 c_6) l_4 - s_5 s_6 l_3
\end{aligned}
$$

$$
\begin{aligned}
J_{r31} &= s_5 * [-c_{23} * c_4 * l_2 + (c_2 * l_1 + c_{23} * l_3 + s_{23} * l_4) * s_4] - c_5 * s_{23} * l_2 \\
J_{r32} &= c_4 * s_5 * (s_3 * l_1 + l_4) - c_5 * (c_3 * l_1 + l_3) \\
J_{r33} &= c_4 * s_5 * l_4 - c_5 * l_3
\end{aligned}
$$

$$
\begin{aligned}
J_{r41} &= -s_{23}(c_4 c_5 c_6 - s_4 s_6) - c_{23} s_5 c_6 \\
J_{r42} &= c_4 s_6 + s_4 c_5 c_6 \\
J_{r43} &= c_4 s_6 + s_4 c_5 c_6 \\
J_{r44} &= -s_5 c_6 \\
J_{r45} &= s_6
\end{aligned}
$$

$$
\begin{aligned}
J_{51}^{P/E} &= s_{23} * (c_4 * c_5 * s_6 + s_4 * c_6) + c_{23} * s_5 * s_6 \\
J_{52}^{P/E} &= c_4 * c_6 - s_4 * c_5 * s_6 \\
J_{53}^{P/E} &= c_4 * c_6 - s_4 * c_5 * s_6 \\
J_{54}^{P/E} &= s_5 * s_6 \\
J_{55}^{P/E} &= c_6
\end{aligned}
$$

$$J_{r61} = -s_{23} * c_4 * s_5 + c_{23} * c_5$$
$$J_{r62} = s_4 * s_5$$
$$J_{r63} = s_4 * s_5$$
$$J_{r64} = c_5$$
$$J_{r66} = 1$$

The dymamics of the robot is expressed by

$$H(q)\ddot{q} + C(q,\dot{q})\dot{q} + f_r\dot{q} + g(q) = \tau - {}^0_6J_r^T F_r^R$$

where

$$H_{11}=p_1+p_3cc_2+p_7ss_{23}+2p_5c_2s_{23}$$
$$H_{12}=p_4s_2+p_8c_{23}+p_9c_2$$
$$H_{13}=p_8c_{23}+p_{12}s_{23}$$
$$H_{22}=p_2+p_6+2p_5s_3$$
$$H_{23}=p_6+p_5s_3+p_{11}c_3$$
$$H_{33}=p_{20}+p_6$$
$$H_{34}=-p_{14}s_4s_5$$
$$H_{35}=p_{14}c_4c_5$$
$$H_{44}=p_{21}+p_{13}$$
$$H_{55}=p_{22}+p_{16}$$
$$H_{66}=p_{19}$$

$$C(q,\dot{q})\dot{q} = V$$

and

$$V_1=(p_4c_2-p_8s_{23}-p_9s_2)\dot{\theta}_2^2+(-p_8s_{23}+p_{12}c_{23})\dot{\theta}_3^2+(2(-p_3sc_2+p_5c_{223}+p_7sc_{23})+p_{10}c_{2233})\dot{\theta}_1\dot{\theta}_2$$
$$+(2(c2(p_5c_{23}-p_{11}s_{23})+p_7sc_{23})+p_{10}c_{2233})\dot{\theta}_1\dot{\theta}_3+(2(-s_4s_5(p_{14}sc_{23}+p_{15}c_2c_{23})+p_{17}c_4s_5))\dot{\theta}_1\dot{\theta}_4$$
$$+(2(p_{14}(-ss_{23}s_5+sc_{23}c_4c_5)+p_{15}c_2(-s_{23}s_5+c_{23}c_4c_5)+p_{17}s_4c_5))\dot{\theta}_1\dot{\theta}_5+2(-p_8s_{23}+p_{12}c_{23})\dot{\theta}_2\dot{\theta}_3$$

$$V_2=-((-p_3sc_2+p_5c_{223}+p_7sc_{23})+0.5p_{10}c_{2233})\dot{\theta}_1^2+(-p_{11}s_3+p_5c_3)\dot{\theta}_3^2+(s_{23}(p_{13}+p_{18}c_{44})+c_4s_5(-p_{14}c_{23}+2p_{15}s_2))\dot{\theta}_1\dot{\theta}_4$$
$$+(-c_{23}s_4(2p_{14}c_5+p_{16})+2p_{15}s_2s_4c_5)\dot{\theta}_1\dot{\theta}_5+2(-p_{11}s_3+p_5c_3)\dot{\theta}_{21}\dot{\theta}_3-2p_{15}c_3s_4s_5\dot{\theta}_2\dot{\theta}_4$$
$$+2(-p_{14}s_5+p_{15}(c_3c_4c_5-s_3s_5))\dot{\theta}_2\dot{\theta}_5-2p_{15}c_3s_4s_5\dot{\theta}_3\dot{\theta}_4+2(-p_{14}s_5+p_{15}(c_3c_4c_5-s_3s_5))\dot{\theta}_3\dot{\theta}_5$$

$$V_3=(-p_8s_{23}+p_{12}c_{23})\dot{\theta}_1^2-(-p_{11}s_3+p_5c_3)\dot{\theta}_2^2+(-p_{14}c_4s_5)(\dot{\theta}_4^2+\dot{\theta}_5^2)+(2p_{14}c_{23}c_4c_5+s_{23}(p_{13}+p_{18}cc_4))\dot{\theta}_1\dot{\theta}_4$$
$$-c_{23}s_4(p_{14}c_5+p_{16})\dot{\theta}_1\dot{\theta}_5-2p_{14}s_5(\dot{\theta}_2\dot{\theta}_5+\dot{\theta}_3\dot{\theta}_5)-2p_{14}s_4c_5\dot{\theta}_4\dot{\theta}_5$$

$$V_4=-(-s_4s_5(p_{14}sc_{23}+p_{15}c_2c_{23})+p_{17}c_4s_5)\dot{\theta}_1^2+p_{15}c_3s_4s_5\dot{\theta}_2^2-(s_{23}(p_{13}+p_{18}c_{44})+c_4s_5(-p_{14}c_{23}+2p_{15}s_2))\dot{\theta}_1\dot{\theta}_2$$
$$-(-2p_{14}c_{23}c_4c_5+s_{23}(p_{13}+p_{18}cc_4))\dot{\theta}_1\dot{\theta}_3-p_{16}s_{23}c_4\dot{\theta}_1\dot{\theta}_5+p_{16}s_4(\dot{\theta}_2\dot{\theta}_5+\dot{\theta}_3\dot{\theta}_5)$$

$$V_5=-(p_{14}(-ss_{23}s_5+sc_{23}c_4c_5)+p_{15}c_2(-s_{23}s_5+c_{23}c_4c_5)+p_{17}s_4c_5)\dot{\theta}_1^2-(-p_{14}s_5+p_{15}(c_3c_4c_5-s_3s_5))\dot{\theta}_2^2$$
$$-(-c_{23}s_4(2p_{14}c_5+p_{16})+2p_{15}s_2s_4c_5)\dot{\theta}_1\dot{\theta}_2+c_{23}s_4(p_{14}c_5+p_{16})\dot{\theta}_1\dot{\theta}_3+p_{16}s_{23}c_4\dot{\theta}_1\dot{\theta}_4-p_{16}s_4(\dot{\theta}_2\dot{\theta}_4+\dot{\theta}_3\dot{\theta}_4)$$

$$V_6 = 0$$

$f_{r1}= 4.94\dot{q}_1+8.43$ if $\dot{q}_1 > 0$

$f_{r1}= 3.45\dot{q}_1-8.26$ if $\dot{q}_1 < 0$

$f_{r1}= 0$ if $\dot{q}_1 = 0$

$f_{r2}= 7.67\dot{q}_1+12.71$ if $\dot{q}_2 > 0$

$f_{r2}= 8.53\dot{q}_1-11.34$ if $\dot{q}_2 < 0$

$f_{r2}= 0$ if $\dot{q}_2 = 0$

$f_{r3}= 3.27\dot{q}_1+5.93$ if $\dot{q}_3 > 0$

$f_{r3}= 3.02\dot{q}_1-5.57$ if $\dot{q}_3 < 0$

$f_{r3}= 0$ if $\dot{q}_3 = 0$

$f_{r4}= 0.41\dot{q}_1+0.85$ if $\dot{q}_4 > 0$

$f_{r4}= 0.41\dot{q}_1 - 1.29$ if $\dot{q}_4 < 0$

$f_{r4}= 0$ if $\dot{q}_{41} = 0$

$f_{r5}= 0.43 * \dot{q}_1+0.67$ if $\dot{q}_5 > 0$

$f_{r5}= 0.43 * \dot{q}_1 - 1.04$ if $\dot{q}_5 < 0$

$f_{r5}= 0$ if $\dot{q}_5 = 0$

$f_{r6}= 0.22\dot{q}_1+0.30$ if $\dot{q}_6 > 0$

$f_{r6}= 0.22\dot{q}_1 - 0.81$ if $\dot{q}_6 < 0$

$f_{r6}= 0$ if $\dot{q}_6 = 0$

$g_2=p_{23}c_2+p_{24}s_{23}+p_{25}s2$

$g_3=p_{24}s_{23}+p_{26}c_{23}$

$g_4=-p_{27}s_{23}s_4s5$

$g_5=p_{27}(c_{23}s_5+s_{23}c_4c_5)$

In these equations, p_i (i = I,...,27) are the inertial parameters. Their values are approximated from those reported by Armstrong, 1986 and they are

$p_1 = 2.7069$, $p_2 = 4.1603$, $p_3 = 1.7044$, $p_4 = 0.7260$, $p_5 = 0.4750$, $p_6 = 0.4387$, $p_7 = 0.4018$, $p_8 = -0.1698$, $p_9 = 0.02375$, $p_{10} = -0.03102$, $p_{11} = -0.01578$, $p_{12} = 0.0$, $p_{13} = 0.0$, $p_{14} = 0.0$, $p_{15} = 0.0$, $p_{16} = 0.0$, $p_{17} = 0.0$, $p_{18} = 0.0$, $p_{19} = 0.193$, $p_{20} = 0.83$, $p_{21} = 0.2$, $p_{22} = 0.179$, $p_{23} = -39.56$, $p_{24} = -10.79$, $p_{25} = 1.024$, $p_{26} = 0.3585$, $p_{27} = -0.0927$

REFERENCES

[1] Adachi, Y., "Touch and Trace on the Free-Form Surface of Virtual Objects," *Proceedings of IEEE Virtual Reality Annual International Symposium*, pp. 162-168, 1993.

[2] Adachi, Y., T. Kumano, and K. Ogino, "Intermediate Representation for Stiff Virtual Objects," *Proceedings of IEEE Virtual Reality Annual International Symposium '95*, pp. 203-210, 1995.

[3] Adachi, Y., T. Kumano, and K. Ogino, "Sensory Evaluation of Virtual Haptic Push-Buttons," *ASME Dynamic Systems and Controls*, DSC-Vol. 55-1, pp. 361-368, 1994.

[4] Adams, R.J., B. Hannaford, "Stable Haptic Interaction with Virtual Environments," *IEEE Transactions on Robotics and Automation*, vol. 15, no. 3, pp. 465-474, 1999.

[5] Adams, R.J., M.R. Moreyra, and B. Hannaford, "Stability and Performance of Haptic Displays: Theory and Experiments," *Proceedings of ASME Dynamic Systems and Control*, vol. 64, pp. 227-234, 1998.

[6] Adelstein, B.D., M.J. Rosen, "Design and Implementation of a Force Reflecting Manipulandum for Manual Control Research," *ASME Dynamic Systems and Control*, DSC-vol. 42, pp. 1-12,1992.

[7] Armstrong B., O. Khatib, and J. Burdick, "The Explicit Dynamic Model and Inertial Parameters of the PUMA 560 Arm", *Proceedings of IEEE International Conference on the Robotics and Automation*, pp. 510-518, San Francisco, Ca, 1986.

[8] Barfield, W., T.A. Furness, *Virtual Environments and Advanced Interface Design*, Oxford University Press: New York, NY, 1995.

[9] Bejczy, A.K., W.S. Kim, and S.C. Venema, "The Phantom Robot: Predictive Displays for Teleoperation with Time Delay," *Proceedings of IEEE International Conference on the Robotics and Automation*, pp. 3-8, January 1990.

[10] Belanger, P.R., P. Dobrovolny, A. Helmy, and X. Zhang, "Estimation of Angular Velocity and Acceleration from Shaft Encoder Measurements," *International Journal of Robotics Research*, vol. 17, no. 11, pp. 1225-1233, November 1998.

[11] Brooks, F.Jr., M. Ouh-Young, J. Batter, and A. Jerome, "Project GROBE-Haptic Displays for Scientific Visualization," *Computer Graphics*, Vol. 24, No. 4, pp. 177-185, 1990.

[12] Brooks, T.L., "Telerobotic Response requirements," *Proceedings of International Conference on Systems, Man, and Cybernetics*, pp. 113-120, Los Angeles, CA, 1990.

[13] Brown, J.M., J.E. Colgate, "Minimum Mass for Haptic Display Simulations," *Proceedings of ASME Dynamic Systems and Control*, DSC-vol. 64, pp. 249-256,1998.

[14] Brown, J.M., J.E. Colgate, "Passive Implementation of Multibody Simulations for Haptic Display," *ASME International Mechanical Engineering Conference and Exhibition*, DSC-vol. 61, pp.85-92, Dallas, TX, 1996.

[15] Bruyninckx, H., O. Khatib, "Gauss' Principle and the Dynamic of Redundant and Constarint Manipulators," *Proceedings of IEEE International Conference on Robotics and Automation*, pp. 2563-2568, San Francisco, CA, April 2000.

[16] Burdea C.G., *Force and Touch Feedback for Virtual Rality*, John Wiley & Sons, New York, NY, 1996.

[17] Caldwell, D., O, Kocak, and U. anderson, "Multi-armed Dextrous Manipulator Operation Using Glove/Exoskeleton Control and Sensory Feedback," *Proceedings of IROS*, pp. 567-572, Pittsburgh, PA, 1995.

[18] Clover, C.L., "Control system design for robots used in simulating dynamic force and moment interaction in virtual reality applications," Doctor of Philosophy dissertation, Iowa State University, 1996.

[19] Colgate, J.E., J.M. Brown, "Factors effecting the z-width of a Haptic display, " *Proceedings of IEEE International Conference on Robotics and Automation*, pp. 3205-3210, 1994.

[20] Colgate, J.E., M.A. Peshkin, and W. Wannasuphoprasit, "Nonholonomic Haptic Display," *Proceedings of IEEE International Conference on the Robotics and Automation*, pp. 539-544, April 1996.

[21] Colgate, J.E., P.E. Grafing, M.C. Stanley, and G. Schenkel, "Implementation of Stiff Virtual Walls in Force-Reflecting Interfaces, " *Proceedings of IEEE Virtual Reality Annual International Symposium*, pp. 202-208, 1993.

[22] Colgate, J.E., W. Wannasuphoprasit, and M.A. Peshkin, "COBOTS: Robots for Collaboration with Human Operators," *Proceedings of the ASME Dynamics Systems and Control Division*, DSC-vol. 58, pp. 433-439, 1996.

[23] Corke, P.I., B. Armstrong, "A search for Consensus Among Model Parameters Reported for the PUMA 560 Robot," *Proceedings of IEEE International Conference on the Robotics and Automation*, pp. 1608-1613, 1994.

[24] Craig, J.J., *Introduction to Robotics: Mechanics and Control*, Addison Wesley, Reading, MA, 1989.

[25] Craignan, C.R., R.R. Cleary, "Closed-Loop Force Control for Haptic Simulation of Virtual Environments," *Haptics-e*, vol. 1, no. 2, pp.1-14, February 2000.

[26] Dede, C., R.B. Loftin, and J.W. Regian, "The Design of Artificial Realities to Improve Learning Newtonian Mechanics," *Proceedings of East-West International Conference on Multimedia, Hypermedia, and Virtual Reality*, Moscow, Russia, 1994.

[27] Doty, K., C. Melchiorri, C. Bonivento, "A Theory of Generalized Inverses Applied to Robotics," *International Journal of Robotics Reserach*, vol. 12, no. 1, pp. 1-19, February, 1993

[28] Doulgeri, Z., N. Fahantidis, and R.P. Paul, "Nonlinear Stability of Hybrid Control," *International Journal of Robotics Research*, vol. 17, no. 7, pp. 792-806, July 1998.

[29] Edwards, J. C. and G. R. Luecke, "Physically Based Models for use in a Force-Feedback Virtual Environment," *Proceedings of the 1996 Japan/USA Symposium on Flexible Automation*, Boston, MA, June 8-10, 1996, pp. 221-228.

[30] Ellis, R.E, O.M. Ismale, and M.G. Lipsett, "Design and Evaluation of a High Performance Prototype Planar Haptic Interface," *Proceedings of ASME Winter Annual Meeting: Advances in Robotics, Mechatronics, and Haptic Interfaces*, pp. 55-64, 1993.

[31] Lewis, F.L, C.T. Abdallah, D. M. Dawson, *Control of Robot Manipulators*, New York: MacMillan Publishing Company, 1993.

[32] Fisher, W.D. , M.S. Mujtaba, "Hybrid Position/Force Control: A Correct Formulation," *The International Journal of Robotics Research*, vol. 11, no. 4, pp. 299-311, August 1992.

[33] Gillespie, B., M. Cutkosky, "Interactive Dynamics With Haptic Display," *Proceedings of ASME Winter Annual Meeting: Advances in Robotics, Mechatronics, and Haptic Interfaces*, pp. 65-72, 1993.

[34] Gillespie, R.B., "A Survey of Multibody Dynamics for Virtual Environments," *ASME International Mechanical Engineering Conference and Exhibition*, DSC-vol. 61, pp.45-54, Dallas, TX, 1996.

[35] Gillespie, R.B., "Haptic Display of Systems with Changing Kinematic Constraints: The Virtual Piano Action," Ph.D., Stanford University, 1996.

[36] Hannaford, B., "A Design Framework For Teleoperators With Kinesthetic Feedback," *IEEE Transactions on Robotics and Automation*, vol. 5, no. 4, pp. 426-434, August 1989.

[37] Hogan, N.H. , "Impedance Control: An Approach to Manipulation: Part I – Theory, Part II – Implementation, Part III - Application", *ASME Journal of Dynamic Systems, Measurement, and Control*, vol. 107, pp. 1-24, March 1985.

[38] Hunter, I.W., et. al., "A Teleoperated Microsurgical Robot and Associated Virtual Environment for Eye surgery," *Presence*, 2(4), pp. 265-280, 1993.

[39] Ishihara, T., "Direct Digital Design of Computed Torque Controllers", *Journal of Robotic Systems*, vol. 11, no. 3, pp. 197-209, 1994

[40] Kane, T.R., D.A. Levinson, *Dynamics: Theory and Applications*, New York: McGraw-Hill Companies, Inc., 1985.

[41] Kazerooni, H., M. Her, "The Dynamics and Control of a Haptic Interface Device," *IEEE Transactions on Robotics and Automation*, vol. 10-4, pp. 453-464, August 1994.

[42] Kazerooni, H., T. Tsay, and K. Hollerbach, "A Controller Design Framework for Telerobotic Systems," *IEEE Transactions on Control Systems Technology*, vol. 1, no. 1, pp. 50-62, March 1993.

[43] Khatib, O., A. Bowling, "Optimization of the Inertial and Acceleration Characteristics of Manipulators," *Proceedings of IEEE International Conference on Robotics and Automation*, pp. 2883-2889, April 1996.

[44] Lawrence, D.A., L.Y. Pao, M.A. Salada, and A.M. Dougherty, "Quantitative Experimental Analysis of Transparency and Stability in Haptic Interfaces," *Proceedings of ASME Dynamic Systems and Control*, DSC-vol. 58,pp. 441-449, November 1996.

[45] Leahy, M.P., K.P. Valavanis, and G.N. Saridis, "Evaluation of Dynamic Models for PUMA robot control," *IEEE Transactions on Robotics and Automation*, vol. 5, no. 2, pp. 242-253, April 1989.

[46] Lenarcic, J., "Alterative Computational Scheme of Manipulator Inverse Kinematics," *Proceedings of IEEE International Conference on Robotics and Automation*, pp. 3235-3240, May 1998.

[47] Luecke, G.R., J.C. Edwards, "Force Interactive Virtual Reality using Local Joint Error Control," *Proceedings of SPIE International Symposium on Intelligent Systems and Advanced Manufacturing*, Boston, MA, November 18-19, pp. 45-52, 1996.

[48] Luecke, G.R., Y. Chai, "Contact Sensation in the Synthetic Environment Using the ISU Force Exoskeleton," *Proceedings of IEEE International Conference on Robotics and Automation*, pp. 192-198,1997.

[49] Marcus, B., P. Churchill, "Sensing Human Hand Motions for Controlling Dextrous Robots," *A.D. Little*, 1988.

[50] Massie, T.H., J.K. Salisbury, " The PHANToM Haptic interface: a device for probing virtual objects", *Proceedings of the 1994 ASME Winter Annual Meeting: Dynamic Systems and Control*, vol. 55-1, pp. 295-301, 1994.

[51] Massimino, M., T. Sheridan, "Sensory Substitution for Force Feedback in Teleoperation," *Presence* 2(4), pp. 344-352, 1993.

[52] Mathewson, B.B., W.S. Newman, "Integration of Force Strategies and Natural Admittance Control," *Proceedings of ASME Winter Annual Meeting; Dynamic Systems and Control*, pp. 237-242, 1994.

[53] McCormick, W., H.M. Schwartz, "An Investigation of Impedance Control for Robot Manipulators," *International Journal of Robotics Research*, vol. 12, no. 5, pp. 473-489, October 1993.

[54] McNeely, W.A., "Robot Graphics: A New Approach to Force Feedback For Virtual Reality," *Proceedings of IEEE Virtual Reality Annual International Symposium*, pp. 336-341, 1986.

[55] Millman, P.A., M. Stanley, and J. E. Colgate, "Design of a High Performance Haptic Interface to Virtual Environments", *Proceedings of IEEE Virtual Reality Annual International Symposium*, pp. 216-222, Seattle, WA, 1993.

[56] Minsky, M, et. al., Feeling and Seeing: Issues in Force Display," Computer Graphics, vol. 24, no.2, pp. 235-243, 1990.

[57] Mussa-Ivaldi, F.A., N. Hogan, "Integrable Solutions of Kinematic Redundancy via Impedance Control," *International Journal of Robotics Research*, vol. 10, no. 1, pp. 481-491, 1991.

[58] Nelson, D.D., E. Cohen, "User Interaction with CAD Models with Nonholonomic Parametric Surface Constraints," *Proceedings of ASME Dynamic Systems and Control*, DSC-vol. 64, pp. 235-242,1998.

[59] Niemeyer, G., J.E. Slotine, "Stable Adaptive Teleoperation," *IEEE Journal of Oceanic Engineering*, vol. 16, no. 1, pp. 152-162, January 1991.

[60] Ouh-young, M., F.P. Brooks, "Using a manipulator for force display in molecular docking," *Proceedings of IEEE Conference on Robotics and Automation*, vol. 3, pp. 1824-1829, Philadelphia, Pa.

[61] Park, J., W. Chung, and Y. Youm, "Unified Motion Specification and Control of Kinematically Redundant Manipulators," *Proceedings of IEEE International Conference on Robotics and Automation*, pp. 3946-3952, San Francisco, CA, April 2000.

[62] Raibert, M.H., J.J. Craig, "Hybrid Position/Force Control Manipulators," *ASME Journal of Dynamic Systems and Control*, vol. 102, pp. 126-133, 1981.

[63] Salcudean, S.E., T.D. Vlaar, "On the Emulation of Stiff Walls and Static Friction with a magnetically Levitated Input/Output Device," ASME International Mechanical Engineering Exposition and Congress, DSC-vol.55-1, pp. 303-310, Chicago, IL, 1994.

[64] Sarkar, N., X. Yun, and V. Kumar, "Control of Mechanical Systems with Rolling Constraints: Application to Dynamic Control of Mobile Robots," *International Journal of Robotics Research*, vol. 13, no. 1, pp. 55-69, February 1994.

[65] Shimoga, K.B., "A Survey of Perceptual Feedback Issues in Dexterous Telemanipulation: Part I: Finger Force Feedback, Part II: Finger Touch Feedback," *Proceedings of IEEE Conference on Robotics and Automation*, pp. 263-279, 1993.

[66] Song, P., A. Goldenberg, "Fundamental Principles of Design of Position and Force Controller for Robot Manipulators," *Proceedings of IEEE International Conference on the Robotics and Automation*, pp. 2246-2251, April 1996.

[67] Whitney, D.E., "Historical Perspective and State of the Art in Robot Force Control", *International Journal of Robotics Research*, pp. 3-14, Spring 1987.

[68] Yabuta, T., "Nonlinear Basic Stability Concept of the Hybrid Position/Force Control Scheme for Robot Manipulators," *IEEE Transactions on Robotics and Automation*, vol. 8, no. 5, pp. 663-670, October 1992.

[69] Yokokohji, Y., R.L. Hollis, and T. Kanade, "What You Can See is What You Can Feel -Development of a Visual/Haptic Interface to Virtual Environment," *IEEE Proceedings of VRAIS '96*, pp. 46-53, January 1996

[70] Yun, X, "State Space Representation of Holonomic and Nonholonomic Constraints Resulting from Rolling Contacts," *Proceedings of IEEE Conference on Robotics and Automation*, pp. 2690-2694, 1995.